CALCULATIONS OF ELASTIC AND INELASTIC ELECTRON SCATTERING IN LIGHT NUCLEI WITH SHELL-MODEL WAVE FUNCTIONS

By

Raad Abdul-Karim Radhi

A DISSERTATION

Submitted to
Michigan State University
In partial fulfillment of the requirements
for the degree of

DOCTOR OF PHILOSOPHY

Department of Physics

1983

ABSTRACT

CALCULATIONS OF ELASTIC AND INELASTIC ELECTRON SCATTERING IN LIGHT NUCLEI WITH SHELL-MODEL WAVE FUNCTIONS

By

Raad Abdul-Karim Radhi

Shell-model wave functions calculated within the complete space of $0p_{3/2}$- $0p_{1/2}$ and $0d_{5/2}$- $1s_{1/2}$- $0d_{3/2}$ configurations are used to calculate elastic and inelastic form factors of electron scattering from p-shell and sd-shell nuclei. We analyze the magnetic elastic scattering data for p-shell and sd-shell nuclei and both the electric and magnetic inelastic electroexcitation of the even-parity states of ^{27}Al. Effective operators for the different multipoles are used to normalize the magnetic elastic form factors to the experimental data. Different effective charges are used for E2 and E4 transitions. The longitudinal form factors and the B(E2) values are well reproduced using these effective charges. Comparisons are made for the single-particle wave functions of the harmonic oscillator and the Woods-Saxon radial wave functions.

To my wife

Shatha

ACKNOLEDGEMENTS

I would like to thank my advisor, Dr. B. H. Wildenthal for suggesting this problem and for his support and guidance during my graduate study. I am also grateful to him for reading and correcting the manuscript.

I would also like to thank Dr. B. A. Brown for his assistance and guidance. His concern for this work was essential to its successful completion. I am grateful to the administration and staff of the cyclotron laboratory for allowing me to make use of the laboratory facilities, particularly the computer

I am grateful to the Iraqi government for the financial support during my graduate study.

I would like to express my deepest thanks to my wife Shatha and my daughter Sima, for their love and for their patience and understanding throughout my graduate study.

Lastly, I would like to thank my parents and my brothers and sisters for their love and encouragement and for their suffering from my absence during the years of study away from home.

TABLE OF CONTENTS

LIST OF TABLES

LIST OF FIGURES

CHAPTER I

INTRODUCTION

Electron scattering has been widely used as a probe of nuclear structure. Theoretical work on electron scattering dates from 1929, when Mott (Ref 1) derived the cross section for the relativistic scattering of Dirac particles by spinless point nuclei of charge Ze where $Z/137 << 1$. For the scattering of high energy electrons from the nucleus, the de Broglie wavelength becomes equal to or smaller than the radius of the nucleus, and the interaction of the electron with the nucleus will be sensitive to the details of the nuclear charge distribution. The effects of finite nuclear size on electron scattering were first considered by Guth (Ref 2) and later independently by Rose (Ref 3). Corresponding to the Mott formula for the scattering of electrons from point nuclei, the finite nuclear size can be taken into account by multiplying the Mott cross section by a factor which depends on the charge, current and magnetization distribution of the target nucleus. This coefficient of the Mott cross section is called the form factor of the nucleus. Experimentally, the form factor can be determined as a function of the momentum transfered (q) to the nucleus, a quantity which is determined by the

energies of the incident and scattered electron and the scattering angle.

The effects of nuclear size were first detected experimentally by Lyman et al. (Ref 4), who measured the scattering cross section of 15.7 MeV electrons by nuclei. Good agreement was obtained between the experimental data and calculations which assumed a uniformly distributed nuclear charge.

The scattering of electrons from a target nucleus can occur in two ways. In one, the nucleus is left in its ground state after the scattering and the energy of the electrons is unchanged. In the other, the scattered electron leaves the nucleus in different excited state and has a final energy reduced from the initial just by the amount taken up by the nucleus in its excited state. These two kinds of processes are refered to as elastic and inelastic electron scattering.

Excitation of nuclear levels by electrons was first discussed theoretically by Mamasachlisov (Ref 5) in 1943. The first experiment on electron excitation of nuclei to discrete levels was done in 1940 by Collins and Waldman (Ref 6). Since that time, electron scattering has become a major technique for studying the structure of the nucleus and many experiments have been performed at different laboratories. The work of Hofstadter et al. (Ref 7) at the Stanford university linear accelator in 1953 is considered as the pioneering experimental study of this subject.

Several review articles have been published discussing the development of this topic and one can find a detailed summary of what has been done in this field and lists of review articles since the early stages of scattering theory in Ref 8, Ref 9 and Ref 10.

Electron scattering is not the only way to probe nuclear structure with electromagnetic interactions. An alternate is photo-excitation. The momentum transfered to the nucleus in this case equal to the excitation energy (ω) since the mass of the photon is zero,

$$q_\mu^2 = q^2 - \omega^2 = 0 \qquad (1)$$

The three-momentum transfer $\vec{q}$ in this case cannot be varied for a given energy level, and the nuclear structure cannot be studied as a function of momentum transfer. In the case of charged-particle excitation of nuclear levels, one can vary q for a fixed ω

$$q_\mu^2 = q^2 - \omega^2 > 0 \qquad (2)$$

and study the form factor of the nucleus as a function of q. This gives detailed information about the charge and current distributions in the nucleus, and at $q = \omega$, the results are in principle exactly the same as those of the photo excitation. Coulomb excitation by heavy charged particles is one such tool for probing nuclear structure,

but for light nuclei and high energy, the incident particle may penetrate the Coulomb barrier and the structure effects of the target cannot be isolated from the strong interaction, where both of them are not known well. The electron, on the other hand can penetrate deeply inside the nucleus with only the electromagnetic force acting between the electron and the nucleus.

The nucleus interacts with the electromagnetic field via its charge and current densities. The interaction of the electron with the charge distributions of the nucleus can be considered in the first Born approximation as an exchange of a virtual photon of angular momentum zero along the direction of q. In this case the electron does not flip spin, due to the conservation of angular momentum. This kind of interaction is called Coulomb or longitudinal scattering. The interaction of the electron with the spin and current distributions of the nucleus gives rise to the transverse part of the cross section, where the process can be considered in the first Born approximation as an exchange of a virtual photon of angular momentum ± 1 along the direction of q. In the limit $q \rightarrow 0$ the transition probabilities are exactly the same as for real photons. The spin of the electron in this case should flip to conserve angular momentum. From parity and time reversal invariance one can see that only electric multipoles can have longitudinal components, while both electric and magnetic multipoles can have transverse components. Transverse multipoles must have

angular momentum greater than zero, while longitudinal multipoles can have angular momentum equal to or greater than zero.

Longitudinal scattering gives information about the charge distribution of the nuclear system, while transverse scattering gives information about the current and magnetization distributions of the nucleus. The transverse part can be separated by doing experiments at 180° (Ref 11) where the transverse form factors dominate the scattering (equations (14), (15) and (17)). For data at other angles, the longitudinal and transverse parts can be separated by making a plot of the cross section against $\tan^2(\theta/2)$ at fixed momentum transfer and energy loss of the electron. The slope of this plot gives rise to the transverse part, while the intercept gives rise to the longitudinal part. Such plots are called Rosenbluth plots.

Our aim in this work is to analyze the electron scattering data for different nuclei in the p-shell and sd-shell with a microscopic theory which is not restricted just to the discription of electron scattering, but has also been widely used for explaining other static and kinematic properties of nuclear structure.

We test the validity of the nuclear multi-particle configuration-mixing shell model in two domains. We analyze the magnetic elastic electron scattering data for p-shell and sd-shell nuclei and both the electric and magnetic inelastic electroexcitation of the even-parity states of

^{27}Al. This nucleus is one of the most interesting systems in this mass region, because it represents the point at which nuclear deformations change from prolate (positive quadrapole moment for ^{26}Mg, or negative spectroscopic quadrapole moment for the 2^+ ^{26}Mg state) to oblate (negative quadrapole moment for ^{28}Si, or positive spectroscopic quadrapole moment for the 2^+ ^{28}Si state) (Ref 12). Recent measurements (Ref 13) of the many even-parity states below 7 MeV have been carried out to high momentum transfers. This allows the comparison of the shell-model calculations for different states over a large region of q.

A brief description of the shell-model calculations is presented in Chapter II. The theoretical formulations of the longitudinal and transverse form factors are presented in Chapter III. Results of the elastic magnetic electron scattering from p-shell and sd-shell nuclei and the electroexcitation of the even-parity states of ^{27}Al are presented and discussed in Chapters IV and V respectively.

CHAPTER II

THE NUCLEAR SHELL MODEL

II.1. Introduction

The configuration-mixing nuclear shell model used here is a generalization of the classical shell model of Mayer and Jensen (Ref 14). In the M-J model the nucleons occupy the lowest available orbits of a spherical potential (which parallels the nuclear matter distribution) according to Pauli principle. The properties of the nucleus are determined by the last unpaired nucleon. Only a few details of nuclear spectroscopy can be explained by this simple model. The configuration-mixing shell model (Ref 15) uses a mixing of different orbits to create the eigenstates. In this extended model it is still asumed that the nucleus contains an inert core and active orbits in which the valence nucleons are distributed according to Pauli principle. For the sd-shell nuclei, ^{16}O is assumed as an inert core and no excitations are allowed out of these filled orbits. The remaining orbits are nlj= $0d_{5/2}$, $1s_{1/2}$ and $0d_{3/2}$ with the valence (A-16) nucleons distributed over them within the limits of Pauli principle. In the p-shell ^{4}He is assumed as an inert core, and the valence (A-4) nucleons are distributed over the $0p_{3/2}$ -$0p_{1/2}$ orbits within

the limits of Pauli principle. The problem of shell-model calculations lies in the specification of the one-body and residual two-body interactions (Ref 16). The eigenstates of these interactions are obtained by diagonalization of the matrices of many-nucleon energy matrix elements. A new empirical Hamiltonian has been formulated (Ref 17) for the complete A= 17-39 region. The wave functions obtained from the diagonalization of this new Hamiltonian are used to calculate the matrix elements of the sd-shell one-body operators corresponding to the M1, M3 and M5 moments and elastic magnetic electron scattering form factors of the odd-mass nuclei from A= 17-39, and for the inelastic electromagnetic multipole excitations of ^{27}Al. In the p-shell we use the eigenstates of the UP " Universal P" interaction of Chitwood and Wildenthal (Ref 18) and of the Cohen-Kurath interaction (Ref 19). Single-nucleon wave functions obtained from either the harmonic oscillator (HO) potential or Woods-Saxon (WS) potential are combined with these matrix elements of one-body operators to create "model-space" transition densities.

As mentioned before, excitations out of the model space are excluded from the wave functions we use. However, from the physical point of view, such excitations must occur at some level. Nuclear properties such as transition rates cannot be reproduced properly by the model-space wave functions if the properties of neutrons and protons are the

same as in free space. The shell-model wave functions have to be renormalized in order to include such "core-polarization" effects in describing different nuclear properties. Renormalizations of the model-space wave functions can be achieved by introducing effective operators (Ref 20). For the electric multipole operators additional charge can be added to the charges of the model space neutrons and protons to form effective charges. Effective charges for the protons and neutrons can be justified from the first-order perturbation theory in terms of 1p-1h transitions (Ref 21 Section 16.7 and Ref 20) to the giant electric resonances. With effective charges, shell-model wave functions can explain the observed values of electric transition rates. Adding these ingredients to the model-space transition densities give total transition densities that can be used in describing different electron scattering processes. Similar renormalizations for the magnetic multipole operators involve the introduction of effective g factors.

The details of the calculations of the matrix elements of one-body opertors are presented in Section II.2. Two different models for the single-nucleon wave functions are described in Section II.3.

II.2. Matrix elements of one-body operators

The one-body operator matrix elements are obtained by taking the matrix elements of a one-body tensor operator of rank L between the eigenstates $|\nu JT>$ of the interaction used. These one-body tensor operators of rank L are expressed in second quantization notation in terms of the reduced matrix elements between the single-nucleon states (Ref 21, p. 318)

$$O(L,p/n)=\sum_{jj'} SNME(O,L,j,j',p/n)\frac{[\,a^{+}(j)\otimes\tilde{a}(j')]^{(L,p/n)}}{\sqrt{(2L+1)}} \qquad (3)$$

The entire set of quantum numbers (n,l,j) are abbreviated by j. The operators $a^{+}(j)(\tilde{a}(j'))$ are the creation (annihilation) operators of a neutron or proton in the single state j (j').

The reduced matrix elements of the tensor operator O^{L} are obtained according to

$$<f||\,O(L,p/n)||i>=\sum_{jj'} OBDM(i,f,L,j,j',p/n)\;SNME(O,L,j,j',p/n) \qquad (4)$$

where the one-body density matrix (OBDM) is given by

$$OBDM(i,f,L,j,j',p/n)=\frac{<f||[a^{+}(j)\otimes\tilde{a}(j')]^{(L,p/n)}||i>}{\sqrt{(2L+1)}} \qquad (5)$$

and

$$SNME(O,L,j,j',p/n) = \langle j||O(L,p/n)||j'\rangle \qquad (6)$$

We abbreviate the initial/final states (Ai/f, Zi/f, vi/f, Ji/f, Ti/f) by i/f.

Since the isospin associated with the shell-model wave functions is a good quantum number, it is convenient to calculate the OBDM in terms of the isospin-reduced matrix elements (see the Appendix)

$$OBDM(p/n) = (-1)^{T_f - T_z}\begin{pmatrix} T_f & 0 & T_i \\ -T_z & 0 & T_z \end{pmatrix} \times\sqrt{2}\quad OBDM\ (\Delta T=0)/2$$

$$(+/-)\ (-1)^{T_f - T_z}\begin{pmatrix} T_f & 1 & T_i \\ -T_z & 0 & T_z \end{pmatrix} \times\sqrt{6}\quad OBDM\ (\Delta T=1)/2 \qquad (7)$$

where OBDM(ΔT) is given by

$$OBDM(i,f,L,j,j',\Delta T) = \frac{\langle f|||[a^{+}(j)\otimes\tilde{a}(j')]^{(L,\Delta T)}|||i\rangle}{\sqrt{(2\Delta T+1)}\sqrt{(2L+1)}} \qquad (8)$$

The triple bars mean that the matrix elements are reduced in both spin and isospin spaces. The values OBDM(ΔT) are given in Tables IV.1 and IV.2 for the ground states of stable sd-shell and p-shell nuclei, respectively, and in Table V.1 for all the excited states of ^{27}Al considered in this work. The occupation probabilities for ^{27}Al are given in Table V.2.

II.3. Radial components of single-nucleon wave functions

The radial components of the single-nucleon wave functions used here are obtained from two different potentials, the harmonic oscillator (HO) potential, characterized by the size parameter b ($b^2 = 41.65/\hbar\omega$), and the Woods-Saxon (WS) potential. The size parameters of the HO potentials are set to the values b_{rms} which reproduce the root-mean-square (rms) charge radii of the sd-shell nuclei (Ref 22) and the p-shell nuclei. The radial components of the single-nucleon wave functions of the WS potential are obtained by solving the equations (Ref 23)

$$\left[-\frac{\hbar^2}{2\mu}\frac{d^2}{dr^2} + \frac{\hbar^2 \ell(\ell+1)}{2\mu r^2} + U(r) \right] R(j,r) = \epsilon\, R(j,r) \qquad (9)$$

where $\mu = m(p/n)(A-1)/A$ is the reduced mass. The potential U(r) contains central, spin-orbit and Coulomb parts (Ref 24)

$$U(r) = V(r) + V_{s0}(r) \langle \vec{\ell} \cdot \vec{\sigma} \rangle + \delta_{pn}\, V_{Coul}(r) \qquad (10)$$

where δ_{pn} is equal to 1 for protons and 0 for neutrons. These three components of the potential are

$$V(r) = V(p/n) \left[1 + \exp(r - R(p/n)/a(p/n)\right]^{-1} \qquad (11)$$

$$V_{Coul}(r) = \begin{cases} \dfrac{Ze^2}{2R_c}\left[3 - (r/R_c)^2\right], & r \leq R_c \\ \dfrac{Ze^2}{r}, & r \geq R_c \end{cases} \qquad (12)$$

$$V_{so}(r) = V_{so}\,\frac{1}{r}\,\frac{d}{dr}\left[1 + \exp(r-R_{so})/a_{so}\right] \qquad (13)$$

where V(p/n), R(p/n) and a(p/n) are the well depth, radius and diffuseness respectively. Their values and the values for $R_c=\sqrt{5/3}$ x the experimental rms charge radius, V_{so}= 12 MeV, $R_{so}= 1.1A^{1/3}$ and a_{so}= 0.65 fm are taken from Ref 25.

CHAPTER III

ELECTRON SCATTERING

III.1. Introduction

The differential cross section for the scattering of an electron of initial energy E_i through an angle θ, from a nucleus of mass M and charge Z and angular momentum J_i, is given in the one-photon exchange approximation by (Ref 9, Ref 10, Ref 26)

$$\frac{d\sigma}{d\Omega} = \left(\frac{d\sigma}{d\Omega}\right)_{Mott} \eta \sum_{L} F^2(L,q), \qquad (14)$$

where $\left(\frac{d\sigma}{d\Omega}\right)_{Mott}$ is the Mott scattering cross section of a relativistic electron from a spinless point charge,

$$\left(\frac{d\sigma}{d\Omega}\right)_{Mott} = \left[\frac{Z\,\alpha\,\cos\theta/2}{2E_i \sin^2\theta/2}\right]^2, \qquad (15)$$

α is the fine structure constant and η is the nuclear recoil factor,

$$\eta = [\,1 + (2E_i/M)\,\sin^2(\,/2)\,]^{-1} \qquad (16)$$

The form factor F^2 is the sum of "longitudinal" F_L^2 and "transverse" F_T^2, terms:

$$F^2(L,q) = \frac{q_\mu^4}{q^4} F_L^2 + \left[\frac{q_\mu^2}{2q^2} + \tan^2(\theta/2) \right] F_T^2 \tag{17}$$

where the four-momentum transfer q_μ is given by

$$q_\mu^2 = q^2 - (E_i - E_f)^2, \tag{18}$$

where

$$q^2 = 4E_iE_f \sin^2(\theta/2) + (E_i - E_f)^2 \tag{19}$$

and E_i and E_f denote, respectively the initial and final total energies of the incident and scattered electron. In the above equations we use $\hbar = c = 1$.

The single-nucleon form factors for the longitudinal electric and the transverse magnetic and electric scattering are presented in Sections III.2, III.3 and III.4 respectively. The multi-particle form factors are discussed in Section III.5. Calculations of the p-shell and sd-shell transition densities are presented in Section III.6. Corrections to the electron scattering form factors are given in Section III.7. A derivation of a conversion factor by which a simultaneous display can be obtained from both the form factor and matrix elements at zero momentum transfer is presented in Section III.8.

III.2. Single-nucleon form factor for the longitudinal operator

The interaction of the electron with the charge distribution of the nucleus gives rise to the longitudinal or Coulomb scattering. The Coulomb multipole operator is defined (Ref 9) by

$$L_{LM}^{C}(q) = \int d\vec{r}\; j_L(qr)\; Y_{LM}(\Omega_r)\; \rho(\vec{r}) \qquad (20)$$

where $\rho(\vec{r})$ is the charge density operator, which is considered in the single-particle model as a sum of the charges of all the nucleons,

$$\rho_{p/n}(\vec{r}) = \sum_{k=1}^{A(p/n)} \delta(\vec{r} - \vec{r}_k) \qquad (21)$$

A(p/n)= Z/N, the number of protons/neutrons in the nucleus.

In the single-particle model, equation (20) reduces to

$$\sum_k L_{LM}^{C}(p/n,q,\vec{r}_k) = \sum_k j_L(qr_k)\; Y_{LM}(\Omega_{r_k}) \qquad (22)$$

The reduced single-particle form factor of the Coulomb operator is given by

$$f_{C,p/n}(L,q) = \langle j||L_L^{C}(p/n,q,\vec{r})||j'\rangle$$

$$= \int dr\ r^2\ \ h_L^C(j,j',r)\ j_L(qr) \qquad (23)$$

The radial function h_L^C is given by

$$h_L^C(j,j',r) = (j||Y_L||j')\ R(j,r)\ R(j',r), \qquad (24)$$

with

$$(j||Y_L||j') = P_L(E,\ell,\ell')\ C_L(j,j') \qquad (25)$$

where the brackets (||) mean that the integration is taken over the angles only. The coefficient $P_L(E,\ell,\ell')$ is the electric parity-selection-rule operator which guarantees the correct parity for the Coulomb operator (Appendix A.3e5 of Ref 21)

$$P_L(E,\ell,\ell') = \frac{1}{2}\left[1 + (-)^{\ell+\ell'+L}\right], \qquad (26)$$

$$C_L(j,j') = (-1)^{j+1/2}\left[\frac{(2j+1)(2L+1)(2j'+1)}{4\pi}\right]^{1/2} \times \begin{pmatrix} j & L & j' \\ 1/2 & 0 & -1/2 \end{pmatrix} \qquad (27)$$

and R(j,r) is the radial component of the single-nucleon wave functions.

III.3. Single-nucleon form factor for the transverse magnetic operator

The transverse form factors arise from the interaction of the scattering electron with the current and magnetization distributions of the nucleus. The transverse form factor is composed of electric and magnetic terms. The multipole magnetic operator is given (Ref 9) by

$$T_{LM}^{mag}(q)=\int d\vec{r}\ \vec{M}_{LLM}(q,\vec{r})\ .\ \vec{J}(\vec{r}) \tag{28}$$

The operator $\vec{M}_{L'LM}(q,\vec{r})$ is defined by

$$\vec{M}_{L'LM}(q,\vec{r})= j_{L'}(qr)\ \vec{Y}_{L'LM}(\Omega_r) \tag{29}$$

where $\vec{Y}_{L'L1}(\Omega_r)$ is the vector spherical harmonic

$$\vec{Y}_{L'L1}(\Omega_r)=\sum_{M',q} \langle L'M'1q|LM\rangle\ Y_{L'M'}(\Omega_r)\ \hat{e}_q \tag{30}$$

$$\hat{e}_{\pm1}=\mp\frac{1}{2}(\hat{e}_x \pm i\ \hat{e}_y) \tag{31}$$

$$\hat{e}_0=\hat{e}_z \tag{32}$$

The factor $\vec{J}(\vec{r})$ is the sum of the convection current, $\vec{J}_c$, and the magnetization current, $\vec{J}_m$, of the nucleus, given by

$$\vec{J}(\vec{r}) = \vec{J}_c(\vec{r}) + \vec{J}_m(\vec{r})$$

$$= \vec{J}_c(\vec{r}) + \vec{\nabla} \times \vec{\mu}(\vec{r}) \tag{33}$$

where the subscripts c and m stand for the convection and magnetization parts of the current respectively, and $\vec{\mu}(\vec{r})$ is the magnetization density operator.

In the single-particle model, the convection current and magnetization densities are given (Ref 26) by

$$\vec{J}_{C,p/n}(\vec{r}) = \frac{e\hbar}{2im_p} \; g_\ell^{p/n} \sum_{k=1}^{A(p/n)} \left\{ \delta(\vec{r} - \vec{r}_k) \; \vec{\nabla}_k \right\}_{symm.} \tag{34}$$

$$\vec{\mu}_{p/n}(\vec{r}) = \frac{e\hbar}{2m_p c} \; (1/2) g_s^{p/n} \sum_{k=1}^{A(p/n)} \delta(\vec{r} - \vec{r}_k) \; \vec{\sigma}_k \tag{35}$$

where m_p is the proton mass and $\vec{\sigma}_k$ are the Pauli matrices.

Using equations (34) and (35), the multipole magnetic operator in the single-particle model reduces to (Ref 9)

$$\sum_k T_{LM}^{mag}(p/n, q, \vec{r}_k) = q(ie\hbar/2m_p c) \left\{ -2 \; g_\ell^{p/n} \sum_k \vec{M}_{LLM}(q, \vec{r}_k) \cdot \frac{1}{q} \; \vec{\nabla}_k \right.$$

$$\left. + (1/2 \; g_s^{p/n}) \sum_k \left[\sqrt{\left(\frac{L+1}{2L+1}\right)} \; \vec{M}_{LL-1M}(q, \vec{r}_k) - \sqrt{\left(\frac{L}{2L+1}\right)} \; \vec{M}_{LL+1M}(q, \vec{r}_k) \right] \cdot \vec{\sigma}_k \right\} \tag{36}$$

where g_ℓ and g_s are the orbital and spin g factors of the

nucleons.

The single-nucleon form factor of the magnetic operator can be reduced to a radial function using relationships between spherical Bessel functions (Ref 10 Appendix A, for example) and integration by parts,

$$f_{T,p/n}^{mag}(L,q) = \langle j||T_L^{mag}(p/n,q,\vec{r})||j'\rangle$$

$$= ie\hbar/2m_pc \times \int dr\ r^2 \Big[g_\ell^{p/n}\ h_L^{mag}(c,j,j',r)\ j_L(qr) + g_s^{p/n}\ h_L^{mag}(m,j,j',r)\ j_L(qr) \Big] \quad (37)$$

where the radial functions of the convection part (c) and magnetization part (m) are given (Ref 27 and Ref 28) by

$$h_L^{mag}(c,j,j',r) = C_L(j,j')\ P_L(M,\ell,\ell')\ A_L(j,j')\ [L(L+1)]^{-1/2} \times (1/r)\ R(j,r)R(j',r) \quad (38)$$

$$h_L^{mag}(m,j,j',r) = \frac{1}{2}[L(L+1)]^{-1/2}\ C_L(j,j')\ P_L(M,\ell,\ell') \times B(j,j')\frac{d}{dr}\Big[R(j,r)R(j',r)\Big] + \Big[B(j,j')-L(L+1)\Big]\ (1/r)\ R(j,r)R(j',r) \quad (39)$$

where R(j,r) are the single-particle radial wave functions, and A_L and B are numerical coefficients given by

$$A_L(j,j') = [\ 1 + B(j,j')/L][1-B(j,j')/(L+1)] \qquad (40)$$

$$B(j,j') = 2 + D(j,\ell) + D(j',\ell') \qquad (41)$$

The numerical coefficient C_L is given in equation (27) above, and the coefficients P_L and D are given by

$$P_L(M,\ell,\ell') = \frac{1}{2}\left[1 + (-1)^{\ell+\ell'+L+1}\right] \qquad (42)$$

$$D(i,k) = i(i+1) - k(k+1) - 3/4 \qquad (43)$$

III.4. Single-nucleon form factor for the transverse electric operator

The transverse electric operator is given (Ref 9) by

$$T_{LM}^{el}(q) = \frac{1}{q}\int d\vec{r}\ \left[\vec{\nabla} x\ \vec{M}_{LLM}(q,\vec{r})\right].\ \vec{J}(\vec{r}) \qquad (44)$$

Using the definition of the vector spherical harmonics $\vec{Y}_{LLM}(\Omega_r)$ with the vector identities (Appendix A.5 of Ref 21)

$$\vec{\nabla} \times (\vec{L}\, M_{LM}(\vec{r})) = iq^2\, \vec{r}\, M_{LM}(\vec{r}) + i\, \vec{\nabla}\left(\frac{\partial}{\partial r}\, r\, M_{LM}(\vec{r})\right) \qquad (45)$$

$$\vec{\nabla} \cdot (a\, \vec{A}) = a\, \vec{\nabla} \cdot \vec{A} + \vec{\nabla} a \cdot \vec{A} \quad , \qquad (46)$$

the transverse electric operator becomes

$$T_{LM}^{el}(q) = T_{LM}^{el1}(q) + T_{LM}^{el2}(q) \qquad (47)$$

where

$$T_{LM}^{el1}(q) = \frac{i}{q}\, [L(L+1)]^{-1/2} \int d\vec{r}\, \{-[\frac{\partial}{\partial r}\, r\, M_{LM}(\vec{r})]\}\, \vec{\nabla} \cdot \vec{J}_C \qquad (48)$$

and

$$T_{LM}^{el2}(q) = \frac{i}{q}\, [L(L+1)]^{-1/2} \int d\vec{r}\, \{\, q^2\, \vec{r}\, M_{LM}(r) \cdot \vec{J}_C$$

$$+\, q^2\, \vec{r}\, M_{LM}(\vec{r}) \cdot (\vec{\nabla} \times \vec{\mu})\, \} \qquad (49)$$

and where

$$M_{LM}(\vec{r}) = j_L(qr)\, Y_{LM}(\Omega_r) \qquad (50)$$

The nuclear current is conserved, and the continuity equation can be used to determine the single-nucleon matrix elements of the transverse electric operator (Ref 26)

$$\frac{\partial J^{\mu}}{\partial x^{\mu}} = \frac{\partial \rho}{\partial t} + \vec{\nabla} \cdot (\vec{J}_C + \vec{\nabla} \times \vec{\mu}) = 0 \tag{51}$$

$$\vec{\nabla} \cdot \vec{J}_C = - \frac{ie}{\hbar} (\epsilon_i - \epsilon_f) \rho(\vec{r}) \tag{52}$$

where ϵ_i and ϵ_f are the single-particle energies of the initial and final states respectively and $\rho(\vec{r})$ is the charge transition density.

In the single-particle model, where the charge, current and magnetization densities are defined in equations (21), (34) and (35), respectively, the reduced single-nucleon matrix elements of the transverse electric operator can be written as

$$f_{T,p/n}^{el}(L,q) = f_{T,p/n}^{ell}(L,q) + f_{T,p/n}^{el2}(L,q),$$

where

$$f_{T,p/n}^{ell}(L,q) = \frac{1}{q} \int dr\, r^2\, h_L^{ell}(c,j,j',r)\, j_L(qr) \tag{53}$$

and

$$f_{T,p/n}^{el2}(L,q) = q \frac{e\hbar}{2m_p c} \int dr\, r^2 \Big[g_{\ell}^{p/n}\, h_L^{el2}(c,j,j',r)\, j_L(qr) + g_s^{p/n}\, h_L^{el2}(m,j,j',r)\, j_L(qr) \Big] \tag{54}$$

and where the radial functions h_L^{ell} are given by

$$h_L^{el1}(c,j,j',r) = \frac{(\epsilon_i - \epsilon_f)}{\hbar c} [L(L+1)]^{-1/2} \times [2\, h_L^C(j,j',r) + r \frac{d}{dr} h_L^C(j,j',r)], \quad (55)$$

$$h_L^{el2}(c,j,j',r) = [L(L+1)]^{-1/2}\ r \left\{ R(j,r) \frac{d}{dr} R(j',r) - [\frac{d}{dr} R(j,r)]\ R(j',r) \right\} \quad (56)$$

and

$$h_L^{el2}(m,j,j',r) = \frac{e\hbar}{2m_p c} \frac{1}{2} P_L(E,\ell,\ell')[\, D(j,\ell) - D(j',\ell')\,] \times [\, L(L+1)]^{-1/2}\, C_L(j,j')\, R(j,r)\, R(j',r) \quad (57)$$

The radial function h_L^C is given by equation (24) above, and the coefficients P_L, $D(j,\ell)$ and $C_L(j,j')$ are defined in equations (42), (43) and (27) respectively.

III.5. Multi-nucleon form factors

The multi-nucleon form factor for Coulomb scattering is

$$F_{C,p/n}(L,q) = \int dr\ r^2\ H_{L,p/n}^C(i,f,r)\ j_L(qr), \quad (58)$$

with the nuclear matrix elements H_L^C given by

$$H_{L,p/n}^C(i,f,r) = \sum_{jj'} OBDM(i,f,L,j,j',p/n)\ h_L^C(j,j',r), \quad (59)$$

where the one-body density matrix (OBDM) is given by equation (7) and the single-particle matrix elements h_L^C are given by equation (24).

The multi-nucleon form factor for the transverse magnetic scattering is

$$F_{T,p/n}^{mag}(L,q) = \frac{ie\hbar}{2m_pc}\left[g_\ell^{p/n} \int dr\ r^2\ H_{L,p/n}^{mag}(c,j,j',r)\ j_L(qr) + g_s^{p/n} \int dr\ r^2\ H_{L,p/n}^{mag}(m,j,j',r)\ j_L(qr)\right] \quad (60)$$

where the multi-particle matrix elements H_L^{mag} are given by

$$H_{L,p/n}^{mag}(c/m,i,f,r) = \sum_{jj'} OBDM(i,f,L,j,j',p/n)\ h_L^{mag}(c/m,j,j',r) \quad (61)$$

The one-body density matrix (OBDM) is given by equation (7) and the single-particle matrix elements h_L^{mag} are given by equations (38) and (39) for the convection and magnetization currents, respectively. The sums in this case extend over all the valence orbits.

The multi-nucleon form factor for the transverse electric scattering are

$$F_{T,p/n}^{el}(L,q) = F_{T,p/n}^{el1}(L,q) + F_{T,p/n}^{el2}(L,q), \quad (62)$$

where

$$F_{T,p/n}^{ell}(L,q) = \frac{1}{q}\int dr\ r^2\ H_{L,p/n}^{ell}(c,i,f,r)\ j_L(qr) \quad (63)$$

and

$$F_{T,p/n}^{el2}(L,q) = \frac{e\hbar}{2m_pc}\ q\ \left\{ \bar{g}_\ell^{p/n} \int dr\ r^2\ H_{L,p/n}(c,i,f,r)\ j_L(qr) \right.$$

$$\left. + g_s^{p/n} \int dr\ r^2\ H_L^{el2}(m,i,f,r)\ j_L(qr) \right\} \quad (64)$$

and where the nuclear matrix elements H_L^{ell} are given by

$$H_L^{ell}(c,i,f,r) = \frac{(E_i - E_f)}{\hbar c}[L(L+1)]^{-1/2}$$

$$x\ [2\ H_L^C(i,f,r) + r\frac{d}{dr}\ H_L^C(i,f,r)] \quad (65)$$

and E_i and E_f are the initial and final energies of the nuclear states respectively. The multi-nucleon matrix elements H_L^C are given in equation (59). The matrix elements H_L^{el2} are given by

$$H_L^{el2}(c/m,i,f,r) = \sum_{jj'} OBDM(i,f,j,j',p/n)\ h_L^{el2}(c/m,j,j',r) \quad (66)$$

where the radial functions h_L^{el2} are given by equations (56) and (57) for the convection and magnetization currents

respectively. The sums extend over all the valence orbits.

III.6. p-shell and sd-shell transition densities

The multi-particle form factor of the Coulomb operator depends on the transition densities $H_L^C(i,f,r)$. The transition density can be divided into two parts, one depending on the model-space transition density and the other depends on the core-polarization transition density.

The model spaces for the p-shell and sd-shell are defined by the complete set of states contructed from the orbits $0p_{3/2}$ -$0p_{1/2}$ and the orbits $0d_{5/2}$ -$1s_{1/2}$- $0d_{3/2}$ respectively. The model-space one-body operator matrix elements are obtained by taking the matrix elements of a one-body tensor operator between the eigenstates of the interaction used

$$G_{L,p/n}(i,f,r) = \sum_{jj'} OBDM(i,f,L,j,j',p/n)\ h_L^C(j,j',r) \qquad (67)$$

where the OBDM are given by equation (7) and the h_L^C are given by equation (24). The sums extend over all the valence orbits for L>0. For L=0, the sums includes all the orbits in the core.

The model-space transition densities G deal with nucleons in the active orbits only and exclude any effects from the core. Many nuclear properties cannot be quantitatively described by using just the model-space transition density, and the effects from outside the model

space must be taken into consideration. The contribution of the core to the transition rates can be explained (Ref 29 p. 334) as a deformation of the core when the active nucleons make a transition from one state to another. The protons in the closed shell are polarized and their orbits are slightly distorted which contributes to the total transition rates by an amount that corresponds to the observed values. Mass and state-independent effective charges have been introduced empirically (Ref 30 and Ref 25) for the model-space protons and neutrons which are able to reproduce the observed B(E2) values in the sd-shell.

Two models for the effective charge are considered here for the core-polarization transition densities. One can assume the transition density to be proportional to the model-space transition density. We will call this the "valence" (V) model

$$C_{L,p/n}{}^{V}(r) = G_{L,p/n}(r) \tag{68}$$

The other model is based on a multipole-multipole interaction which connects the ground state to the L-multipole $n\hbar\omega$ giant resonance. The shape of the core-polarization transition density in this case is given by the Tassie (T) model (Ref 31)

$$C_{L,p/n}{}^{T}(r) = r^{L-1} \frac{d}{dr} G_{L=0,p/n}(r) \tag{69}$$

where $G_{L=0}(r)$ is the ground state density given in equation (67).

The total transition densities are obtained by combining the model-space transition densities with each of the two models for the radial distribution for the core polarization. The total transition density corresponding to first-order perturbation theory is given by

$$H_{L,p/n}{}^{C}(i,f,r) = G_{L,p/n}(i,f,r) + N_{C,p/n}\, C_{L,p/n}(i,f,r) \qquad (70)$$

where G(r) is the model-space transition density given in equation (67) above, and C(r) is the core-polarization transition density given by equations (68) and (69) for the valence and the Tassie models, respectively, and N_C is a normalization constant to be determined from the matrix elements of the L-multipole gamma-ray-transition operator M_L,

$$M_L = \int r^L \; H_L{}^{C}(r)\; r^2\, dr \qquad (71)$$

The r^L radial integrals of model-space and core-polarization transition densities are given by

$$G_L = \int r^L \; G_L(r)\; r^2\, dr \qquad (72)$$

$$C_L = \int r^L \; C_L(r)\; r^2\, dr \qquad (73)$$

The gamma-ray-transition matrix elements defined at $q = E_f - E_i$, expressed in terms of the effective charges, are given (Ref 22) by

$$M_{L,p} = G_{L,p}(1+\delta_{pp}) + G_{L,n}\delta_{pn} \quad (74)$$

$$M_{L,n} = G_{L,n}(1+\delta_{nn}) + G_{L,p}\delta_{np} \quad (75)$$

where δ_{cv} is the polarization charge that arises from the interaction of the valence nucleons (v) with the core nucleons (c). Their relations to the conventional effective charges e_p and e_n are given by

$$\delta_{pp} = \delta_{nn} = e_p - 1 \quad (76)$$

$$\delta_{pn} = \delta_{np} = e_n \quad (77)$$

It has been found (Ref 30 and Ref 22), that for the complete sd-shell model space, average values of the effective charges for E2 and E4 are close to $e_p + e_n = 1.7e$ and $e_p + e_n = 2.0e$ respectively. These values are used throughout the calculations considered in this work, together with the isovector effective-charge defined by $e_p - e_n = 1e$ (Ref 25).

The normalization constants of equation (70) are obtained by comparing the integrals of both sides of equations (74) and (75),

$$N_{c,p} = (\delta_{pp}G_p + \delta_{pn}G_n)/C_p \tag{78}$$

$$N_{c,n} = (\delta_{nn}G_n + \delta_{np}G_p)/C_n \tag{79}$$

The electromagnetic transition strength $B(L,J_i,J_f)$ is given by

$$B(L,J_i,J_f) = \frac{1}{2J_i+1} |M_{L,p}|^2 \tag{80}$$

III.7. Corrections to the electron scattering

The shell-model wave functions used in describing transition densities give rise to additional non-physical excited states called spurious states, due to the fact that the interaction potential represents an average potential with respect to a fixed origin. The Hamiltonian in this case is in general not translational invariant, and the motion of the center of mass is responsible for these spurious states. These states can be isolated from the exact observed states of the intrinsic motion of the nucleons in the case of the HO potential (Ref 10), where the Hamiltonian can be separated into two parts, one representing the motion of the center of mass, and the other representing the intrinsic motion of the nucleus. This is done by including a factor G_{cm} given by the HO in the nuclear form factor. The center of mass correction factor G_{cm} is (Ref 32)

$$G_{cm}(q) = \exp(q^2\, b^2\, /4A) \tag{81}$$

where b is the oscillator length parameter. We use $b = b_0$ obtained from a global formula for the oscillator length

$$\hbar\omega_0 = 41.46/b_0^2 = 45\,A^{-1/3} - 25\,A^{-2/3} \quad , \qquad (82)$$

where A is the total number of nucleons in the nucleus.

The form factor discussed in the previous sections assumed the nucleons as point particles. A correction due to the finite nucleon size should be considered. For longitudinal scattering, the form factor becomes (Ref 33)

$$F_C(L,q) = N_F \left\{ F_{C,p}(L,q)\, G_{fs,p}(q) + F_{C,n}(L,q)\, G_{fs,n}(q) \right\} \times G_{cm}(q) \qquad (83)$$

where $F_{C,p/n}(L,q)$ is given by equation (58), and the free-nucleon form factors $G_{fs,p}$ and $G_{fs,n}$ are taken from Ref 34, including the small Darwin-Foldy relativistic correction in G_{fs} (Ref 35). The normalization factor N_F is given by

$$N_F = \frac{1}{Z}\left[\frac{4\pi}{2J_i + 1}\right]^{1/2} \qquad (84)$$

For inelastic scattering we use the approximation

$$\frac{F_{C,p}}{Z} = \frac{F_{C,n}}{N} \qquad (85)$$

where the number of protons and neutrons in the nucleus are denoted by Z and N respectively. The Coulomb form factor reduces to

$$F_C(L,q) = N_F \; F_{C,p}(L,q) \; \left[G_{fs,p}(q) + N/Z \; G_{fs,n}(q)\right] \; G_{cm}(q) \qquad L>0 \qquad (86)$$

For the transverse form factor, the correction for the finite nucleon size G_{fs} described in Ref 36 is used for both protons and neutrons. The transverse form factors are

$$F_T^{mag,el}(L,q) = N_F \; \left[F_{T,p}^{mag,el}(L,q) + F_{T,n}^{mag,el}(L,q)\right] \times G_{cm}(q) \; G_{fs,p}(q) \qquad (87)$$

where $F_{T,p/n}^{mag,el}(L,q)$ is given by equation (60) and (62), respectively and $G_{cm}(q)$ is the center of mass correction given in equation (81).

The total form factor is obtained from the sum over all form-factor multipoles $F^2(L,q)$ given in equation (17),

$$F^2(q) = \sum_L F^2(L,q) \qquad (88)$$

where L is determined from the parity selection rule

$$\Delta\pi^{el} = (-1)^L \qquad (89)$$

$$\Delta\pi^{mag} = (-1)^{L+1} \qquad (90)$$

From the parity and time reversal invariance one can see that only electric multipoles can have longitudinal components, while both electric and magnetic multipoles can have transverse components. Transverse multipoles must have angular momentum greater than zero, while longitudinal multipoles can have angular momentum equal to or greater than zero. For elastic scattering, only even multipoles contribute to the longitudinal scattering, while only odd multipoles contribute to the magnetic scattering. There are no contributions from the transverse electric elastic scattering.

The form factors discussed in the previous sections are formulated in terms of the first Born approximation, in which the initial and final states of the electron are pure plane waves. This type of approximation is called the plane wave Born approximation (PWBA). For nuclei in which $Z\alpha << 1$, the PWBA is expected to describe the electron scattering data very well, except in the region of the diffraction minima where the PWBA goes to zero. An improvement to the first Born approximation can be obtained by including the effects of the distortion of the plane wave by the Coulomb field. This higher-order effect is incorporated into the distorted wave Born approximation (DWBA). To first order, the effect of the Coulomb field is to increase the momentum transfered to the nucleus and an effective momentum transfer can be used to include these effects. The effective momentum transfer q_{eff} is related to q (Ref 10) by

$$q_{eff} = q\left[\,1 - \frac{V(r)}{E_i(MeV)}\right] \tag{91}$$

$$q_{eff} = q\left[\,1 + \frac{f_c\ Z\ e^2}{E_i(MeV)\ R_c\ (fm)}\right] \tag{92}$$

where $R_c = \sqrt{5/3}\ \langle r^2\rangle^{1/2}$, $e^2 = \alpha\hbar c = 1.44$ MeV fm and α is the fine structure constant. The value of f_c is determined from the Coulomb potential energy

$$V(r) = \frac{-Z\ e^2}{2\ R_c^{\,3}}\ [\ 3R_c^{\,2} - r^2\ ] \tag{93}$$

where $f_c = 3/2$ if the scattering occurs at the center of the nucleus, and 1.0 if the scattering occurs at the surface. An excellent overlap between DWBA and PWBA is obtained (Ref 37) if the experimental data are plotted as a function of q_{eff} for the elastic magnetic scattering with $f_c = 1.2$ and the theoretical form factors calculated in PWBA are plotted against q. In Figure III.1 we show the difference between the DWBA, calculated with the code Duels (Ref 38), and the PWBA for the elastic magnetic scattering of ^{27}Al. The DWBA and the experimental data are plotted versus q_{eff} with $f_c = 1.2$, while the PWBA are plotted vs. q. No significant differences appear between the DWBA and the PWBA calculations. All the magnetic elastic scattering form factors presented in this work are calculated in PWBA and plotted vs. q with the data plotted vs. q_{eff} with

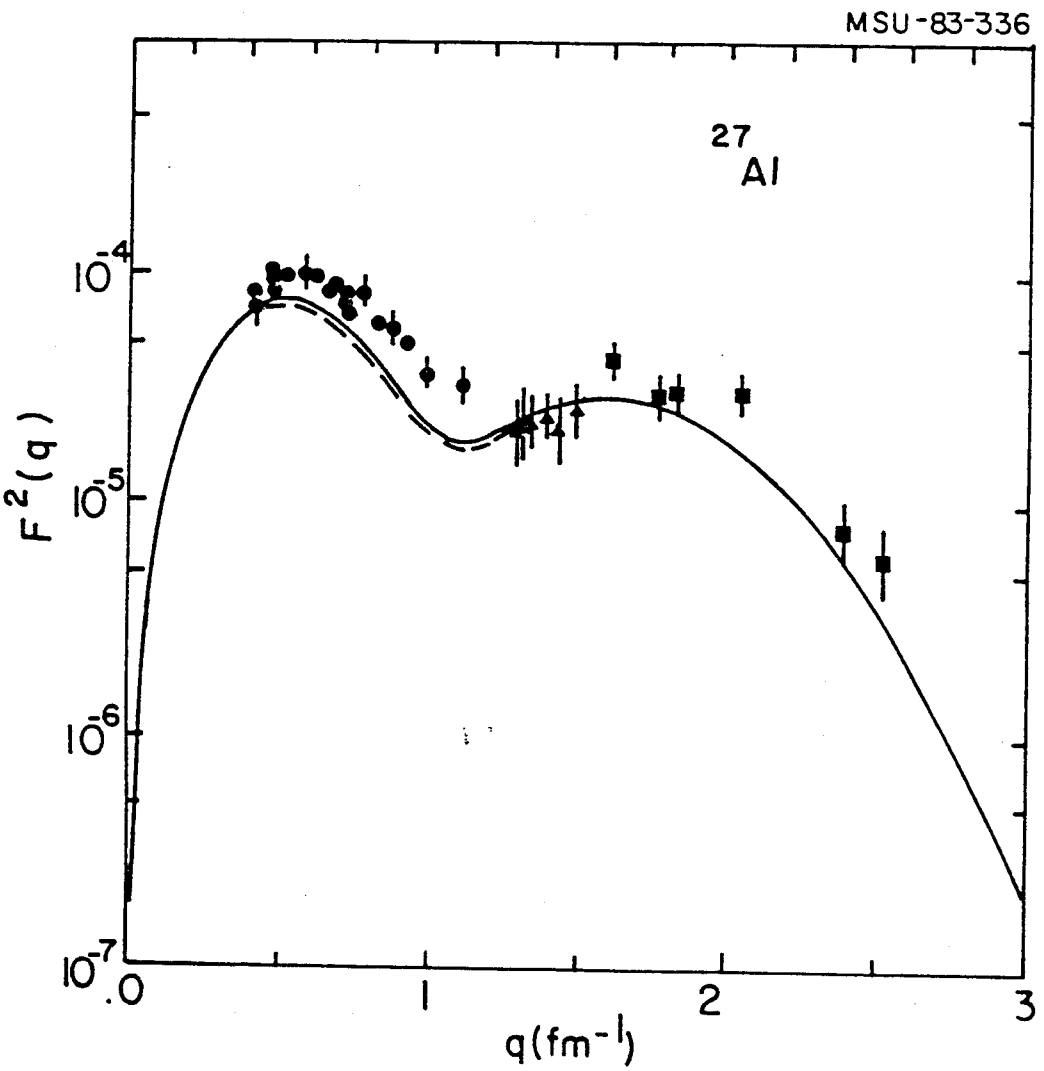

Figure III.1, DWBA form factor for the elastic magnetic scattering from ^{27}Al (solid line) in comparison with the PWBA (dashed line). The calculations incorporate the single-nucleon wave functions of the HO potential of $b=b_{rms}$. The data are taken from Ref 40 (circles), Ref 41 (triangles) and Ref 42 (squares).

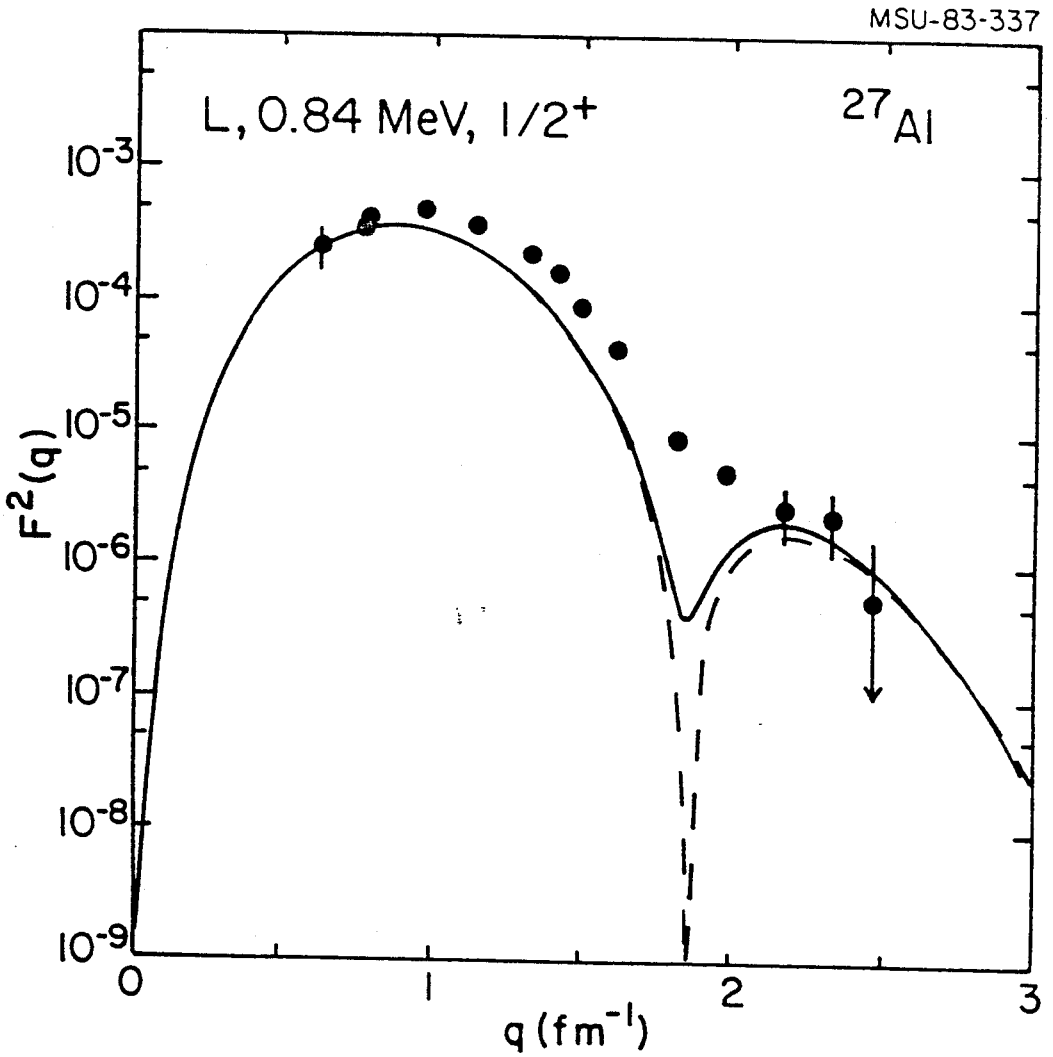

Figure III.2. DWBA form factor for the 0.844 MeV, $1/2^+$ state of ^{27}Al (solid line) in comparison with the PWBA for the same state (dashed line). The calculations incorporate the single-nucleon wave functions of the HO potential of $b=b_{rms}$. The data are taken from Ref 13.

f_C=1.2.

The value of f_C=3/2 has been widely used for the elastic and inelastic electric scattering. In Figure III.2 we show the difference between the DWBA calculated with the code Duels (Ref 38) for the $1/2^+$ state (0.844 MeV) of ^{27}Al and the PWBA. The DWBA and the experimental data are plotted versus q_{eff} with f_C= 3/2, while the PWBA are plotted vs. q. The difference between these two calculations are significant only in the region of the first diffraction minimum, where the PWBA goes to zero, and no significant differences appear at other values of the momentum transfer. All the excited states of ^{27}Al are calculated also in PWBA and plotted vs. q with the data plotted vs. q_{eff} with f_C= 3/2. The Coulomb elastic scattering of ^{27}Al is calculated in DWBA of the MIT elastic phase-shift code (Ref 39).

III.8. Conversion of form factors to q-dependent matrix elements M(q)

We present here a representation for form factors in which we can display simultaneously both the form factor and matrix elements at zero momentum transfer. Formally, we wish to utilyze coversion functions D(L,q) such that $M(q) = F(L,q)/D(L,q)$.

In the limit of small momentum transfer, the PWBA longitudinal form factor is related to the gamma-transition matrix element $M_{L,p}$ defined in equation (74),

$$\lim_{q \to 0} F_C(L,q) = \frac{1}{Z} \sqrt{\frac{4\pi}{2J_i + 1}} \frac{q^L}{(2L+1)!!} M_{L,p} \qquad (94)$$

To remove some of the trivial q dependence at larger q values, the form factor can be divided by the exponential dependence $\exp(-b^2 q^2/4)$ which is contained in the HO radial wave functions. The q- and L-dependent conversion factor for the Coulomb scattering is written as

$$D_C(L,q) = \frac{1}{Z} \sqrt{\frac{4\pi}{2J_i + 1}} q^L \exp(-b_0^2 q^2/4) (2L+1)!! \; D_{cm}(q,b_0) \; D_{fs}(q) \qquad (95)$$

where D_{cm} and D_{fs} are the center of mass and finite proton size corrections, given by

$$D_{cm}(q,b_0) = \exp(b_0^2 q^2/4A), \qquad (96)$$

and

$$D_{fs}(q) = \exp(-0.43 q^2/4), \qquad (97)$$

where b_0 is the harmonic oscillator length parameter obtained from the oscillator length given in equation (82).

For the transverse magnetic scattering, the form factor in the small momentum transfer limit can be written as

$$\lim_{q \to 0} F_T^{mag}(q) = \frac{1}{Z} \sqrt{\frac{4\pi}{2J_i + 1}} C(L) \; M(L) \; q^L \qquad (98)$$

where M(L) is the magnetic multipole moment and C(L) is given by

$$C(L)=\left[\quad 2mc/\hbar\sqrt{\frac{L}{L+1}}\quad(2L+1)!!\quad X\right]^{-1} \tag{99}$$

where

$$X=\sqrt{\frac{4\pi}{2L+1}}\begin{pmatrix} J_i & L & J_i \\ J_i & 0 & -J_i \end{pmatrix} \tag{100}$$

for the elastic magnetic scattering and X=1 for the inelastic magnetic scattering.

In the region of small momentum transfer, the lowest M multipole dominates the scattering, and a q- and L- dependent conversion factor is chosen such that division of the inelastic magnetic form factor by this conversion factor with L set equal to the lowest multipole gives the matrix elements at $q \to 0$.

Hence,

$$D_T^{mag}(L,q)=\frac{1}{Z}\sqrt{\frac{4\pi}{2J_i+1}}q^L\exp(-b_0^2\,q^2/4)\;C(L)$$

$$D_{cm}(q,b_0)\;D_{fs}(q) \tag{101}$$

where D_{cm} and D_{fs} are the center of mass and finite proton size corrections given in equations (96) and (97), respectively.

For the elastic magnetic scattering, we have chosen a

function which is proportional to q at low-q values and proportional to $q^{L_{max}}$ at high-q values. Division of the form factors by this function yields results which clearly display the individual contributions of the different multipoles and which have a slower variation with change in q at region of high momentum transfer. For this function we have chosen the expression

$$H(L_{max},q)=\left[\frac{1}{q}e^{-(q/\alpha)^{L_{max}+1}} + \frac{1}{q^{L_{max}}}\left(1- e^{-(q/\alpha)^{L_{max}+1}}\right)\right]^{-1} \qquad (102)$$

where α is a numerical constant chosen to be 1 and L_{max} is the highest multipole in the shell, L_{max}= 1, 3 and 5 in the 0s, 0p and 1s-0d shells respectively. The complete q- and L-dependent conversion factor is written as

$$D_T^{mag}(L_{max},q)= \frac{1}{Z}\sqrt{\frac{4\pi}{2J_i+1}}\ \exp(-b_0^2\, q^2/4)\ H(L_{max},q)\ C(L=1) \times\ D_{cm}(q,b_0)\ D_{fs}(q) \qquad (103)$$

where D_{cm} and D_{fs} are the center of mass and finite proton size corrections given in equations (96) and (97).

The new representation for the form factor is

$$M(q)= \frac{|F(q)|}{D(L,q)}, \qquad (104)$$

where D(L,q) is given in equations (95), (101) and (103) with L=2 for the Coulomb, L=1 for transverse magnetic and L= L_{max} for magnetic elastic scattering. For the magnetic elastic scattering, the form factor M(q) is plotted vs. q, and for the longitudinal scattering and transverse inelastic scattering, the form factor M(q) is plotted vs. q^2.

The two representations of the form factors $F^2(q)$ and M(q) are shown in Figure III.3 and III.4 for the elastic magnetic scattering and longitudinal E2 transition of $1/2^+$ state in ^{27}Al, respectively.

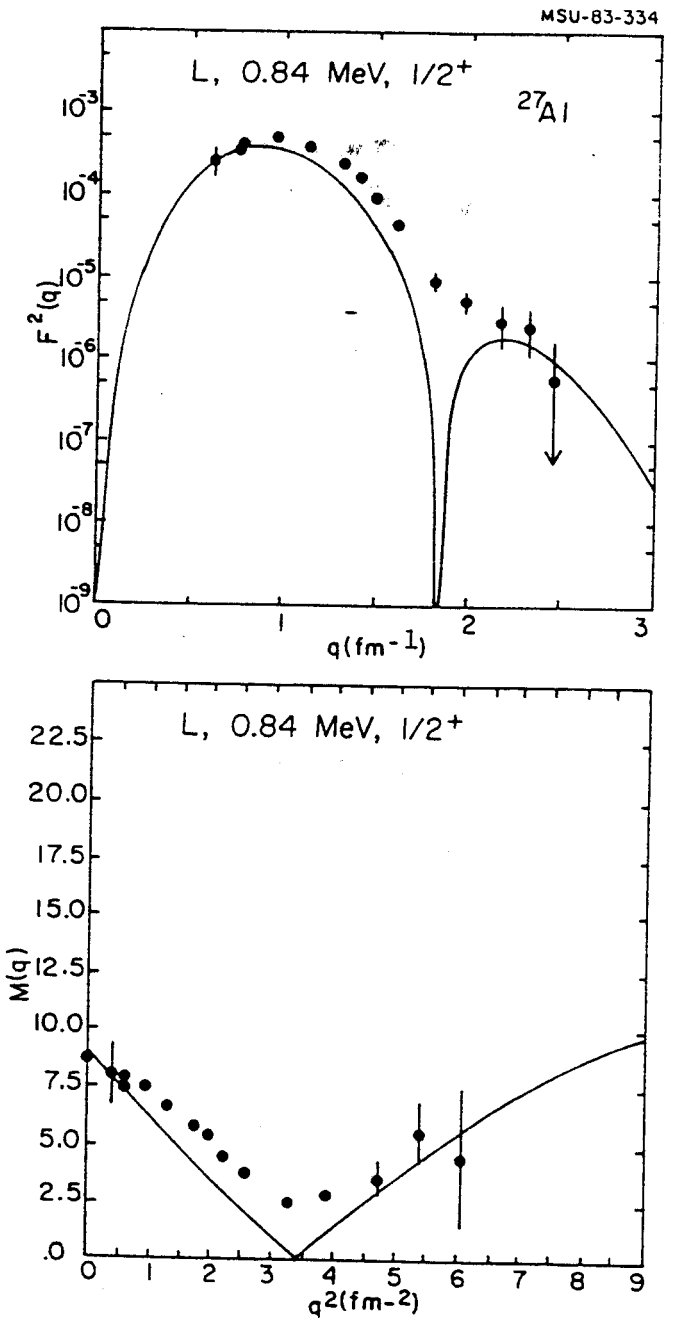

Figure III.3. Magnetic elastic electron scattering for ^{27}Al calculated with the HO potential, presented in the two forms $F^2(L,q)$ and M(q) as explained in section III.8. The magnetic multipoles contributing to the scattering are M1 (dotted line), M3 (dashed line) and M5 (dashed-dotted line). The solid line represents the total incoherent sum of these three multiploles. The magnetic dipole moment is displayed in the M(q) representation. The data are taken from Ref 40 (circles), Ref 41 (triangles) and Ref 42 (squares).

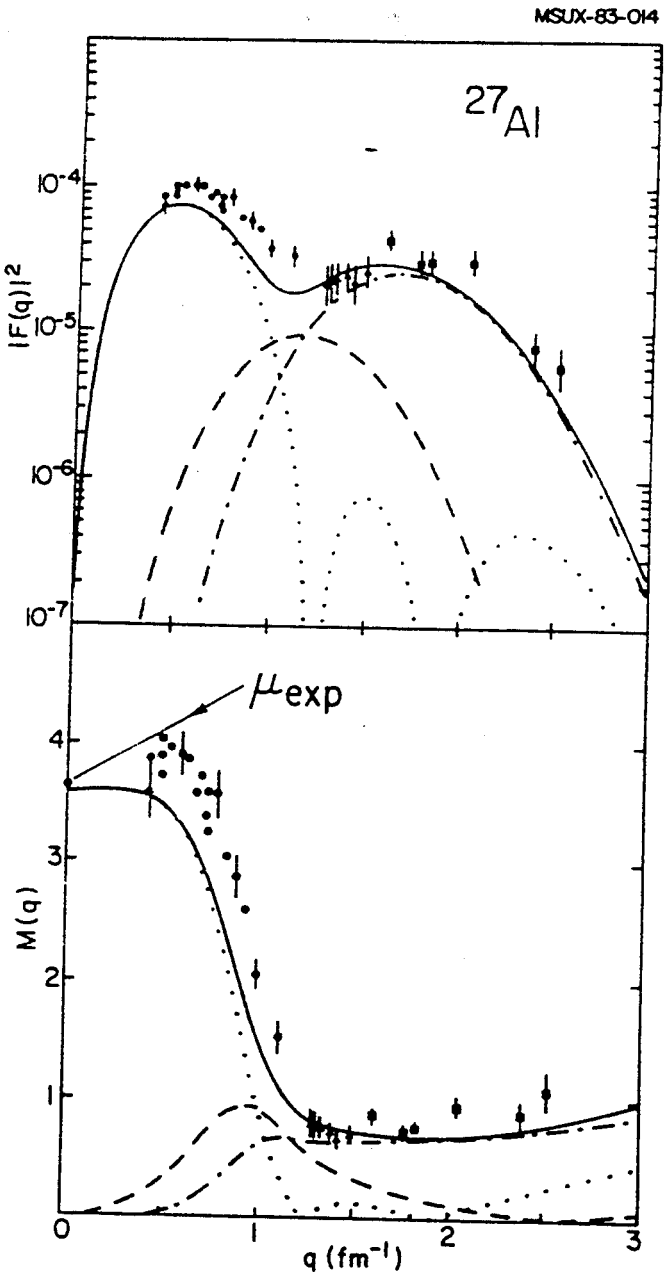

Figure III.4. Longitudinal E2 form factor for the 0.844 MeV, $1/2^+$ state for ^{27}Al calculated with the HO potential, presented in the two forms $F^2(L,q)$ and M(q) as explained in section III.8. The measured B(E2) value is displayed in the M(q) plot at q=0. The data are taken from Ref 13.

CHAPTER IV

MAGNETIC ELASTIC ELECTRON SCATTERING

IV.1. Introduction

The configuration-mixing shell model used here allows the mixing of different orbits to give the full basis eigenstate. In this case, all the model-space valence nucleons share in the scattering process, rather than just the one unpaired nucleon as in the simple shell model. In the calculation of the one-body density matrix (OBDM), we assume that the core is inert and only the motion of the valence nucleons need to be considered. However, it has been shown that higher-order effects such as core polarization and meson-exchange currents are very important and must be taken into consideration (Ref 43, Ref 44, Ref 45 and Ref 46). Assuming an effective two-body interaction between the core and the valence nucleons, one can carry out microscopic calculations to include these effects. Such microscopic calculations lead to the introduction of effective single-nucleon matrix elements which are different from the free-space values. Renormalization of the free-space values of the single-nucleon matrix elements of the different operators might take care of the core-polarization effects. The renormalization of the single-nucleon matrix elements

might be approximated by introducing L-dependent effective g factors. The effects of the meson-exchange current might be explained by using radial parameters for the valence nucleons different from those required to match the rms radius.

We compare the shell-model calculations with experimental data for odd-A 1s-0d-shell and 0p-shell nuclei. Good data are available for the nuclei ^{17}O, ^{27}Al and ^{39}K. Comprehensive comparisons are made for these nuclei using different effective g factors for the different multipoles. We plot the new representation of the form factor M(q) vs. q for all the cases considered in this study, which permits display of the magnetic dipole moment at q=0. We will use the term " form factor" for the new representation M(q).

IV.2. Magnetic elastic scattering from $1/2^+$ nuclei

The stable odd-A nuclei of spin $1/2^+$ in the sd-shell nuclei are ^{19}F, ^{29}Si and ^{31}P. Only the M1 multipole contributes to the magnetic scattering for these systems.

In Figure IV.1 we show the magnetic elastic form factors for these nuclei using the HO radial wave functions of parameter $b=b_{rms}$. The crosses, plusses, and solid lines represent the calculations with the single-particle model, the configuration-mixing shell model with free-nucleon g factors and the configuration-mixing shell model with effective g factors, respectively. We use effective M1 g

Figure IV.1. Form factors for the magnetic elastic scattering of ^{19}F, ^{29}Si and ^{31}P calculated with the HO radial wave functions of $b = b_{rms}$. The cross signs represent the calculations with the single-particle model with free-nucleon g factors. The configuration-mixing shell model calculations using free-space g factors and effective M1 g factors are represented by plus signs and solid lines respectively. The values for the M1 effective g factors are $g_s^p = 5.$, $g_s^n = -3.442$, $g_\ell^p = 1.078$ and $g_\ell^n = -0.044$. The data for ^{19}F are taken from Ref 47 (circles). The data for ^{29}Si and ^{31}P are taken from Ref 48 (triangles) and Ref 49 (circles).

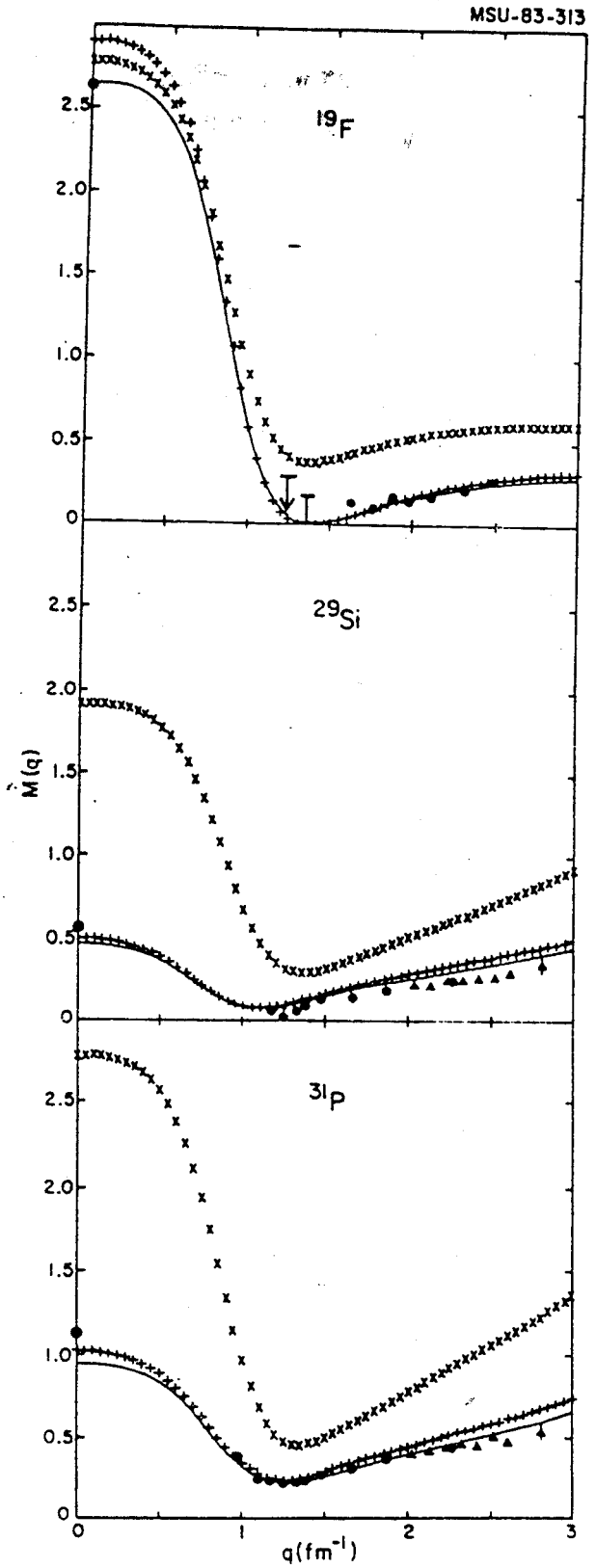

Figure IV.1

factors resulting from a Chi-square fitting to the magnetic dipole moments of all the stable odd-A sd-shell nuclei. These values are [$g_s{}^p$= 5., $g_s{}^n$ = -3.442, $g_\ell{}^p$= 1.028, $g_\ell{}^n$= -0.044].

The single-particle picture of ^{19}F is one proton in the $s_{1/2}$ orbit. From Figure IV.1, we notice that with the single-particle picture (cross signs) neither the magnetic dipole moment nor the scattering data are reproduced satisfactorily. The free-nucleon g factors-configuration mixing shell model does explain the scattering data much better than the single-particle model. However, the measured magnetic dipole moment is not reproduced by the free-nucleon g factors. The effective g factors-configuration mixing shell model explains the experimental data very well (solid lines), and the measured magnetic dipole moment is reproduced properly for ^{19}F, but it slightly underestimated for ^{29}Si and ^{31}P.

IV.3. Magnetic elastic scattering from other odd-A sd-shell nuclei

We calculate the magnetic elastic form factors for all other stable sd-shell nuclei. We compare the results of the single-nucleon shell model (cross signs) with the configuration-mixing shell model. The calculations for ^{17}O, ^{25}Mg and ^{27}Al are presented in Figure IV.2, those for ^{21}Ne, ^{23}Na and ^{33}S are presented in in Figure IV.3 and those for

^{35}Cl, ^{37}Cl and ^{37}K are presented in Figure IV.4. The configuration-mixing shell model form factors are calculated with two different values of the g factors. The lines denoted by plusses represent the calculations with the free-nucleon g factors for all the multipoles that contribute to the scattering, while the solid lines represent the calculations with effective M1 g factors obtained from the Chi-square fitting to the magnetic dipole moments of all the nuclei considered in this study. The values for the effective g factors [$g_s^p = 5.$, $g_s^n = -3.442$, $g_\ell^p = 1.078$ and $g_\ell^n = -0.044$] are used for the M1 multipole. Also, the M3 contribution is quenched to 60% of the free-space value. We use the free M5 g factors for both cases. The multipole decompositions M1 (dotted line), M3 (dashed lines) and M5 (dashed-dotted lines) are those of the empirical g factors discussed above.

With the empirical g-factors, the agreement with the measured magnetic dipole moments becomes worse for some nuclei and improved for others, like ^{21}Ne, ^{23}Na, ^{25}Mg, ^{35}Cl, ^{37}Cl and ^{39}K. A common feature noticed in the regions of high momentum transfer ($q > 2$ fm^{-1}) is that the data are higher than the theory for those states which are dominated by M3 and M5 multipoles. Also, the free-nucleon M3 contribution is an overestimate in the region where it is important.

In the case of ^{25}Mg, good agreement with the measured

Figure IV.2. Form factors for the magnetic elastic scattering of ^{17}O, ^{25}Mg and ^{27}Al calculated with the HO radial wave functions of $b = b_{rms}$. The cross signs represent the calculations with the single-particle model and free-space g factors. The configuration-mixing shell model calculations using free-space g factors are shown by plus signs and those of effective M1 and M3 g factors are shown by solid lines. The values for the effective M1 g factors are those used in Figure IV.1. The M3 contribution is quenched to 60% of the free-space value. We use the free M5 g factors for both cases. The decomposition of the multipoles are M1 (dotted lines), M3 (dashed lines) and M5 (dashed-dotted lines), calculated with the empirical g factors discussed above. The data for ^{17}O are taken from Ref 50 (circles). The data for ^{25}Mg are taken from Ref 37 (squares) and Ref 51 (circles). The data for ^{27}Al are taken from Ref 40 (circles), Ref 41 (triangles) and Ref 42 (squares).

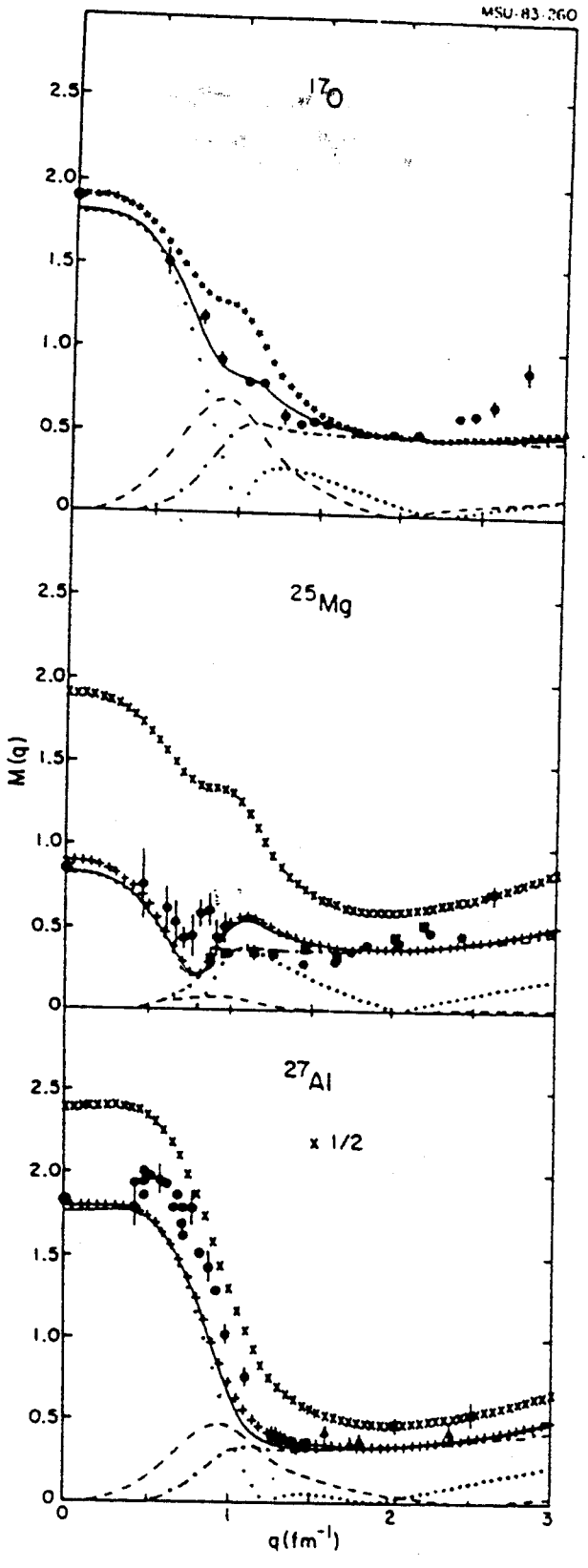

Figure IV.2

Figure IV.3. Form factors for the magnetic elastic scattering of ^{21}Ne, ^{23}Na and ^{33}S. The conventions of the presentation are the same as given in the caption of Figure IV.2. The data for ^{23}Na are taken from Ref 52 (circles).

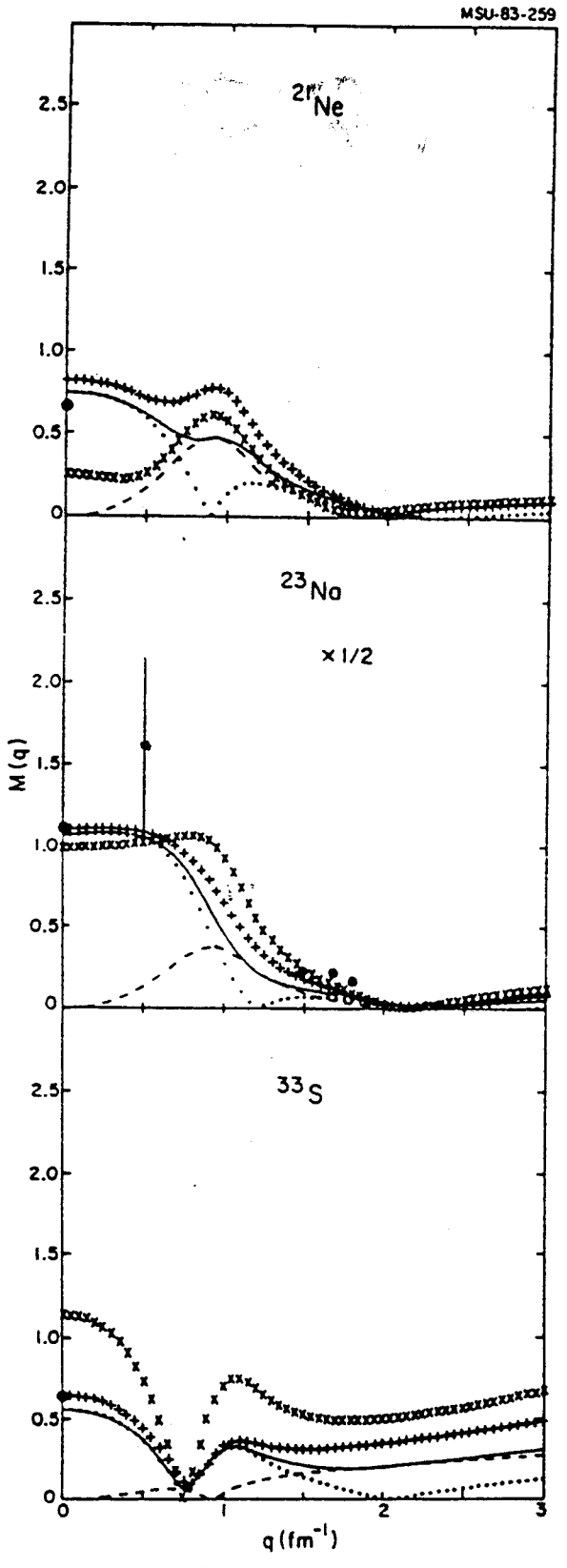

Figure IV.3

Figure IV.4. Form factors for the magnetic elastic scattering of ^{35}Cl, ^{37}Cl and ^{39}K. The conventions of the presentation are the same as given in the caption of Figure IV.2. The data for ^{39}K are taken from Ref 53 (circles) and Ref 54 (squares).

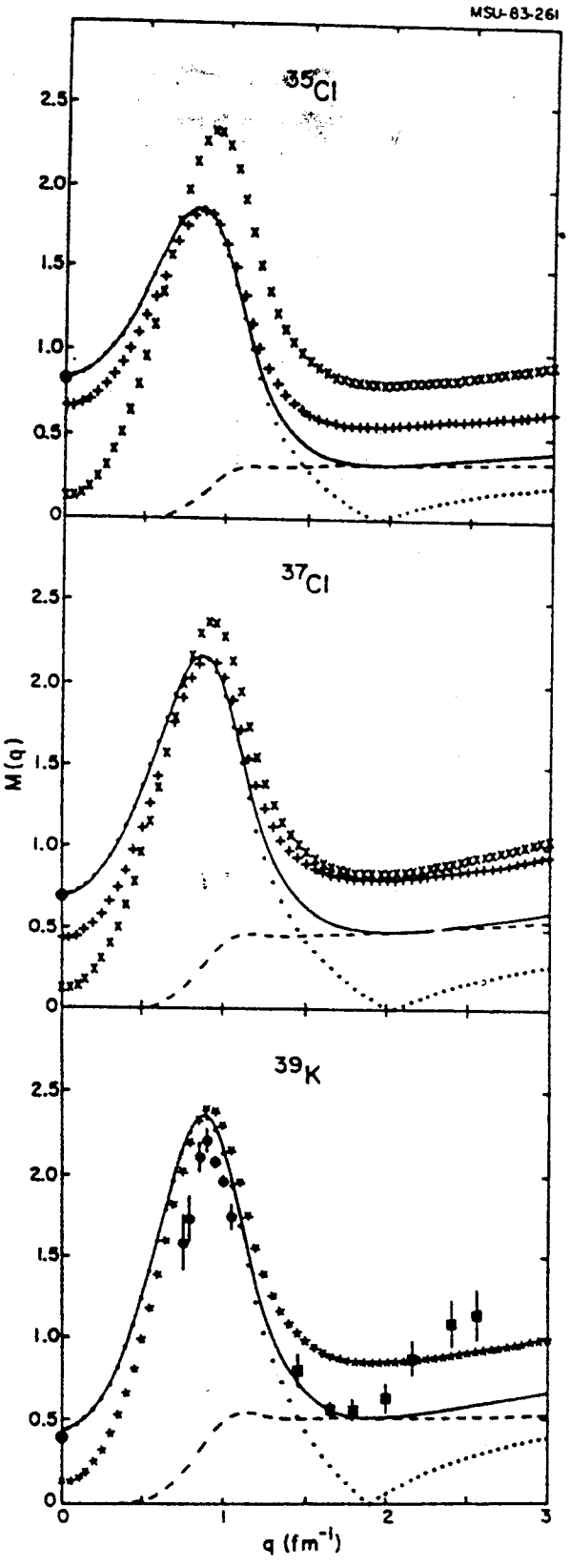

Figure IV.4

dipole moment is obtained, but the quality of the form factor data in the region of small- and medium-q values limits the usefullness of the comparison with theory.

IV.4. Magnetic elastic scattering from ^{17}O

The complete sd-shell space shell-model picture of ^{17}O is identical to the single-nucleon shell-model picture, since this nucleus corresponds to only one neutron outside the ^{16}O inert core. All of the nuclear properties are determined by this unpaired neutron in the model. The calculated form factor with this model is shown in Figure IV.5a and IV.5a' using single-nucleon radial wave functions of the HO potential and the WS potential, respectively. The free-space neutron g factors are used in these calculations. From Figures IV.5, it can be concluded that the M3 contribution is too large and that the calculated form factor is too small in the region of $q > 2$ fm^{-1} .

As mentioned before, the core-polarization effects will alter the results both of simple-single particle and full sd-shell model calculations. We will assume that these effects can be introduced in the form of L-dependent effective g factors. The form factor calculated with effective g factors for the M3 multipole of the neutron equal to 60% of their free-space values are shown in Figure IV.5b and IV.5b'. Quenching the M3 multipole to 60% of the

free-space value gives better agreement with the experimental data in the region where M3 is important but does not improve agreement between experiment and theory in the region of high momentum transfer ($q > 2.0$ fm^{-1}). The discrepancy between theory and experimental data at high momentum transfers has been discussed for medium-heavy nuclei (Ref 55). Meson-exchange corrections (MEC) effects are found to be important in this momentum transfers region. Simple quenching of the M5 form factors (dashed-dotted lines) will not help in resolving this discrepancy.

In Figures IV.5c and IV.5c' we plot the form factors calculated with the M3 multipole quenched to 60% of the free-nucleon values and the rms radii of the valence orbit reduced by 5% from those required to fit the rms charge radii in the respective model for the single-nucleon wave functions. With these reductions, enhancements of the form factor are obtained at high-q values. Reduction of the rms radius of the valence orbit also has small effects in the region of small-q values. Best overall agreement between theory and experiment is obtained with the 0.6 quenching of the g factors for the M3 multipole and the smaller radial size parameters.

It was found in studies of beta-decay (Ref 56) that the spin g factor of the Gammow-Teller matrix elements should be quenched 80% from the free-nucleon value have explored the

Figure IV.5. Form factor for magnetic elastic electron scattering for ^{17}O. The single-nucleon radial wave functions used here are those of the HO potential of $b = b_{rms}$ (Figure IV.5a) and of the WS potential discused in Section II.3 (Figure IV.5a'). Free-space values for the neutron-g factors are used in both calculations. The corresponding calculations with quenching the g factor of the M3 contributions to 60% are shown in Figure IV.5b and Figure IV.b'. Figure IV.5c and Figure IV.5c' are the same as Figure IV.5b and IV.5b' except that the rms radius of the valence orbit is reduced by 5%. The same conventions are used for the different multipoles as in Figure IV.2. The data are taken from Ref 50 (circles).

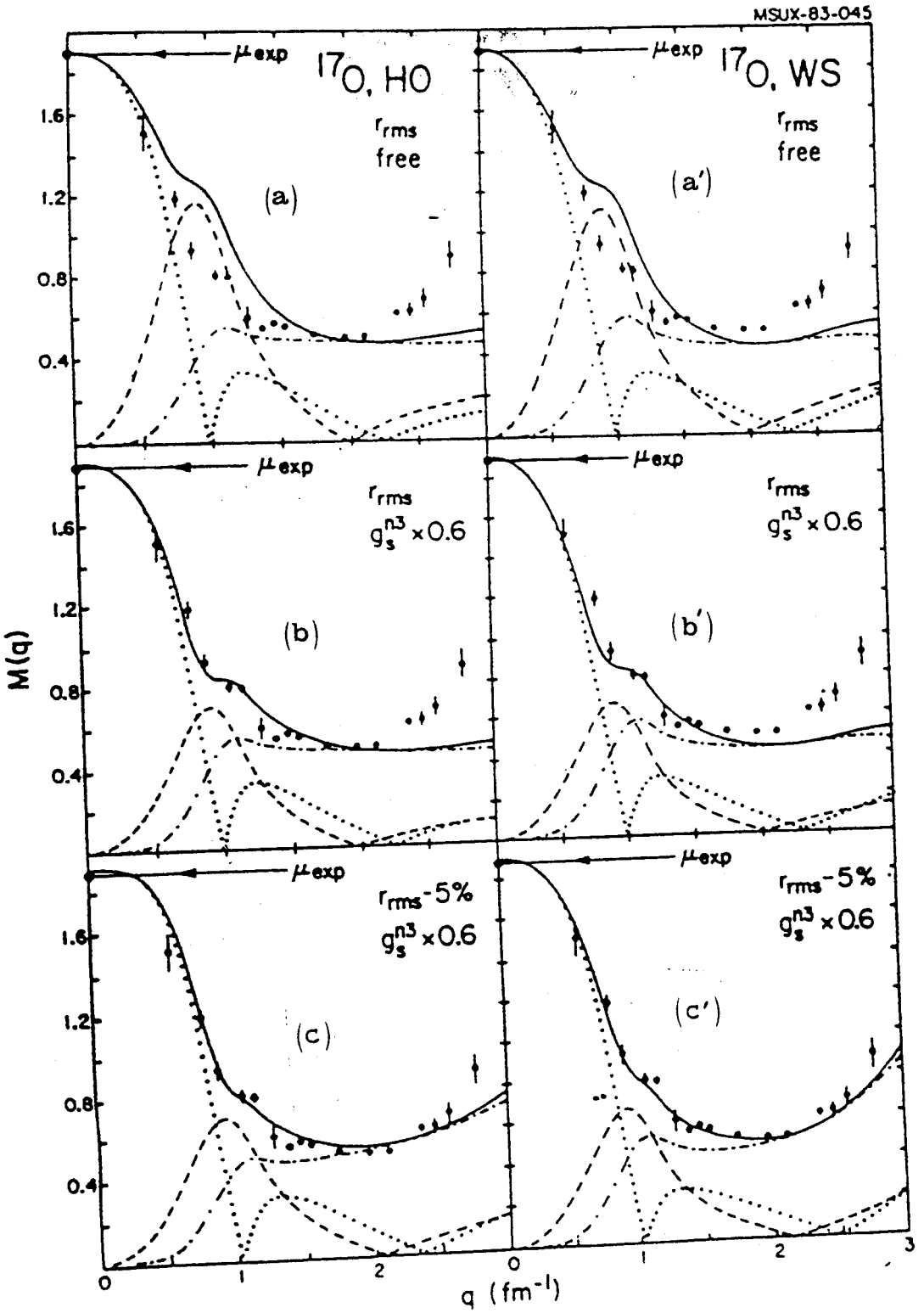
MSUX-83-045
μexp
17O, HO
rrms
free
(a)
μexp
17O, WS
rrms
free
(a')
μexp
rrms
gs n3 ×0.6
(b)
μexp
rrms
gs n3 ×0.6
(b')
μexp
rrms-5%
gs n3 ×0.6
(c)
μexp
rrms-5%
gs n3 ×0.6
(c')
M(q)
q (fm-1)
0.4
0.8
1.2
1.6
0
1
2
3

Figure IV.5

Figure IV.6. Form factors for the magnetic elastic scattering of ^{17}O. The conentions of the presentation are the same as given in the caption of Figure IV.5c' except effective g factors for the M1 contributions are used ($g_s^n(\text{eff}) = 0.8 \times g_s^n$, $g_\ell^n(\text{eff}) = g_\ell^n - .182$).

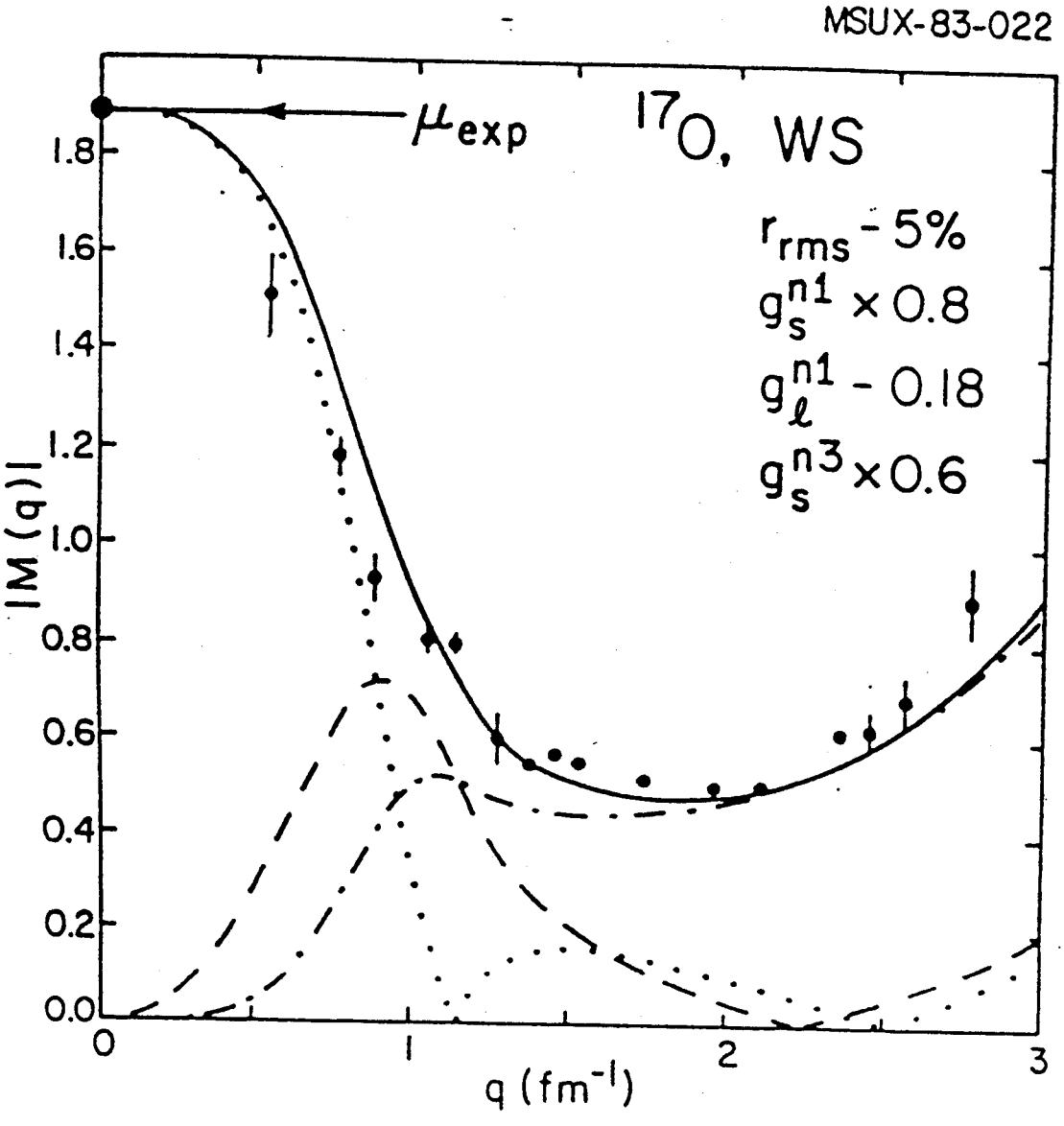
MSUX-83-022
μ_{exp}
^{17}O, WS
r_{rms} - 5%
$g_s^{n1} \times 0.8$
g_ℓ^{n1} - 0.18
$g_s^{n3} \times 0.6$
|M(q)|
q (fm^{-1})
0.0
0.2
0.4
0.6
0.8
1.0
1.2
1.4
1.6
1.8
0
1
2
3

Figure IV.6

consequences of imposing this same quenching upon the magnetic dipole g_s . With this effective g_s for the M1 multipole, the measured magnetic dipole moment cannot be reproduced without also reducing g_ℓ . In Figure IV.6, we show the form factor calculated with the same WS radial wave functions that used in Figure IV.5c'. Effective g factors for the M1 multipole [g_s^n(eff)= 0.8xg_s^n, g_ℓ^n(eff)= g_ℓ^n-.182] are used, which exactly reproduce the dipole magnetic moment. It is seen that even with the magnetic dipole moment reproduced exactly, the agreement with the form factor data at small momentum transfer data is not as good as was obtained with the free-space M1 g factors, (Figure IV.5c').

No major differences appear between the HO and the WS potentials in describing the data except in the region of high-q values, where the WS potential gives better agreement with the experimental data than the HO potential (Figure IV.5c' and IV.5c).

IV.5 Magnetic elastic scattering from ^{27}Al

In the single-particle model, ^{28}Si is considered as a closed shell, and ^{27}Al as one proton hole in the $d_{5/2}$ orbit. The form factor calculated with this model is shown in Figure IV.7a using the HO radial wave functions with the value of the "b" parameter fixed to reproduce the rms charge radius. This model overestimates the magnetic dipole moment

Figure IV.7. Form factors for magnetic elastic electron scattering for ^{27}Al. Calculations with the HO potential of b= b_{rms}, assuming only one proton hole in the $d_{5/2}$ orbit are shown in Figure IV.7a. The configuration-mixing contributions of the HO potential of $b=b_{rms}$ and of b reduced 9% from b_{rms} are shown in Figure IV.7b and Figure IV.7c respectively. Free-nucleon values for the g factor are used in these calculations. The effect of reducing b-value of the HO potential by 5% is shown in Figure IV.7d using different values for g factors for M1 contributions to get the exact magnetic dipole moments ($g_s^p(eff)= 0.8xg_s^p$, $g_\ell^p(eff)= g_\ell^p x1.25$). Figure IV.7e is the same as Figure IV.7d except the proton g factor of M3 contributions is quenched to 60% of the free-space value. Figure IV.9f is the same as Figure IV.7e except the wave functions of the WS potential whose valence orbits rms radius reduced 5% are used in place of the HO wave functions. The same conventions are used for the different multipoles as in Figure IV.2. The data are taken from Ref 40 (circles), Ref 41 (triangles) and Ref 42 (squares).

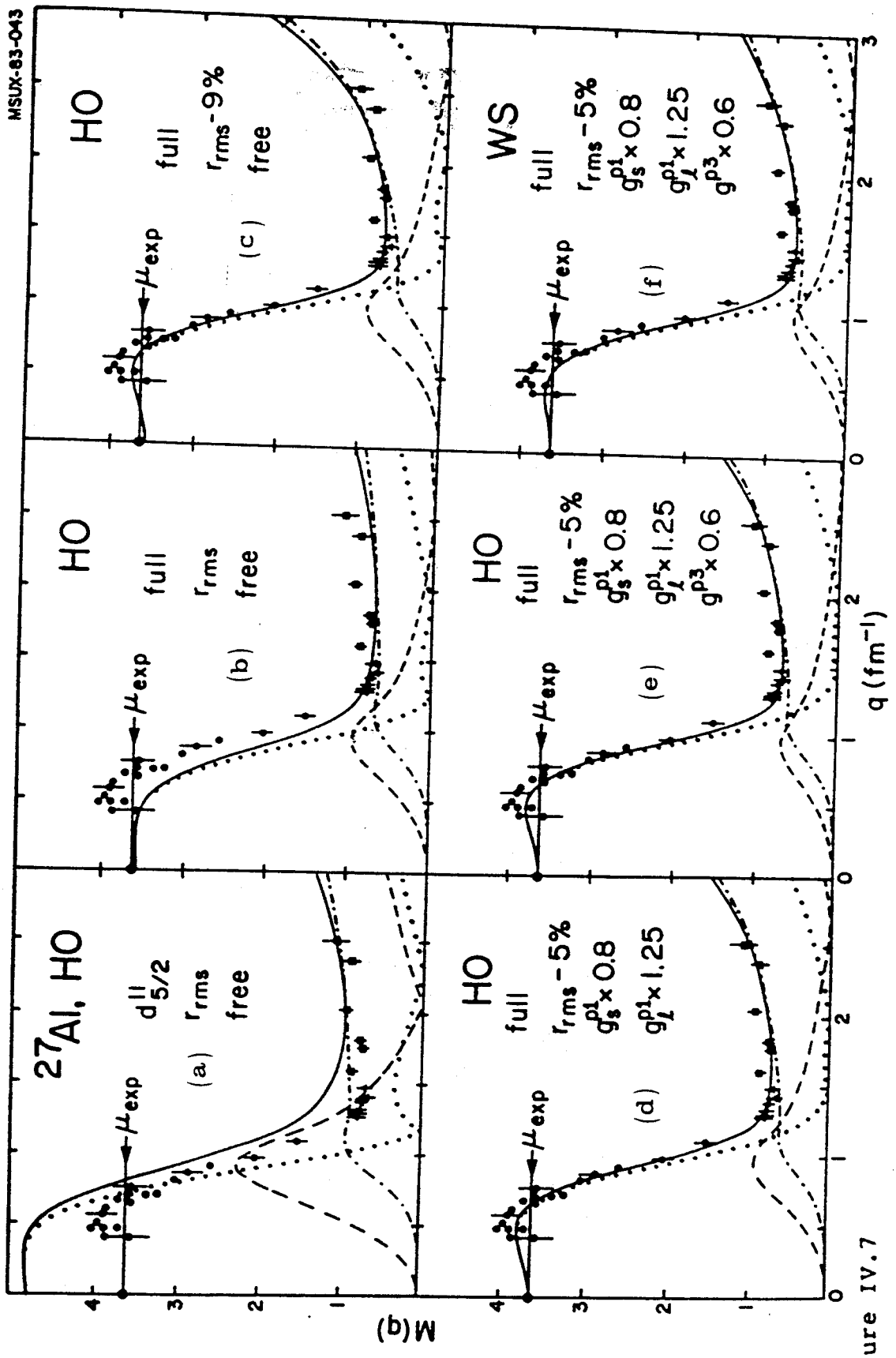
MSUX-83-043
^{27}Al, HO
$d^{II}_{5/2}$
(a) r_{rms} free
HO
full
r_{rms}
(b) free
HO
full
r_{rms}-9%
(c) free
HO
full
r_{rms}-5%
g_s^{p1}×0.8
g_l^{p1}×1.25
(d)
HO
full
r_{rms}-5%
g_s^{p1}×0.8
g_l^{p1}×1.25
g^{p3}×0.6
(e)
WS
full
r_{rms}-5%
g_s^{p1}×0.8
g_l^{p1}×1.25
g^{p3}×0.6
(f)
μ_{exp}
M(q)
q (fm^{-1})

Figure IV.7

by a factor of 1.2. The form factor data are also not explained satisfactorily. In Figure IV.7b, we present the form factor calculated with the multi-particle shell model using the HO radial wave functions whose b parameter is fixed to reproduce the rms charge radius. The configuration-mixing shell model reduces the M1 form factor in the region of small-q values by a factor of 1.4 from that of the single-particle picture. It similarly reduces the M3 form factor by a factor of 2. It yields good agreement with the measured magnetic dipole moment. Overall, the configuration-mixing shell model gives much better agreement with the experimental data than the single-particle model discussed above. However, in the region of low momentum transfer, the theoretical form factor falls below the values of the data. It would seem that the M1 multipole needs to be renormalized to get agreement with those data but this would tend to destroy the agreement with the measured magnetic dipole moment. The agreement with the low-q data can be improved by reducing the radial size of the valence nucleons from that required by the rms radius, as shown in Figure IV.7c.

In Figure IV.7d, we use effective M1 g factors ($(g_s^p(\text{eff}) = 0.8 \times g_s^p$, $g_\ell^p(\text{eff}) = g_\ell^p + 0.247$) to reproduce the measured magnetic dipole moment. We use HO radial wave functions of radial size 5% smaller than that required by the rms radius. An enhancement of the M1 form factor at the

region of low-q values is thereby obtained, such that the experimental data at this region of q are well decribed. Also, an enhancement of the M5 multipole is obtained at high-q values. The corresponding calculation in which the M3 form factor is quenched to 60% of the free-space value is shown in Figure IV.7e. In Figure IV.7f we show the calculation in which the quenching factors are the same as in Figure IV.7e, but in which single-nucleon wave functions of the WS potential whose valence nucleons radial size parameter reduced 5% from that required by the rms radius are used in place of the HO wave functions. From Figures IVe and IVf one can see that an overall agreement can be obtained between theory and the experimental data and that there are no significant differences between the results of HO and the WS potentials throughout the momentum-transfer regions studied.

Even though both protons and neutrons are active outside the closed ^{16}O core in the multi-particle configuration-mixing model of ^{27}Al, the magnetic scattering is dominated by protons (Figure IV.8a). The contribution of the neutrons is small (Figure IV.8b). The valence protons contribute to the magnetic scattering both through their spin and orbital angular momentum. In the region of high momentum transfer, only the spin part is important, the orbital part having very small effects, as shown in Figure IV.8c and IV.8d respectively.

Figure IV.8. Form factors for magnetic elastic electron scattering for ^{27}Al calculated with single-nucleon radial wave functions of HO potential of b= b_{rms} using free-space values for the g factors. Protons contributions only are shown in Figure IV.8a. The neutrons contributions only are shown in Figure IV.8b. Figure IV.8c and Figure IV.8d show the proton g_s and g contributions respectively. The same conventions are used for the different multipoles as in Figure IV.1. The data are taken from Ref 40 (circles), Ref 41 (triangles) and Ref 42 (squares).

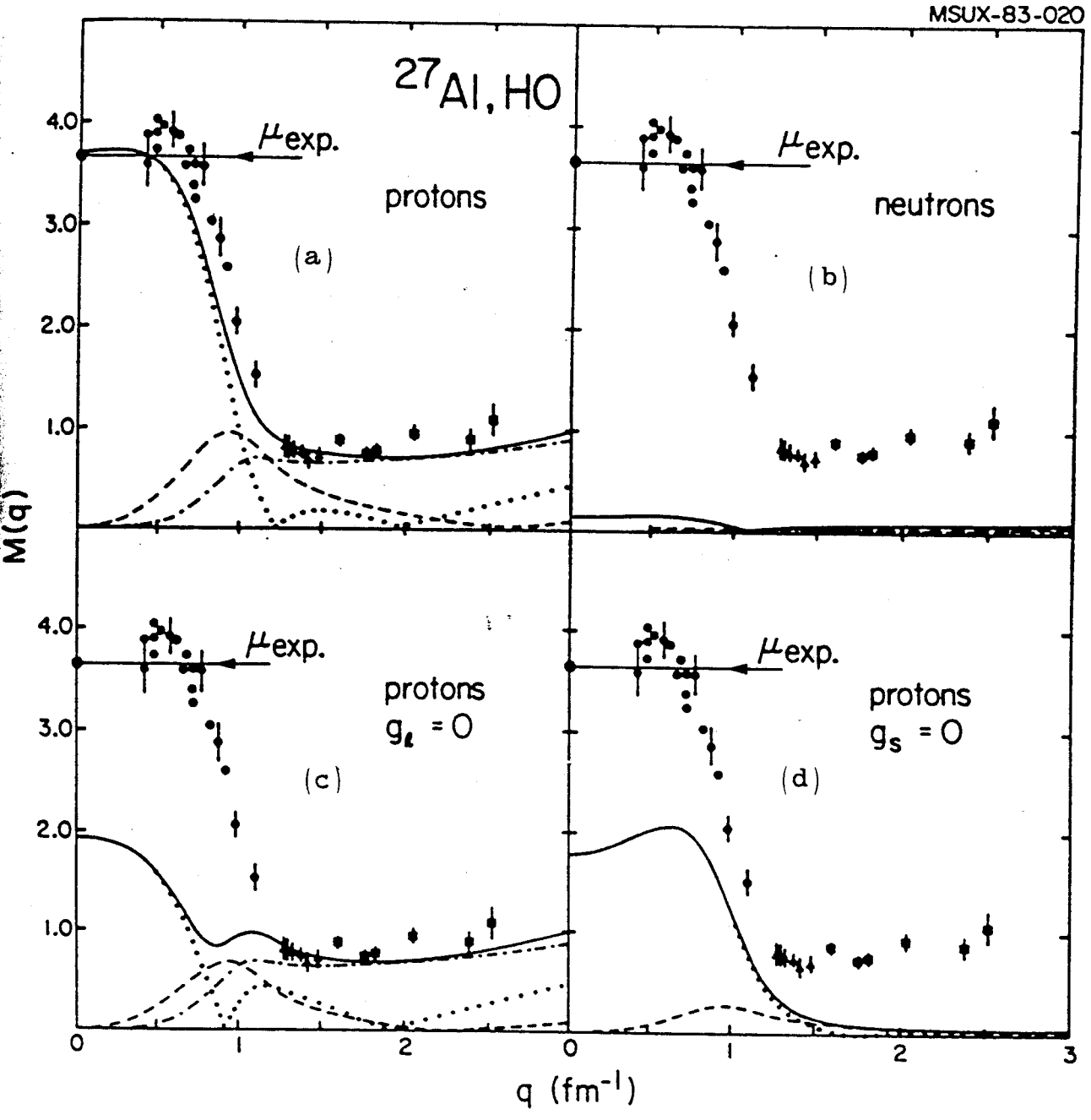
MSUX-83-020
^{27}Al, HO
μexp.
protons
(a)
μexp.
neutrons
(b)
μexp.
protons
g_ℓ = 0
(c)
μexp.
protons
g_s = 0
(d)
M(q)
q (fm^{-1})
4.0
3.0
2.0
1.0
0
1
2
3

Figure IV.8

IV.6. Magnetic elastic scattering from ^{39}K

In Figures IV.9 and IV.10 we show form factors for magnetic elastic electron scattering in ^{39}K. One proton hole in the $d_{5/2}$ orbit is responsible for the scattering. The single-nucleon shell model and the configuration-mixing shell model are identical in this case. The form factor calculated with HO radial wave functions of $b=b_{rms}$ and the free-proton value for the g factor is shown in Figure IV.9a. The calculated magnetic dipole moment disagrees with the measured value. In the region of medium-q values, where the M3 multipole is important, the predicted form factor is too large. This is the same behaviour noticed in ^{17}O at this region of q. This suggests that the need to quench the M3 strength is a common feature for the electron scattering process in this mass region.

Quenching the proton g factor of the M3 multipole to 60% of its free space value improves the agreement between theory and experiment at low and medium momentum transfers values (Figure IV.9b). At the region of high-q values ($q > 2$ fm^{-1}), the agreement is still poor and the data are increasing as function of q, while the theory varies smoothly and approximately steadily as function of q.

In Figure IV.10a we show the calculation which uses the same quenching factor as those used in Figure IV.9b, and a radial size parameter reduced 5% from that required to fit the rms radius. The agreement at high-q values is improved

Figure IV.9. Form factors for the magnetic elastic electron scattering for ^{39}K calculated with single-nucleon radial wave functions of the HO potential of $b=b_{rms}$. Free-space values for the g factors of the M1 and M3 contributions are shown in Figure IV.9a. Figure IV.9b is the same as Figure IV.9a except the proton g factor of the M3 contributions is quenched to 60% of the free-nucleon value. The orbital angular momentum contributions alone are shown in Figure IV.9c. Figure IV.9d shows only the spin contributions. The same conventions are used for the different multipoles as in Figure IV.2. The data are taken from Ref 53 (circles) and Ref 54 (squares).

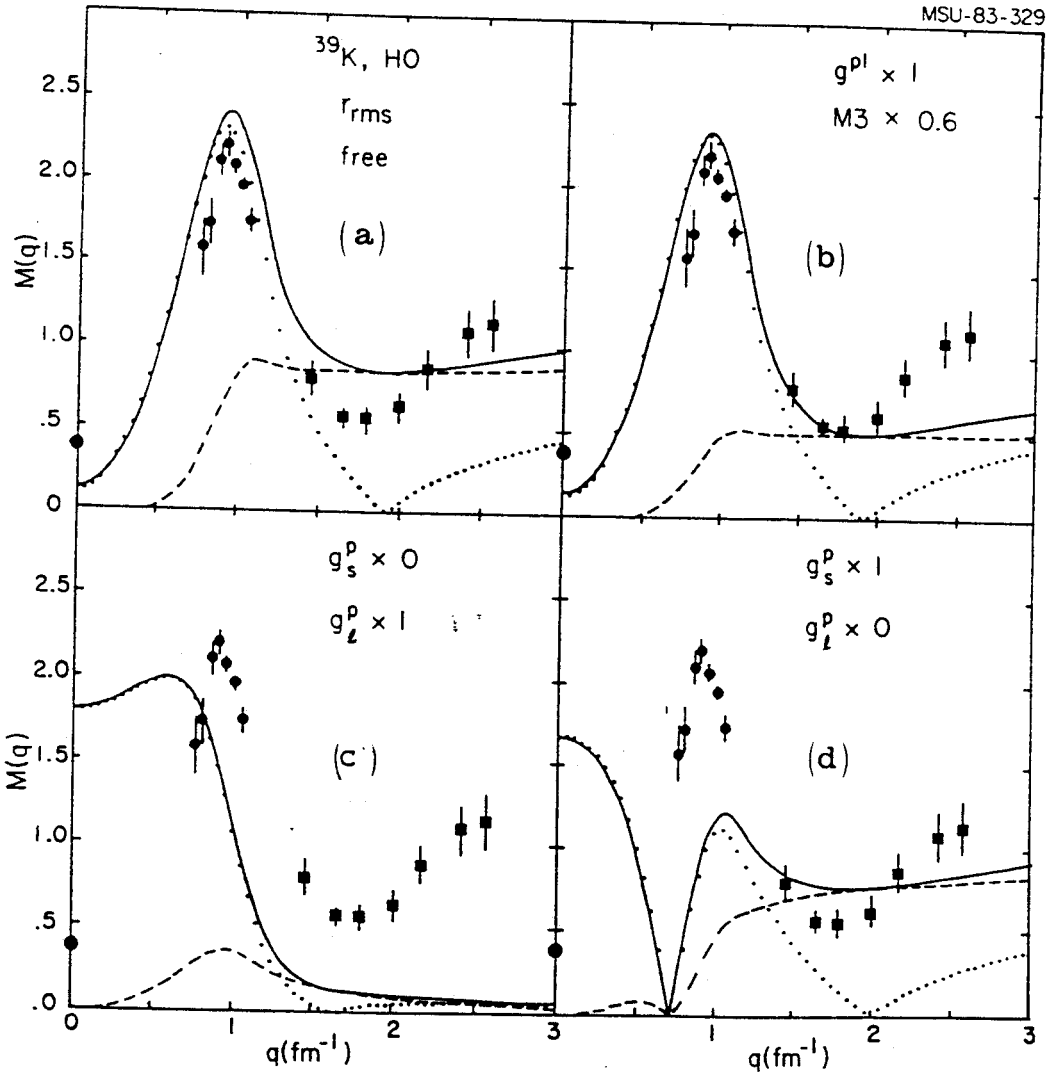
MSU-83-329
^{39}K, HO
r_{rms}
free
(a)
g^{pl} × 1
M3 × 0.6
(b)
g_s^p × 0
g_l^p × 1
(c)
g_s^p × 1
g_l^p × 0
(d)
M(q)
q(fm^{-1})
0
.5
1.0
1.5
2.0
2.5
3

Figure IV.9

by this reduction.

To reproduce the measured magnetic dipole moment, we choose an effective M1 orbital g factor for the proton of $g_\ell^{\,p}(\text{eff}) = g_\ell^{\,p} + 0.15$. These calculations are shown in Figure IV.10b. The M1 form factor is increased throughout the momentum transfer regions except at the high-q values. The fact that the high-q values do not change is because the orbital contribution is important only at low-q values as shown in Figure IV.9c. Figure IV.9d shows the spin contribution to the elastic magnetic scattering. The form factors decrease as a function of q at small-q values, while the high-q values are dominated by the spin part.

Giving the proton effective M1 g factors ($g_s^{\,p}(\text{eff}) = 0.8 \times g_s^{\,p}$) and $g_\ell^{\,p}(\text{eff}) = 0.962 \times g_\ell^{\,p}$) reproduces the measured magnetic dipole moment. These calculations are shown in Figure IV.10c and IV.10d with the HO and WS radial wave functions respectively. The radial size parameter of the valence proton is reduced 5% from that required by the rms radius. Much better agreement is obtained with these empirical values. The WS radial wave functions reproduce the high-q values better than the HO.

The octupole moment can be calculated using the formula

$$\Omega = -\frac{3}{70}(g_s - 4g_\ell)\,\langle r^2 \rangle, \qquad (105)$$

with $\langle r^2 \rangle^{1/2} = 3.606$ fm calculated with the WS radial wave functions. The binding energy of the valence orbit is fixed

Figure IV.10. Form factors for the magnetic elastic electron scattering for ^{39}K calculated by quenching the g factor of the M3 contributions to 60% of the free-space value. Figure IV.10a shows the calculations with free-nucleon values for the M1 contributions. Figure IV.10b shows the calculations with $g_\ell^p(\text{eff}) = g_\ell^p \times 1.15$ and $g_s^p(\text{eff}) = g_s^p(\text{free})$ for the M1 contributions. Fiure IV.10c are calculated with $g_s^p(\text{eff}) = 0.8 \times g_s^p$ and $g_\ell^p(\text{eff}) = 0.962 g_\ell^p$ for the M1 contributions. Figure IV.10d is the same as Figure IV.10c but usig the WS potential whose valence orbits rms reduced 5%. The same conventions are used for the different multipoles as in Figure IV.2. See caption of Figure IV.9 for the data.

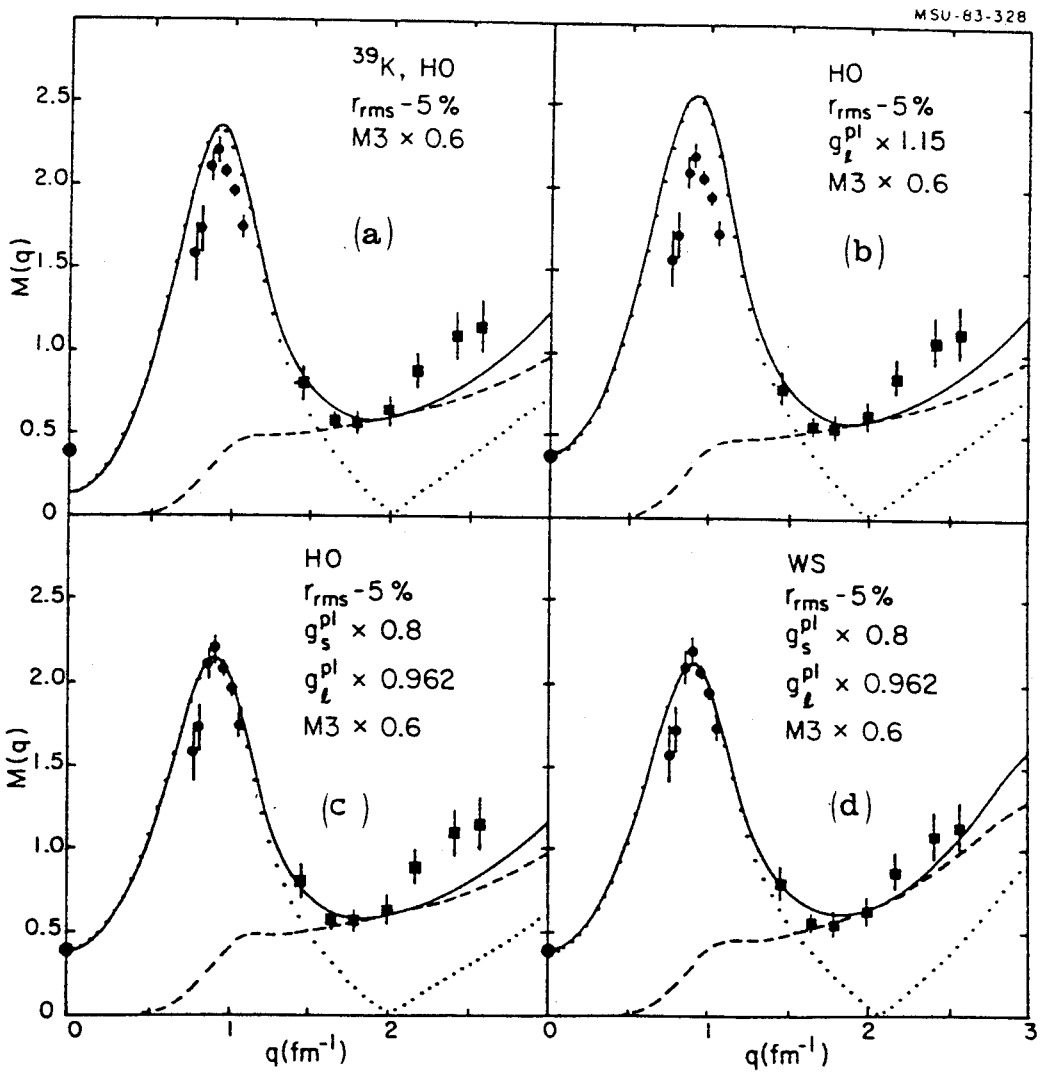
MSU-83-328
^{39}K, HO
r_{rms} - 5 %
M3 × 0.6
(a)
HO
r_{rms} - 5 %
g_ℓ^{pl} × 1.15
M3 × 0.6
(b)
HO
r_{rms} - 5 %
g_s^{pl} × 0.8
g_ℓ^{pl} × 0.962
M3 × 0.6
(c)
WS
r_{rms} - 5 %
g_s^{pl} × 0.8
g_ℓ^{pl} × 0.962
M3 × 0.6
(d)
M(q)
q(fm^{-1})

Figure IV.10

to be 8.329 MeV. According to this formula, the single-particle moment is found to be -0.88 μ_N fm^2. The value with quenching M3 to 60% of the free-nucleon value (g_s(eff)=0.6 g_s and g_ℓ (eff)=0.6 g_ℓ) is found to be -0.48 μ_N fm^2. The rms radius of the valence orbit in this case is reduced 5% from that required by the rms radius. Experimental data for the octupole moment of ^{39}K has been quoted by Lapikas (Ref 53) by extracting the data to q=0, which cannot be considered as an accurate value. Suzuki (Ref 46) has calculated the octupole moment by including the effects of first order core polarization, pair currents, one-pion exchange currents and isobar currents due to π - and ρ -meson exchanges corrections. He obtains the value -1.454 μ_N fm^2.

IV.7. Magnetic elastic scattering from p-shell nuclei

In the p-shell region we study the nuclei ^{6}Li, ^{7}Li, ^{9}Be, ^{10}B, ^{11}B, ^{13}C, ^{14}N, and ^{15}N . The calculations for ^{6}Li and ^{14}N are presented in Figure IV.11, those for ^{7}Li and ^{9}Be are presented in Figure IV.12, those for ^{10}B and ^{11}B are presented in Figure IV.13 and those for ^{13}C, and ^{15}N are presented in Figures IV.14. The lines denoted by crosses represent the calculations with the single-particle model. The solid lines and the lines denoted by plusses represent the calculations with a new empirical Hamiltonian (Ref 18) and the Cohen-Kurath interaction (Ref 19), respectively, with

Figure IV.11. Form factors for the magnetic elastic electron scattering for ^{6}Li and ^{14}N calculated with two different wave functions, MSU wave functions (solid lines) and the Cohen-Kurath wave functions (plus signs) using the HO potentials of $b=b_{rms}$. The data for ^{6}Li are taken from Ref 57(circles), Ref 58 (squares) and Ref 59 (triangles), and for ^{14}N are taken from Ref 58 (squares)), and Ref 60 (circles).

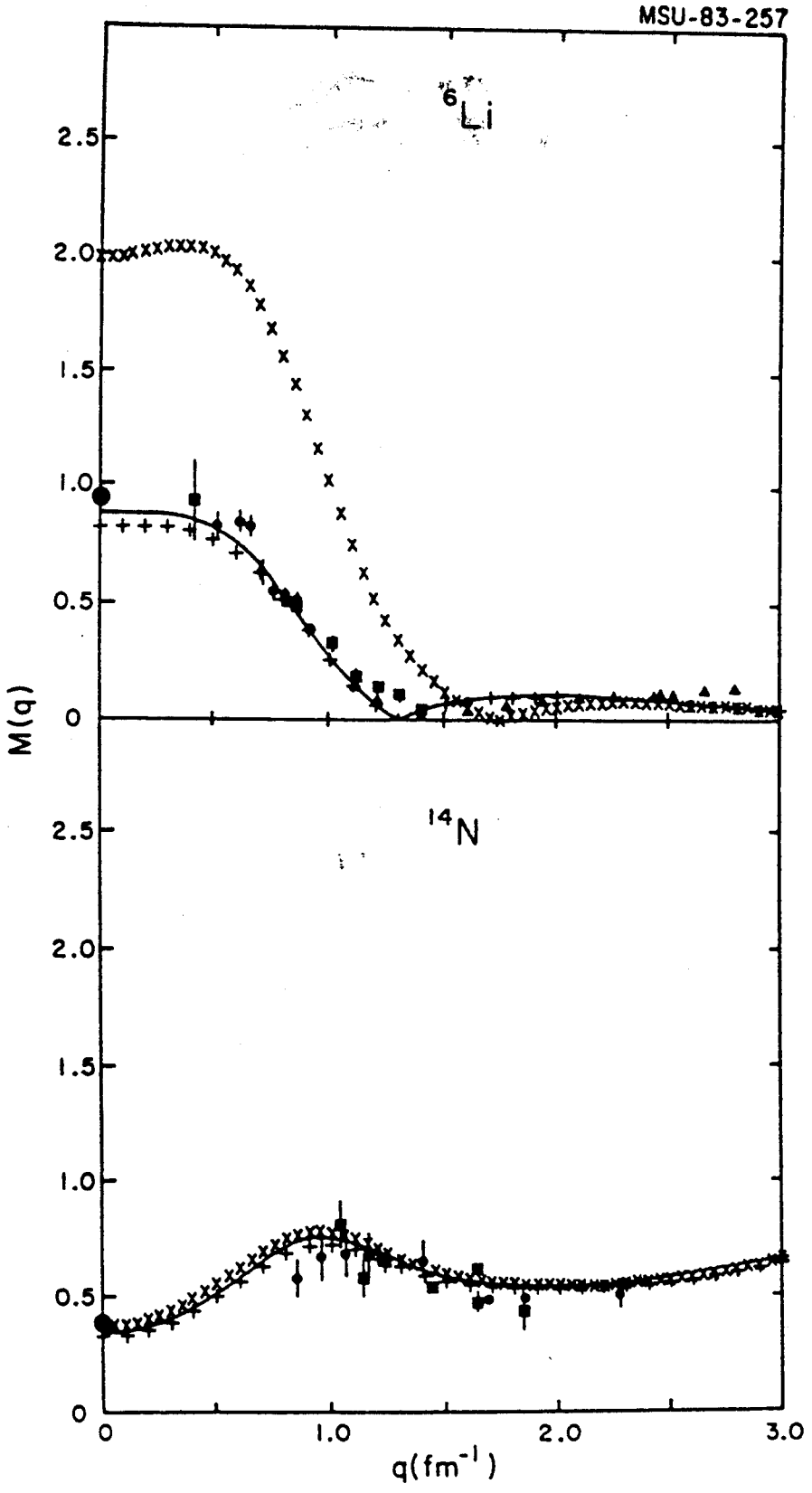

Figure IV.11

Figure IV.12. Form factors for the magnetic elastic scattering of ^{7}Li and ^{9}Be. The conventions of the presentation are the same as given in the caption of Figure IV.11. The decomposition of the multipoles calculated with the MSU wave functions are M1 (dotted lines) and M3 (dashed lines). Free-nucleon values are used here for the g factors. The data for ^{7}Li are taken from Ref 61 (circles) and Ref 62 (traingles), for ^{9}Be are taken from Ref 63 (circles), Ref 64 and Ref 58 (squares).

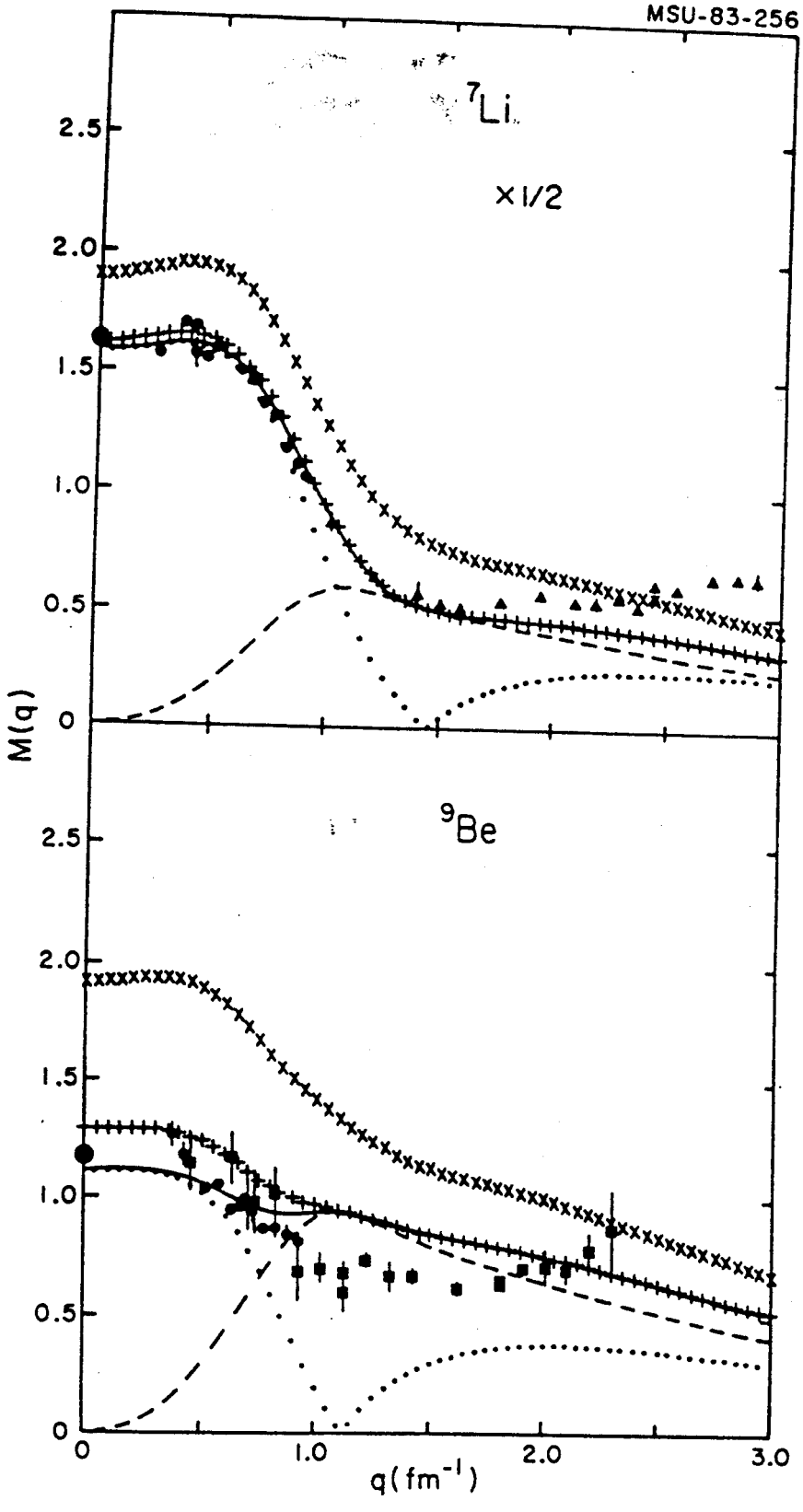

Figure IV.12

Figure IV.13. Form factors for the magnetic elastic scattering of ^{10}B and ^{11}B. The conventions of the presentation are the same as given in the caption of Figure IV.12. The data are taken from Ref 58 (squares) and Ref 57 (circles).

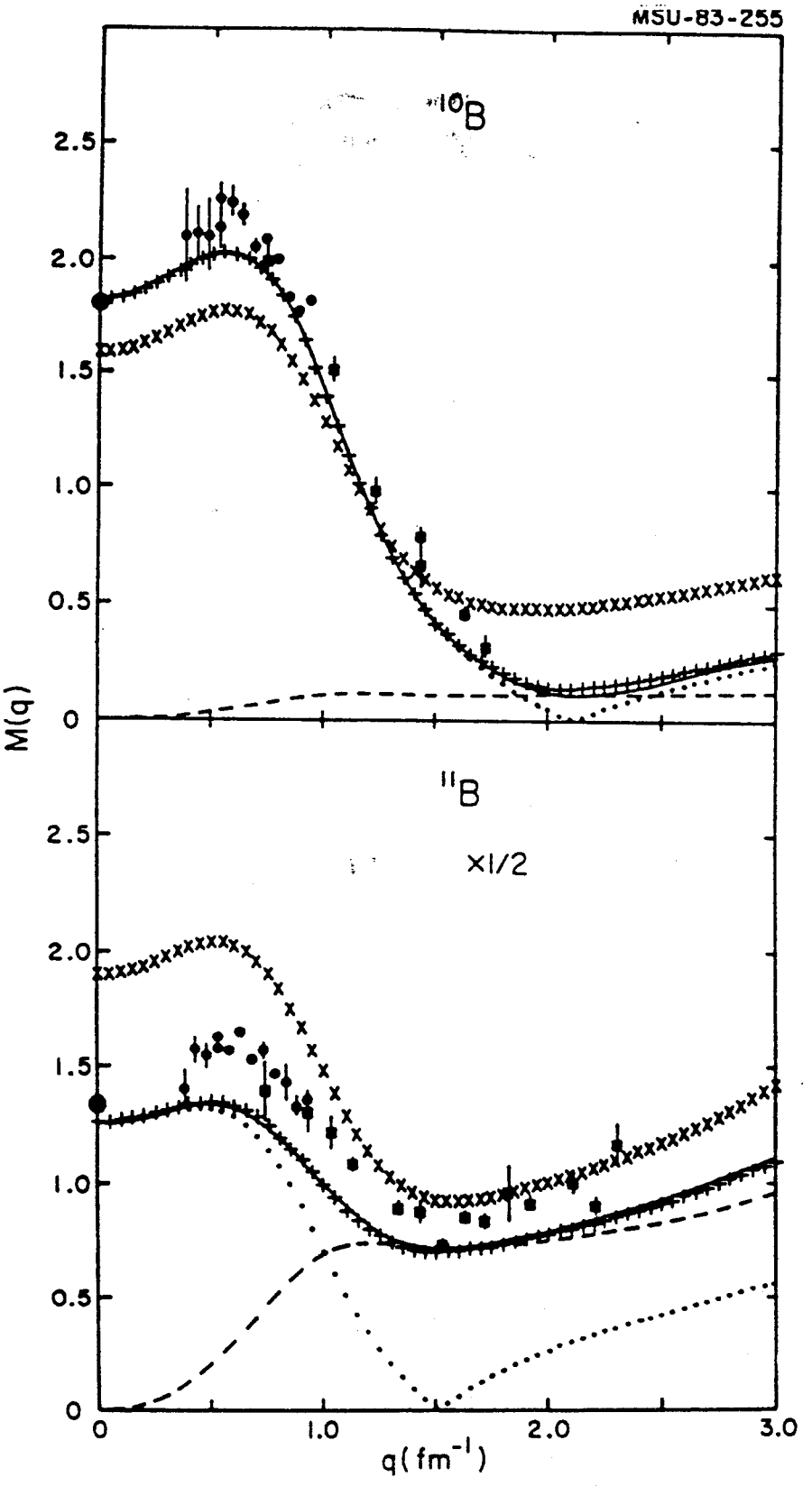

Figure IV.13

Figure IV.14. Form factors for the magnetic elastic scattering of ^{13}C and ^{15}N. The conventions of the presentation are the same as given in the caption of Figure IV.12. The data for ^{13}C are taken from Ref 63 (circles) and Ref 65 (triangles), and for ^{15}N are taken from Ref 66 (squares)

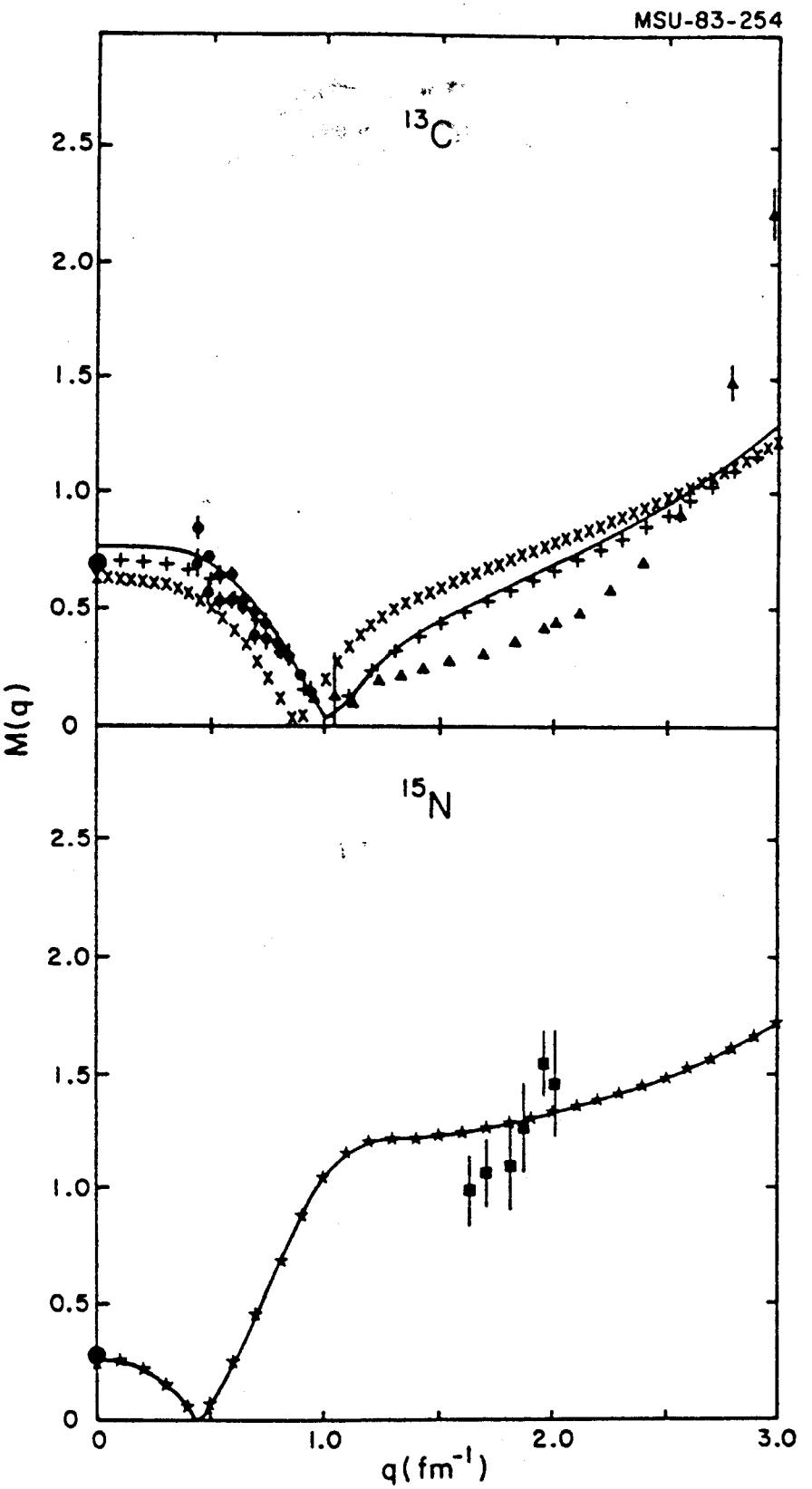

Figure IV.14

single-nucleon wave functions of HO potentials of b= b_{rms} and free-nucleon g factors. Good agreement is obtained for those nuclei where the M1 is the only multipole which contributes to the scattering. In the case of ^{9}Be, the M3 multipole is overestimated and needs to be quenched to describe the data in this region. The behaviour of the data at large-q values is the same as in sd-shell nuclei; normaly they increase as a function of q. To get a better reproduction of these data with theory, the rms radius of the valence nucleons must be reduced. The reduction of the rms radius might help also in ^{7}Li, ^{10}B and ^{11}B, where the behaviour is almost the same as in ^{27}Al, normaly the calculated form factors at low-q values are lower than the data.

IV.8. Conclusions

From these comparisons, we conclude that the configuration-mixing shell model succeeds in describing the magnetic elastic scattering data if we allow for small modifications to the free-space forms of the magnetic operators. We use two different types of single-particle radial wave functions, obtained from the HO and WS potentials. No major differences between these two potentials appear in describing the data except in the region of high momentum transfers. There the WS potential gives better agreement with the experimental data than the HO potential in ^{17}O (Figure IV.5c and IV.5c') and ^{39}K

(Figure IV.10c and Figure IV.10d). For those nuclei in which higher multipoles contribute to the scattering, the high-momentum-transfer data are not be described by these two potentials when the valence nucleons have a radial size determined by the rms radius. Reduction of the radial parameters by 5% seems to resolve the discrepancy at high momentum transfers for these nuclei. Also in some cases the lower multipoles are improved by this reduction, as in ^{27}Al, where the calculated peak at lower momentum transfer falls lower than the data when the radial parameter of the valence nucleons determined by the rms radius. For those nuclei in which M1 is the only multipole which contributes to the scattering, the radial size parameter determined by the rms radius seems to describe the data at high-q values without any reduction in the radius. The M3 contributions are overestimated in almost all instances. This suggests that the core-polarization effects cannot be ignored and can be taken into account by giving the nucleon an M3 effective g-factor less than its free value.

Table IV.1. Calculated one-body transition density matrix elements for the ground state of stable sd-shell nuclei for the wave functions of Ref 17.

		OBDM(i,f,L,j,j',ΔT)								
$A;J^{\pi}$	$2j-2j'$ =	5-5	5-1	5-3	1-1	1-5	1-3	3-5	3-1	3-3
	$2\Delta T$									
$17;5/2^+$										
L=1,3,5	0	1.0000	0.0000	0.0000	0.0000	0.0000	0.0000	0.0000	0.0000	0.0000
	2	1.0000	0.0000	0.0000	0.0000	0.0000	0.0000	0.0000	0.0000	0.0000
$19,1/2^+$										
L=1	0	0.1228	0.0000	-0.1217	0.4451	0.0000	0.0120	0.1217	-0.0120	-0.0543
	2	-0.2411	0.0000	0.1055	-0.4078	0.0000	0.0128	-0.1055	-0.0128	0.0121
$21;3/2^+$										
L=1	0	0.5141	0.0000	-0.0812	-0.1247	0.0000	0.0088	0.0812	-0.0088	0.0776
	2	0.3587	0.0000	-0.1003	-0.0690	0.0000	0.0091	0.1003	-0.0091	0.0256
L=3	0	-0.6270	0.0821	0.0687	0.0000	0.0821	0.0000	-0.0687	0.0000	0.0261
	2	-0.5474	0.0508	0.1020	0.0000	0.0508	0.0000	-0.1020	0.0000	0.0452
$23;3/2^+$										
L=1	0	0.4985	0.0000	-0.0578	-0.1076	0.0000	0.0172	0.0578	-0.0172	0.1014
	2	-0.2917	0.0000	0.0994	0.0969	0.0000	-0.0725	-0.0994	0.0725	-0.0308
L=3	0	-0.5268	0.0429	0.0559	0.0000	0.0429	0.0000	-0.0559	0.0000	0.0595
	2	0.5383	-0.0571	-0.0816	0.0000	-0.0571	0.0000	0.0816	0.0000	-0.0853
$25;5/2^+$										
L=1	0	0.9662	0.0000	0.0778	0.0321	0.0000	-0.0236	-0.0778	0.0236	0.0531
	2	0.7005	0.0000	0.0319	0.0448	0.0000	0.0279	-0.0319	-0.0279	-0.0347
L=3	0	0.4424	-0.0645	0.0281	0.0000	-0.0645	0.0000	-0.0281	-0.0000	0.0091
	2	0.2056	-0.0248	-0.0144	0.0000	-0.0248	0.0000	0.0144	0.0000	-0.0073
L=5	0	0.6792	0.0000	0.0000	0.0000	0.0000	0.0000	0.0000	0.0000	0.0000
	2	0.6366	0.0000	0.0000	0.0000	0.0000	0.0000	0.0000	0.0000	0.0000
$27;5/2^+$										
L=1	0	0.9419	0.0000	0.1105	0.0964	0.0000	0.0084	-0.1105	-0.0084	0.0781

Table IV.1. (cont'd.)

	2	-0.6799	0.0000	-0.1113	-0.2015	0.0000	-0.0989	0.1113	0.0989	0.0273
L=3	0	0.6346	-0.1405	0.0358	0.0000	-0.1405	0.0000	-0.0358	0.0000	-0.0112
	2	-0.6095	0.1274	-0.0225	0.0000	0.1274	0.0000	0.0225	0.0000	0 .0413
L=5	0	0.7276	0.0000	0.0000	0.0000	0.0000	0.0000	0.0000	0.0000	0.0000
	2	-0.7195	0.0000	0.0000	0.0000	0.0000	0.0000	0.0000	0.0000	0.0000
$29;1/2^+$										
L=1	0	0.1153	0.0000	0.1966	0.5721	0.0000	-0.0249	-0.1966	0.0249	-0.0803
	2	0.1111	0.0000	0.1856	0.5529	0.0000	-0.0142	-0.1856	0.0142	-0.0875
31;1/2										
L=1	0	0.0882	0.0000	0.1817	0.6446	0.0000	-0.0127	-0.1817	0.0127	-0.0527
	2	-0.0507	0.0000	-0.1590	-0.5487	0.0000	0.0113	0.1590	-0.0113	0.1207
$33;3/2^+$										
L=1	0	0.0627	0.0000	-0.0409	-0.0190	0.0000	0.1051	0.0409	-0.1051	0.8887
	2	0.0032	0.0000	-0.1010	-0.0485	0.0000	0.0789	0.1010	-0.0789	0.7564
L=3	0	0.0010	0.0028	0.0826	0.0000	0.0028	0.0000	-0.0826	0.0000	0.8194
	2	-0.0363	0.0072	0.0325	0.0000	0.0072	0.0000	-0.0325	0.0000	0.7566
$35;3/2^+$										
L=1	0	0.0479	0.0000	-0.0602	-0.0095	0.0000	0.1182	0.0602	-0.1182	0.9135
	2	-0.0031	0.0000	0.0709	0.0169	0.0000	-0.0355	-0.0709	0.0355	-0.6858
L=3	0	-0.0038	0.0016	0.0639	0.0000	0.0016	0.0000	-0.0639	0.0000	0.8388
	2	0.0168	-0.0065	-0.0513	0.0000	-0.0065	0.0000	0.0513	0.0000	-0.6913
$37;3/2^+$										
L=1	0	0.0261	0.0000	0.0431	-0.0006	0.0000	-0.0157	-0.0431	0.0157	0.9513
	2	-0.0323	0.0000	0.0125	-0.0340	0.0000	-0.0760	-0.0125	0.0760	0.6413
L=3	0	0.0040	-0.0016	0.0047	0.0000	-0.0016	0.0000	-0.0047	0.0000	0.9216
	2	-0.0240	-0.0073	-0.0441	0.0000	-0.0073	0.0000	0.0441	0.0000	0.6672
$39;3/2^+$										
L=1	0	0.0000	0.0000	0.0000	0.0000	0.0000	0.0000	0.0000	0.0000	1.0000
	2	0.0000	0.0000	0.0000	0.0000	0.0000	0.0000	0.0000	0.0000	-1.0000
L=3	0	0.0000	0.0000	0.0000	0.0000	0.0000	0.0000	0.0000	0.0000	1.0000
	2	0.0000	0.0000	0.0000	0.0000	0.0000	0.0000	0.0000	0.0000	-1.0000

Table IV.2. Calculated one-body transition density matrix elements for the ground state of stable p-shell nuclei for the wave functions of Ref 18 and Ref 19.

			OBDM(i,f,L,j,j',ΔT)			
$A;J^{\pi}$	ref	2j-2j' = 3-3	3-1	1-3	1-1	
		$2\Delta T$				
$6;1^+$						
L=1	a	0	0.50116	-0.43568	0.43568	-0.17060
	b	0	0.51828	-0.31022	0.31022	-0.22473
$7;3/2^-$						
L=1	a	0	0.98732	-0.02161	0.02161	0.04009
		2	-0.29741	0.33561	-0.33561	0.26912
	b	0	0.98594	-0.01682	0.01682	0.04447
		2	-0.37212	0.30047	-0.30047	0.23792
L=3	a	0	0.63188	0.00000	0.00000	0.00000
		2	-0.65016	0.00000	0.00000	0.00000
	b	0	0.72854	0.00000	0.00000	0.00000
		2	-0.62924	0.00000	0.00000	0.00000
$9;3/2^-$						
L=1	a	0	0.97682	0.11030	-0.11030	0.07329
		2	0.63727	-0.03971	0.03971	-0.09598
	b	0	0.99265	0.07927	-0.07927	0.02325
		2	0.67171	-0.06522	0.06522	-0.08804
L=3	a	0	0.78341	0.00000	0.00000	0.00000
		2	0.73450	0.00000	0.00000	0.00000
	b	0	0.84834	0.00000	0.00000	0.00000
		2	0.75134	0.00000	0.00000	0.00000
$10;3^+$						
L=1	a	0	1.66784	0.14446	-0.14446	0.01732
	b	0	1.68331	0.18029	-0.18029	-0.03158
L=3	a	0	0.31373	0.00000	0.00000	0.00000

Table IV.2. (cont'd.)

	b	0	0.39980	0.00000	0.00000	0.00000
11;3/2$^-$						
L=1	a	0	0.99489	0.21692	-0.21692	0.01615
		2	-0.68575	-0.11247	0.11247	0.25977
	b	0	0.99985	0.22396	-0.22396	0.00047
		2	-0.70255	-0.11637	0.11637	0.23566
L=3	a	0	0.73701	0.00000	0.00000	0.00000
		2	-0.78990	0.00000	0.00000	0.00000
	b	0	0.78576	0.00000	0.00000	0.00000
		2	-0.75915	0.00000	0.00000	0.00000
13;1/2$^-$						
L=1	a	0	0.03275	0.03952	-0.03952	0.89645
		2	-0.11993	-0.03815	0.03815	0.81506
	b	0	0.01737	0.02962	-0.02962	0.94506
		2	-0.09112	-0.03091	0.03091	0.81325
14;1$^+$						
L=1	a	0	0.02502	0.09508	-0.09508	1.33510
	b	0	0.05497	0.15510	-0.15510	1.24037
15;1/2$^-$						
L=1	a	0	0.00000	0.00000	0.00000	1.00000
		2	0.00000	0.00000	0.00000	-1.00000
	b	0	0.00000	0.00000	0.00000	1.00000
		2	0.00000	0.00000	0.00000	-1.00000

a) Ref 18
b) Ref 19

Table IV.3. Experimentally determined rms charge radii of stable p-shell and odd-A, sd-shell-nuclei and the corresponding values calculated in the harmonic-oscillator model with length parameters b_{rms} and in the Woods-Saxon model.

NUCLEUS	rms(fm) exp	b_{rms}(fm)	Exp.Ref	rms(fm) HO	rms(fm) WS
^{6}Li	2.510(100)	1.880	a		
^{7}Li	2.350(100)	1.740	a		
^{9}Be	2.519(12)	1.763	b		
^{10}B	2.400(26)	1.611	c		
^{11}B	2.400(26)	1.611	c		
^{13}C	2.472(15)	1.628	d		
^{14}N	2.529(25)	1.645	e		
^{15}N	2.580(26)	1.678	b		
^{17}O	2.712(5)	1.763	f	2.716	2.692
^{19}F	2.898	1.833	g	2.903	2.855
^{21}Ne	(2.984)	1.845		2.989	2.961
^{23}Na	2.896(9)	1.810	g	2.992	3.034
^{25}Mg	3.003(11)	1.793	h	3.010	3.097
^{27}Al	3.058(5)	1.804	g	3.064	3.158
^{29}Si	3.122(15)	1.825	i	3.134	3.216
^{31}P	3.187(3)	1.848	g	3.197	3.271
^{33}S	(3.264)	1.881	g	3.274	3.321
^{35}Cl	3.351(16)	1.921	i	3.360	3.363
^{37}Cl	3.351(17)	1.921	j	3.359	3.349
^{39}K	3.437(2)	1.95	g	3.442	3.436

a) Ref 67

Table IV.3. (cont'd.)
b) Ref 68

c) Ref 69

d) Ref 70

e) Ref 71

f) Ref 72

g) Ref 73

h) Ref 37

i) Ref 74

j) Ref 75

Table IV.4. Measured and calculated magnetic dipole moments for p-shell and sd-shell nuclei.

NUCLEUS	J^{π}	(sd)[a] (μ_N)	(sd)[b] (μ_N)	Experiment[c,d] ($q \to 0$) (μ_N)
^{6}Li	1^+	0.878	0.824	0.822
^{7}Li	$3/2^-$	3.169	3.234	3.256
^{9}Be	$3/2^-$	-1.115	-1.289	-1.177
^{10}B	3^+	1.819	1.811	1.801
^{11}B	$3/2^-$	2.509	2.532	2.688
^{13}C	$1/2^-$	0.763	0.701	0.702
^{14}N	1^+	0.339	0.326	0.403
^{15}N	$1/2^-$	-0.264	-0.264	-0.283
^{17}O	$5/2^+$	-1.911		-1.893
^{19}F	$1/2^+$	2.911		2.628
^{21}Ne	$3/2^+$	-0.824		-0.662
^{23}Na	$3/2^+$	2.219		2.218
^{25}Mg	$5/2^+$	-0.908		-0.855
^{27}Al	$5/2^+$	3.584		3.642
^{29}Si	$1/2^+$	-0.501		-0.555
^{31}P	$1/2^+$	1.023		1.132
^{33}S	$3/2^+$	0.651		0.644
^{35}Cl	$3/2^+$	0.663		0.822
^{37}Cl	$3/2^+$	0.433		0.684
^{39}K	$3/2^+$	0.124		0.391

a) Calculated magnetic moments based on the complete p-shell and sd-shell space wave functions of Ref 17 Ref 18

Table IV.4. (cont'd.)
and the free-nucleon g factors.

b) Calculated magnetic moments based on the coplete p-shell space wave functions of Ref 19 and the "free-nucleon" g factors.

c) Ref 76 ,Ref 77 and Ref 78 for p-shell nuclei.

d) Ref 79, Ref 80, Ref 81, Ref 82 and Ref 12 for sd-shell nuclei.

CHAPTER V

ELECTROEXCITATION OF EVEN PARITY STATES OF ^{27}Al

V.1. Introduction

The nucleus ^{27}Al is one of the most interesting nuclei in the sd-shell because it represents a point at which the nuclear deformation changes from prolate (for ^{26}Mg) to oblate (for ^{28}Si) (Ref 12). The electroexcitation of ^{27}Al has been analyzed previously (Ref 83 and Ref 13) in terms of the full $0d_{5/2}$- $1s_{1/2}$- $0d_{3/2}$ space with the restriction of $J^{\pi} \geq 5/2^{+}$ levels, and with a truncated space in which at least 6 particles were restricted to the $0d_{5/2}$ shell. In this study we use the full $0d_{5/2}$-$1s_{1/2}$-$0d_{3/2}$ space for all states to obtain the eigenfunctions of a new empirical Hamiltonian (Ref 17). In Figure V.1, we show the measured ^{27}Al (e,e') spectrum taken from Ref 13 in comparison with the calculated spectrum. The experimental and theoretical energy levels are shown in Figure V.2. In this chapter, we compare the form factors for all the measured positive-parity states that have definite assignments of spin and parity.

Complete separations between the longitudinal and transverse form factors have been done only for those states of excitation energies $E_x \leq 3.0$ MeV. The calculated

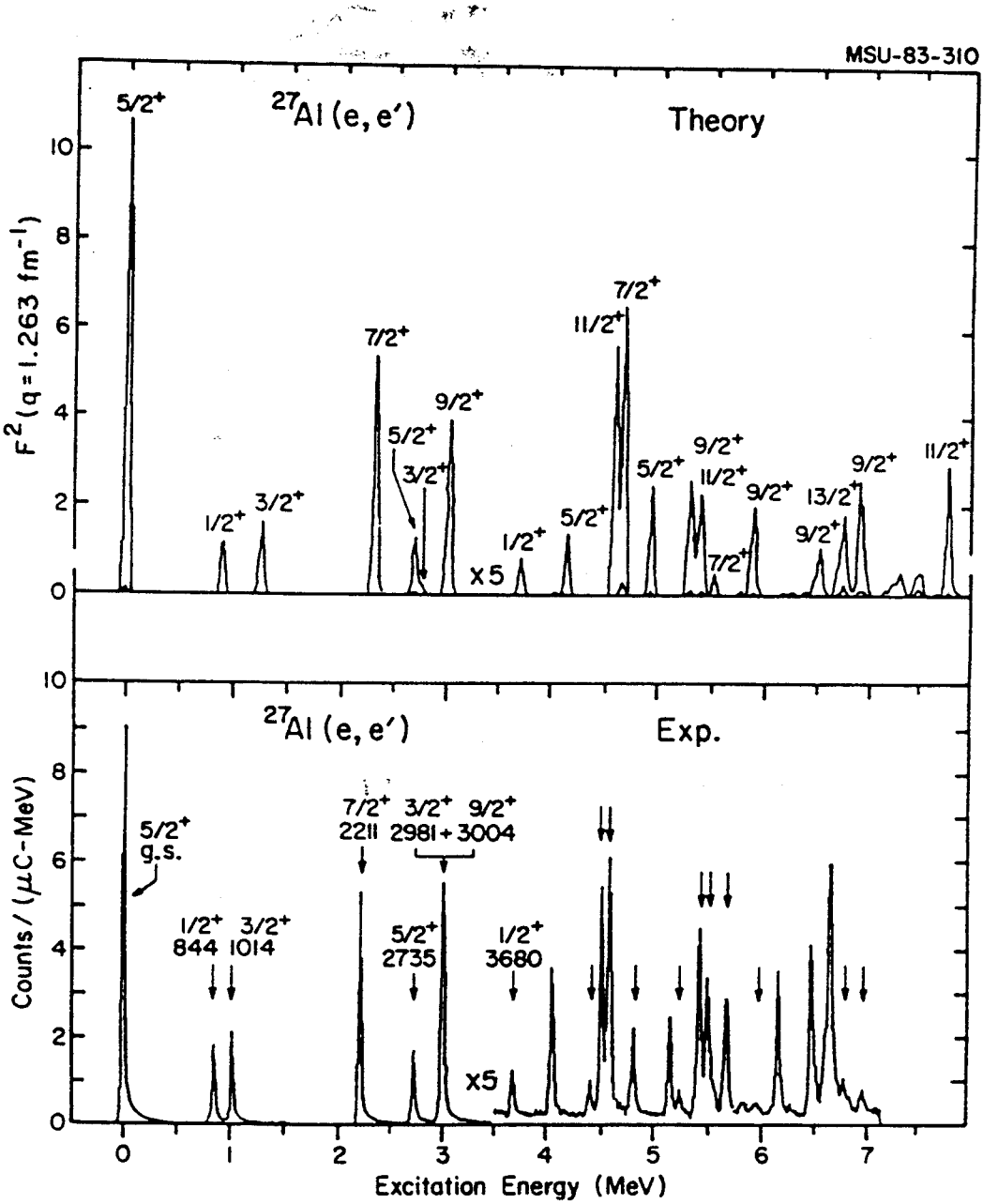

Figure V.1. Experimental spectrum of ^{27}Al (e,e') in comparison with the theoretical form factors of the positive-parity states calculated at the same angle and incident energy as the measured spectrum.

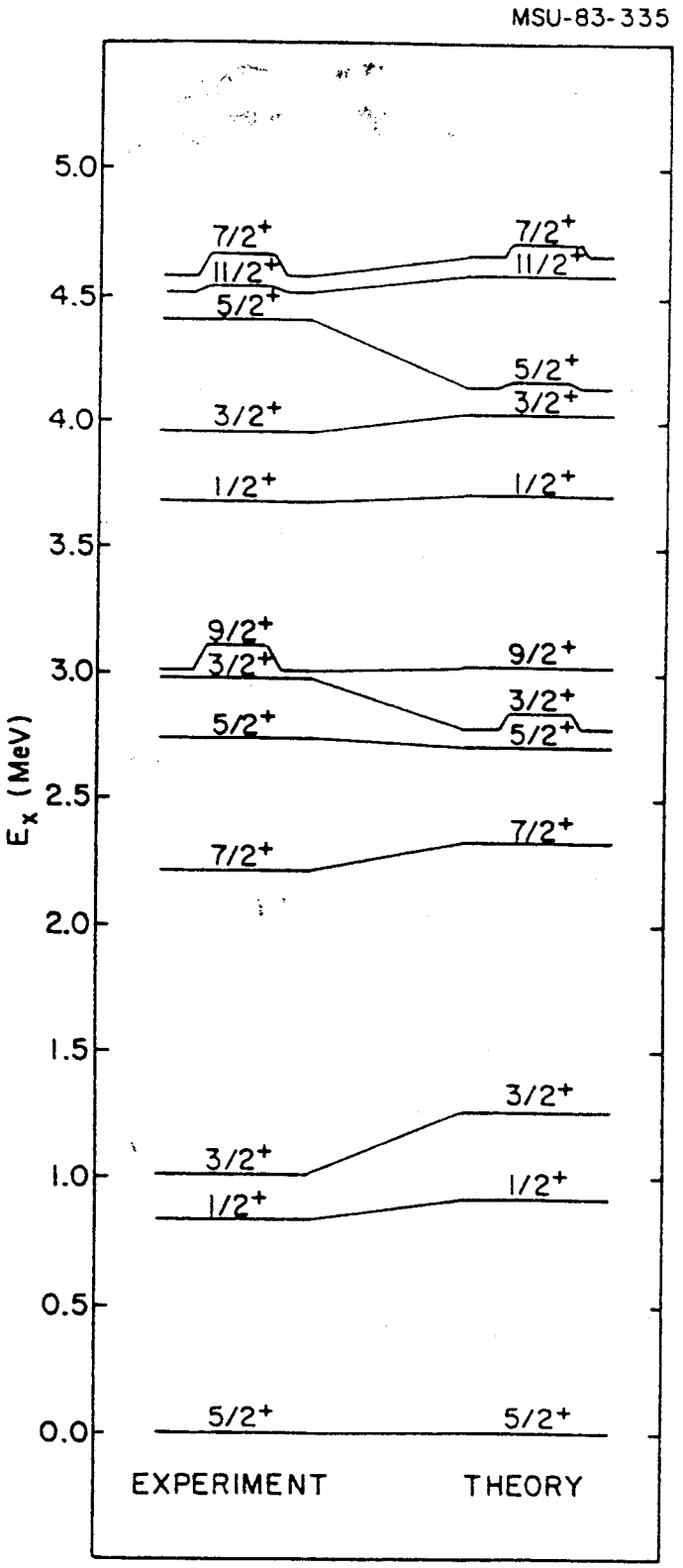

Figure V.2. Measured positive-parity energy levels of ^{27}Al in comparison with the shell-model calculations.

longitudinal form factors are compared with the experimental data for these states only. For higher-lying states, calculated transverse and total form factors are compared with the data.

V.2. Elastic scattering for the $5/2^+$ ground state

The measured elastic form factor for the $5/2^+$ ground state is shown in Figure V.3 in comparison with the DWBA calculations which incorporate single-nucleon wave functions of the HO potential with $b=b_{rms}$ (solid line) and WS potential (dashed line). The different multipoles that contribute to the elastic scattering are E0 (dotted line), E2 (plus signs) and E4 ("Y" signs). These multipoles are calculated with the HO potential of $b=b_{rms}$. The elastic form factor is dominated by E0 up to momentum transfer 2.3 fm^{-1} where E2 becomes more important. The E4 contribution is very small and has a negligible contribution to the scattering. In the region of small momentum transfers, the HO radial wave functions describe the scattering data very well up to the first diffraction minimum. Beyound that region, the HO results fall below the WS results. The latter fit the data very well in this region. This behaviour is similar to that noticed for other cases studied in the sd-shell region (Ref 33).

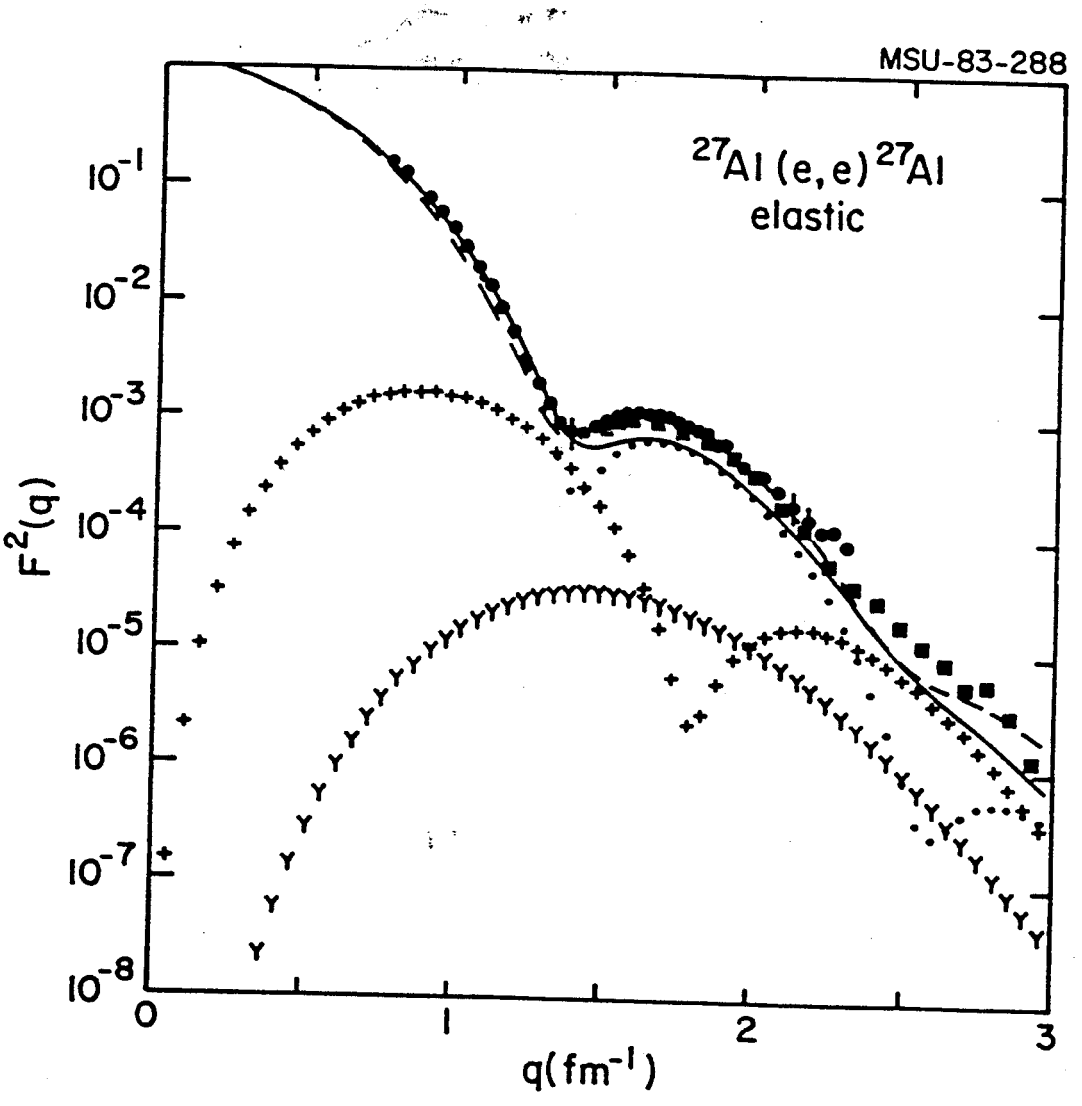

Figure V.3. DWBA elastic scattering form factor calculated with the single-nucleon wave functions of the HO potential of $b=b_{rms}$(solid line) and of the WS potential (dashed line). The different multipoles E0, E2 and E4 (dotted lines, plus and "Y" signs, respectively) are calculated with the single-nucleon wave functions of the HO potential of $b=b_{rms}$. The data are taken from Ref 42 (circles)-250 MeV, (squares)-500 MeV.

V.3. Inelastic scattering to the 0.844 MeV, $1/2_1^+$ state

The longitudinal E2 form factor M(q) for the inelastic scattering of the 0.844 MeV, $1/2_1^+$ state is shown in Figure V.4, where we compare two models for the core-polarization transition density, the valence model (dashed line) and the Tassie model (solid line). The low-q values favour the valence model.

Figure V.5 shows the form factor M(q) calculated with the HO potential of length parameter $b=b_{rms}$ (solid line) and the WS potential (dashed line) using the Tassie model for the core-polarization transition density. The measured B(E2) value is reproduced reasonably well but the scattering data are higher than the theory in the region of momentum transfer $1< q^2 < 4$ fm^{-2}. No differences between these two potentials appear in describing the data except at the photon point, where the measured B(E2) value is reproduced better with the HO radial wave functions.

The transverse form factor is shown in Figure V.6 (dashed-dotted line) calculated with the HO radial wave functions of $b=b_{rms}$. In this Figure we show the different contributions from the spin and orbital parts. The different multipoles that contribute to the scattering are E2 (plus signs) and M3 (cross signs). The transverse form factor is dominated by the spin contribution. The orbital contribution is important only in the region of the diffraction minimum. The contributions of both multipoles are important in the

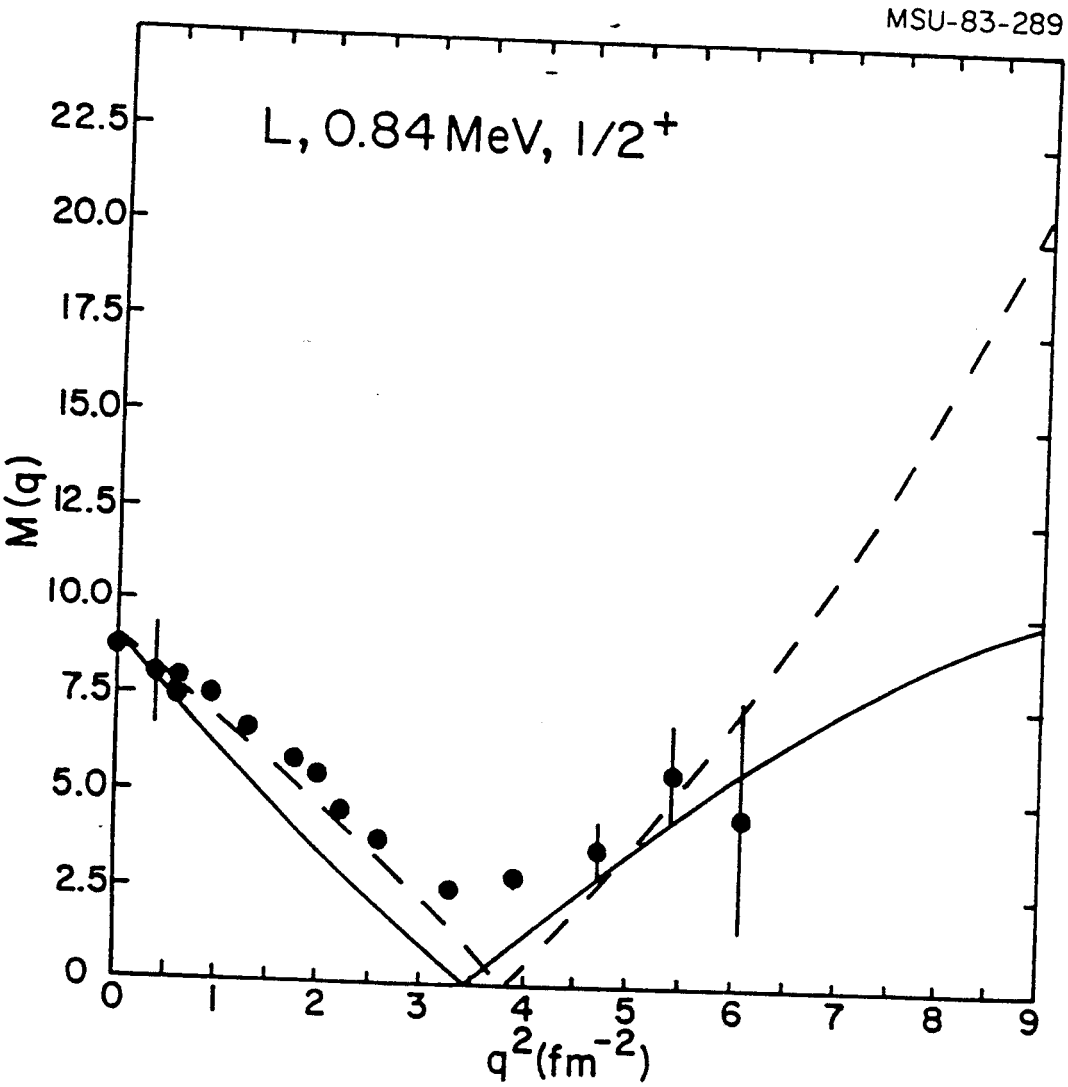

Figure V.4. Longitudinal E2 form factor M(q) for the $1/2_1^+$ state in ^{27}Al calculated with the single-nucleon wave functions of the HO potential combined with the Tassie and valence models (solid and dashed lines, respectively) The data are taken from Ref 13.

region of low-q values up to $q \approx 1.7$ fm^{-1}. Beyond that, the transverse form factor is dominated by the magnetic scattering. From the discussions of the magnetic elastic scattering in the previous chapter, we conclude that the M3 form factor needs to be quenched to get a reasonable explanation of the experimental data. The result of quenching the M3 form factor to 60% of the free-nucleon value is shown also in this Figure. Quenching the M3 form factor improves the agreement with the low-q data. At $q >$ 1.5 fm^{-1} the form factor is underestimated by a factor of 2.5. From here on in our discussions all the calculations are presented with the M3 form factor quenched to 60% of its free-space value.

In Figure V.7 we show the total form factor for the 0.844 MeV, $1/2_1^+$ state calculated at $\theta = 90^\circ$ by the solid line. The longitudinal contribution is shown by the dashed line. The dashed-dotted line shows the transverse form factor, including the kinematic factor $(1/2+\tan^2 \theta/2)$. In the region of low and medium momentum transfer the scattering is mostly longitudinal, while at the large momentum transfers, both longitudinal and transverse are important.

V.4. The 1.014 MeV, $3/2_1^+$ state

Form factors for the 1.014 MeV, $3/2_1^+$ state are shown in Figure V.8, calculated with the radial wave functions of the HO potential of $b=b_{rms}$. The longitudinal E2+ E4 form

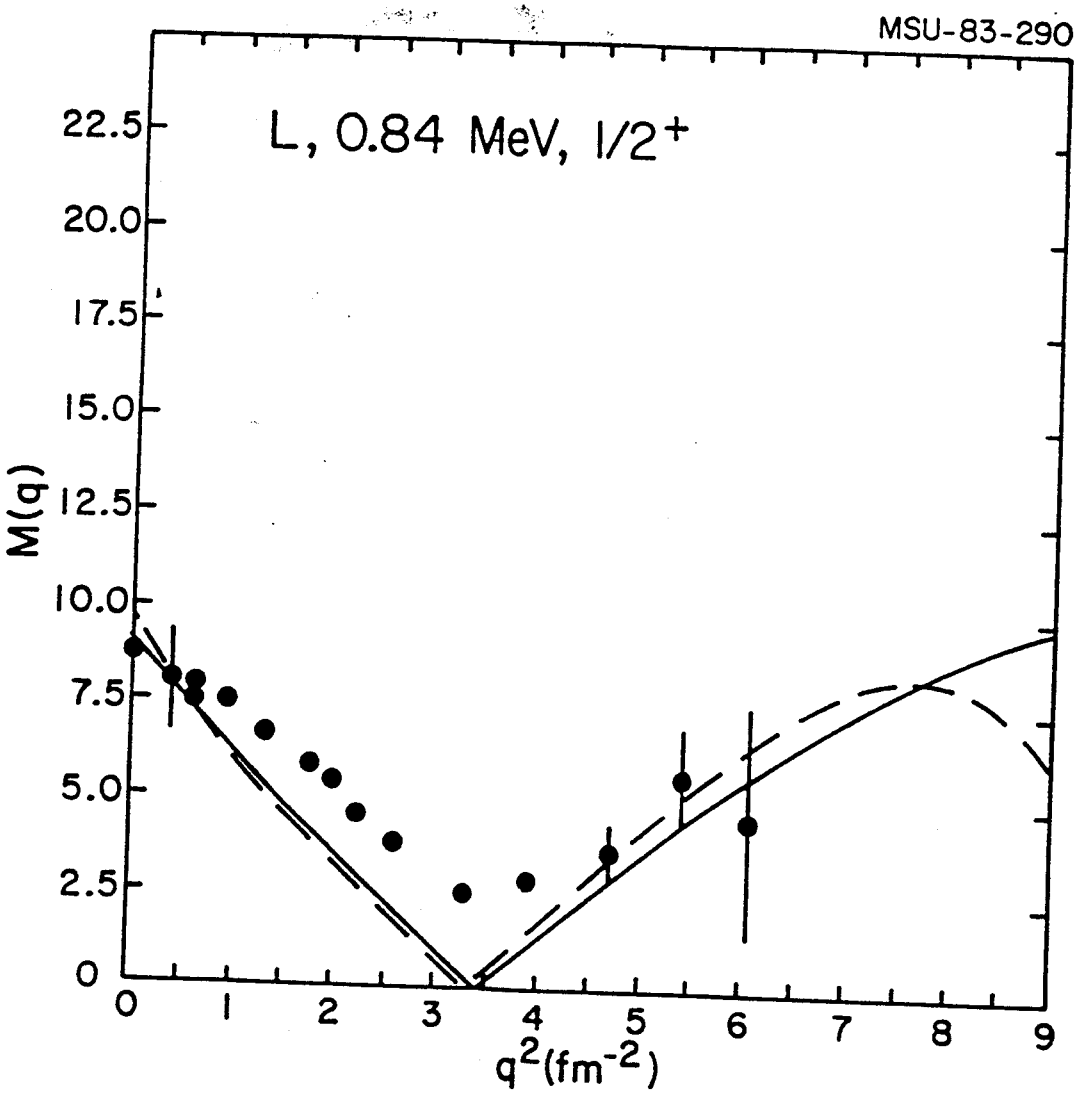

Figure V.5. Longitudinal E2 form factor M(q) for the $1/2_1^+$ state in ^{27}Al calculated with the Tassie model combined with single-nucleon wave functions of the HO potential of $b=b_{rms}$ (solid line) and of the WS potential (dashed line). The data are taken from Ref 13.

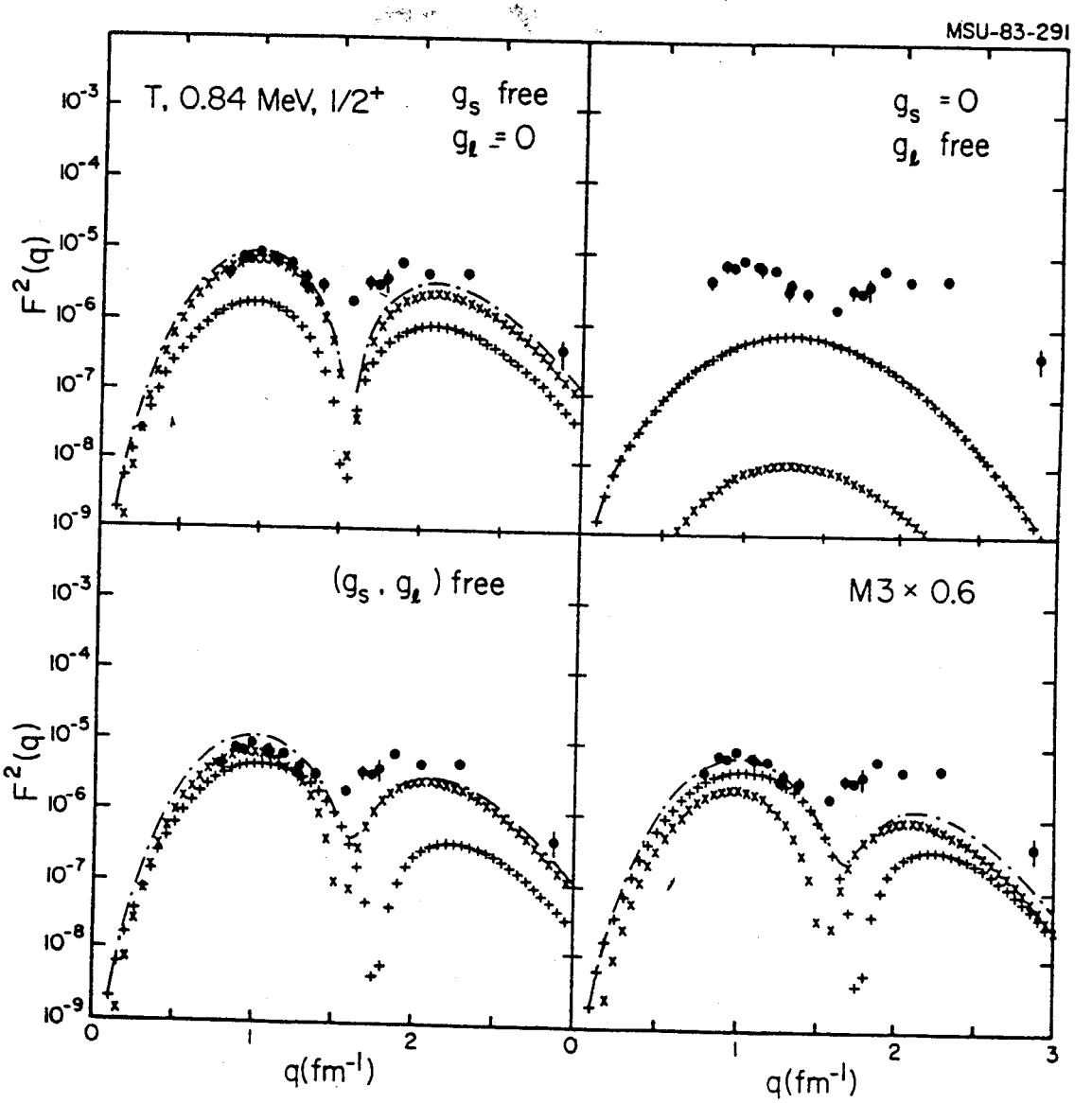

Figure V.6. Transverse form factors for the 0.844 MeV, $1/2_1^+$ state calculated with the HO radial wave functions of $b=b_{rms}$. The upper two Figures show the contributions from the spin and orbital g factors respectively. The lower two Figures calculated with free M3 g factors and quenched M3 g factors to 60% of the free-nucleon values, respectively. E2 and M3 multipoles are shown by the plus and cross signs respectively. The data are taken from Ref 13.

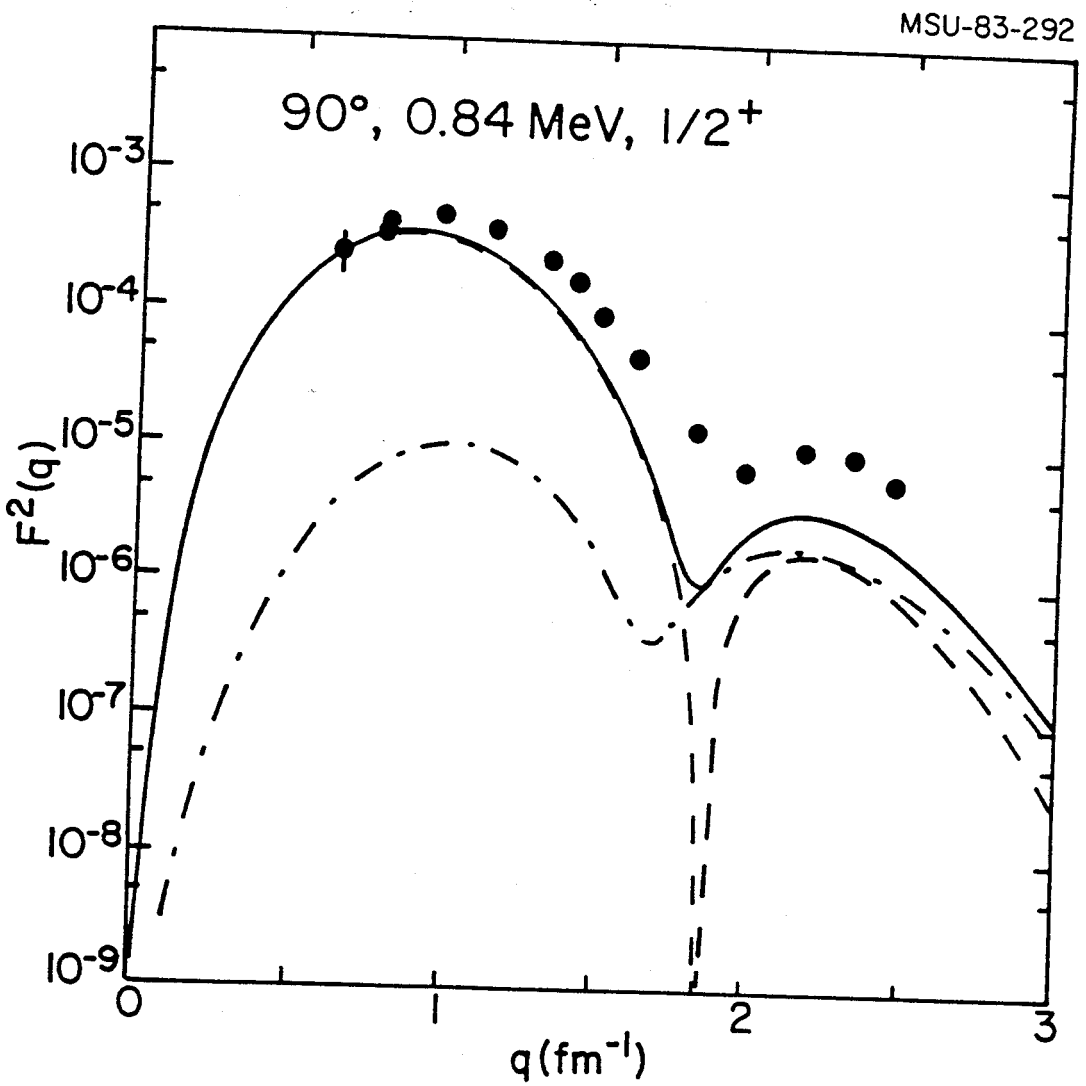

Figure V.7. Total form factor for the 0.844 MeV, $1/2_1^+$ state calculated at $\theta = 90^\circ$ (solid line). The dashed line represents the longitudinal form factor, and the dashed-dotted line represents the transverse form factor $1.5\ F_T^2$. The data are taken from Ref 13.

factor (dashed line) is dominated by the E2 contribution (plus signs). The E4 multipole ("Y" signs) makes a negligible contribution to the longitudinal scattering. The data is reasonably well explained, although it is slightly underestimated in the region of $1 < q < 1.5$ fm^{-1}.

The total transverse form factor is shown by the dashed-dotted line. The multipole decompositions that contribute to the transverse scattering are M1 (dotted line), E2 (plus signs), M3 (cross signs) and E4 ("Y" signs). Good agreement is obtained at low- and high-q values, while in the region of medium-q values, the form factor is underestimated by a factor of 2.

The total form factor of the 1.014 MeV, $3/2_1^+$ state is shown in this Figure by the solid line, calculated at $\theta=90^o$. The scattering is mostly longitudinal (dashed line) except at the region of the diffraction minimum where the transverse contribution 1.5 F_T^2 is also important (dashed-dotted line)

In Figure V.9 we plot the form factor M(q) vs. q^2 using the two models for the core polarization, the valence model (dashed line) and the Tassie model (solid line). The high-q values are very well explained by the Tassie model, while no big diference appears between these two models at the low-q values. The measured B(E2) value is well reproduced as shown in this Figure as $q \rightarrow 0$. From previus study (Ref 33) it was found that the longitudinal scattering data are well

Figure V.8. Form factors for the 1.014 MeV, $3/2_1^+$ state calculated with the single-nucleon radial wave functions of the HO potential of $b=b_{rms}$. The longitudinal, transverse and total form factors are represented by the dashed, dashed-dottted and solid lines, respectively. The plus and "Y" signs in the longitudinal plot represent the contribution of the E2 and E4 multipoles of the longitudinal form factors. The decomposition of the multipols of the transverse form factor are M1 (dotted line), E2 (plus signs), M3 (cross signs) and E4 ("Y" signs). The total form factor is calculated at $\theta=90^\circ$. The data are taken from Ref 13.

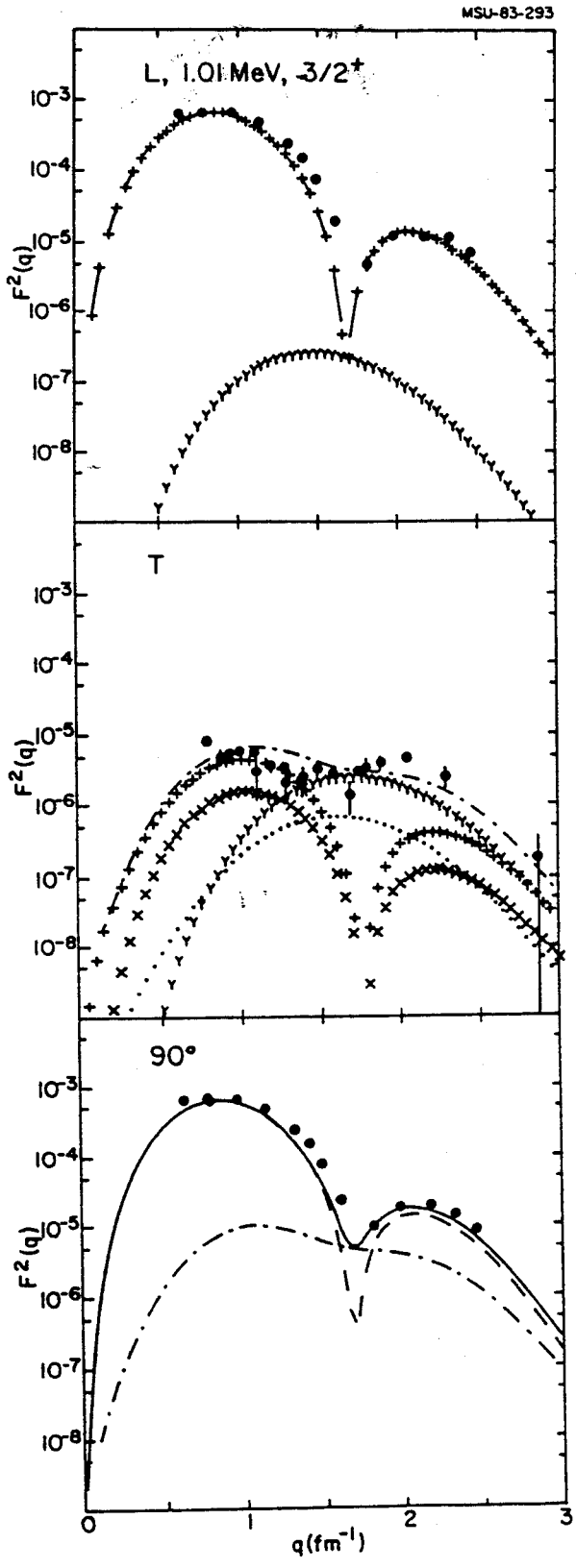

Figure V.8

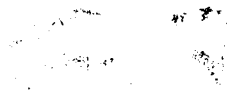

Figure V.9. Longitudinal and transverse M(q) form factors for the 1.014 MeV, $3/2_1^+$ state of ^{27}Al calculated with the single-nucleon wave functions of the HO potential of $b=b_{rms}$. In the longitudinal plot, the solid and dashed lines represent the calculations with the Tassie and valence models respectively. The measured B(E2) value and B(M1) value are shown at q= 0 in the longitudinal and transverse plots respectively. The data are taken from Ref 13.

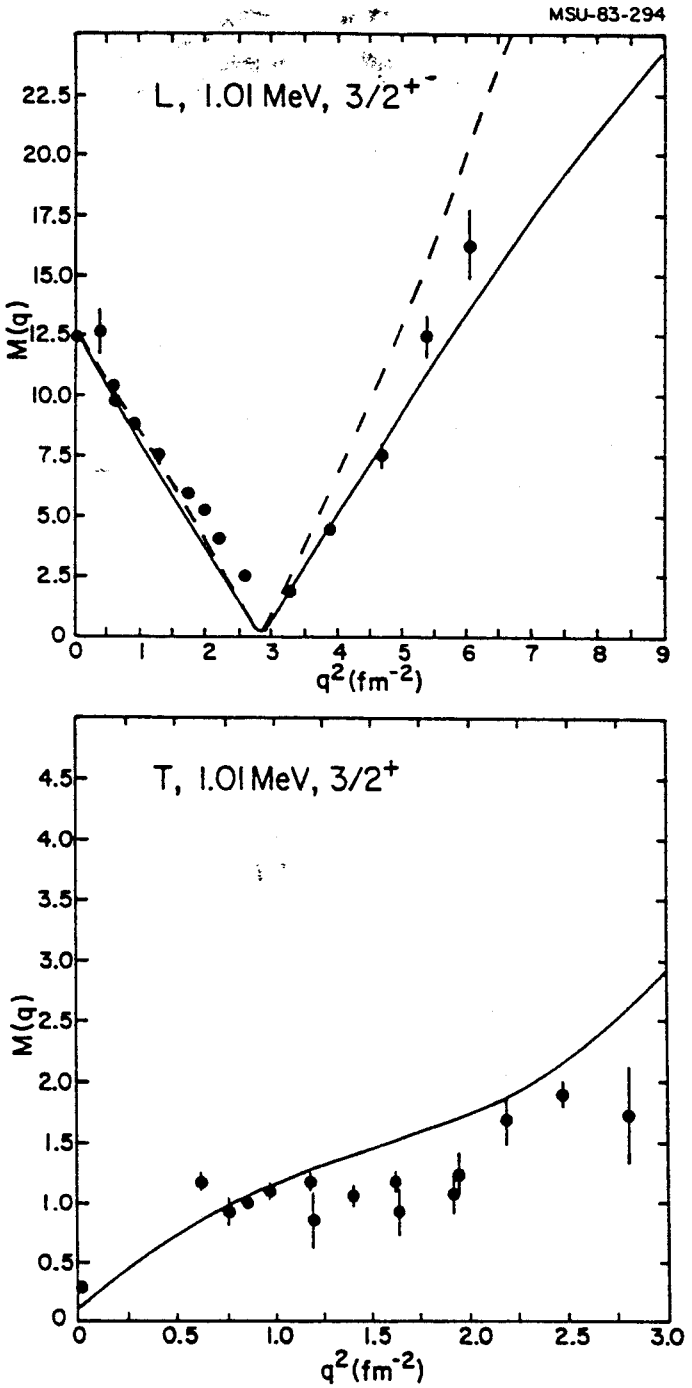

Figure V.9

described by the Tassie model in this mass region. We will use the HO radial wave functions of $b=b_{rms}$ and the Tassie model for the core-polarization transition density throughout the calculations of the excited states of ^{27}Al. The predicted magnetic dipole transition matrix element is slightly smaller than the measured value, as shown in the M(q) plot for the transverse scattering.

V.5. The 2.211 MeV, $7/2_1^+$ state

Form factors for the 2.211 MeV, $7/2_1^+$ state are shown in Figure V.10 calculated with the radial wave functions of the HO potential of $b=b_{rms}$. The longitudinal E2+ E4 form factor (dashed line) is dominated by the E2 contribution (plus signs), as the E4 multipole ("Y" signs) makes a negligible contribution to the longitudinal scattering. The experimental data are very well described throughout the different momentum transfer regions.

The total transverse form factor is shown by the dashed-dotted line. The decomposition of the multipoles that contribute to the transverse scattering are M1 (dotted line), E2 (plus signs), M3 (cross signs), E4 ("Y" signs) and M5 (triangles). The shape of the form factor is very well reproduced, but the magnitudes are slightly underestimated.

The total form factor for the 2.211 MeV, $7/2_1^+$ state is shown in this Figure by the solid line, calculated at $\theta=90^\circ$. Once again, the scattering is mostly longitudinal

Figure V.10. Form factors for the 2.211 MeV, $7/2_1^+$ state. The convections of the presentation are the same as given in the caption to Figure V.8. The M5 multipole is shown by the triangles. The data are taken from Ref 13 (circles), Ref 84 (triangles).

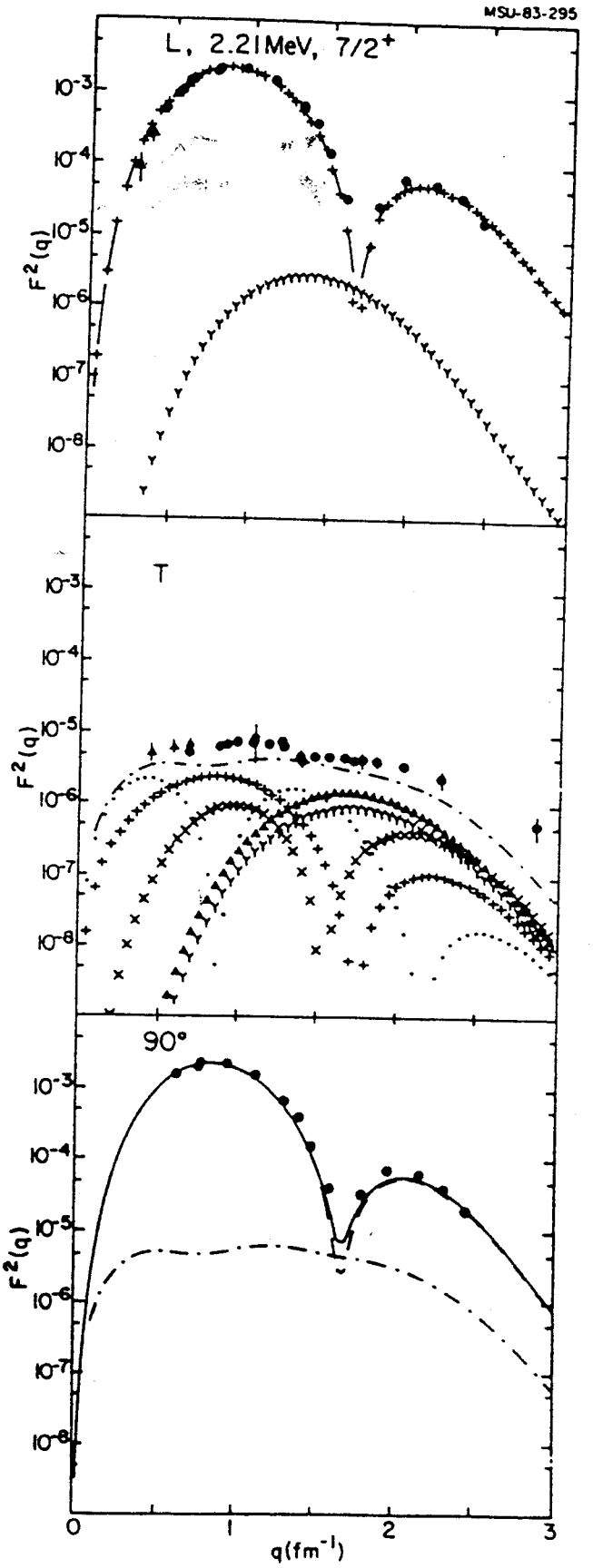

Figure V.10

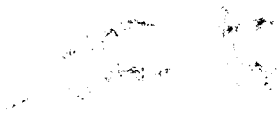

Figure V.11. Longitudinal and transverse M(q) form factors for the 2.211 MeV, $7/2_1^+$ state. The convections of the presentation are the same as given in the caption of Figure V.9. The data are taken from Ref 13 (circles), Ref 84 (triangles).

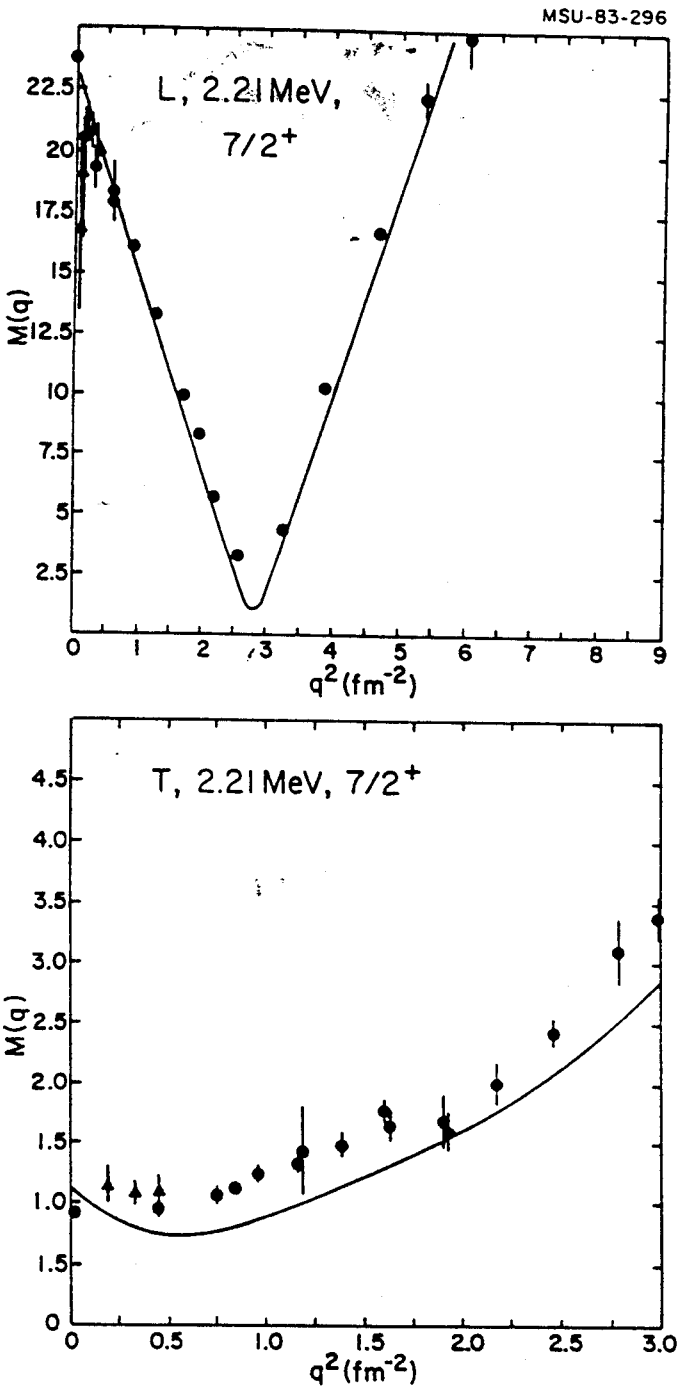

Figure V.11

(dashed line), while the transverse part, 1.5 F_T^2 (dashed-dotted line), makes a negligible contribution. The experimental data are very well reproduced at all q values. Good agreement is obtained with the measured B(E2) value, as shown in Figure V.11. The predicted B(M1) is higher than the measured one by a factor of 2, as shown in the transverse M(q) plot.

V.6. The 2.735 MeV, $5/2_2^+$ state.

Form factors for the 2.735 $5/2_2^+$ state are shown in Figure V.12, calculated with the radial wave functions of the HO potential of $b=b_{rms}$. In the region of low-q values, the longitudinal E0+ E2+ E4 form factor (dashed line) is dominated by the E2 contribution (plus signs), while in the region of medium-q values it is dominated by the E4 contribution ("Y" signs). In the region of high-q values the E2 and E4 multipoles contribute equally to the longitudinal scattering. The E0 contribution (dotted line) is very small compared to the E2 and E4 multipoles. The shape and magnitude are very well reproduced except at the region of q between 1-1.5 fm^{-1} where the form factor is slightly underestimated.

The total transverse form factor is shown by the dashed-dotted line. Good agreement is obtained between theory and experiment. The decomposition of the multipoles that contribute to the transverse scattering are M1 (dotted

Figure V.12. Form factors for the 2.735 MeV, $5/2_2^+$ state. The convections of the presentation are the same as given in the caption to Figure V.8. The convections for the different multipoles are the same as those in Figure V.3 and Figure V.10. The data are taken from Ref 13.

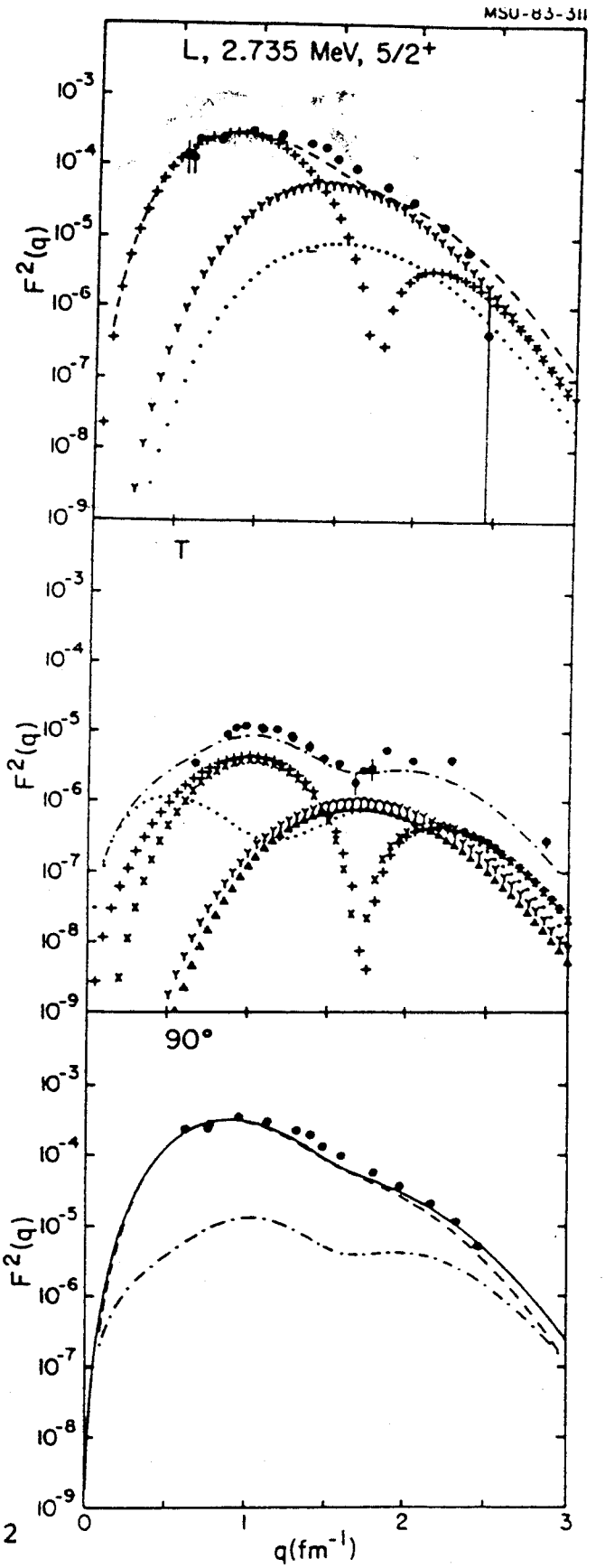

Figure V.12

line), E2 (plus signs), M3 (cross signs), E4 ("Y" signs) and M5 (triangles).

The total form factor $F^2(q)$ is shown by the solid line, calculated at $\theta = 90^\circ$ where the scattering is mostly longitudinal (dashed line). The transverse form factor, $1.5F_T^2$ (dashed-dotted line), makes a negligible contribution to the total form factor except in the region of $q > 2$ fm^{-1}. The measured B(E2) value is reasonably well reproduced, as shown in Figure V.13. The measured B(M1) value is also well reproduced, as shown in the transverse M(q) plot.

V.7. The (2.98,3.004) MeV, ($3/2_2^+$, $9/2_1^+$) doublet

The theoretical form factor of this unresolved doublet is obtained by adding the calculated form factors of the $3/2_2^+$ and $9/2_1^+$ states (Figure V.14). The total longitudinal E2+ E4 form factor is shown by the dashed line. The largest contribution is due to the E2 form factor (plus signs). The E2 form factor is dominated by that of the $9/2_1^+$ state, while the $3/2_2^+$ state makes a negligible contribution to the E2 form factor. The E4 form factors of both states ("Y" signs) contribute approximately equally to the longitudinal scattering and they make negligible contributions except in the region of the diffraction minimum. The experimental data are slightly underestimated in the region of $q > 1$ fm^{-1}.

The total transverse form factor is shown by the dashed-dotted line. The decomposition of the multipoles that

Figure V.13. Longitudinal and transverse M(q) form factors for the 2.735 MeV, $5/2_2^+$ state. The convections of the presentation are the same as given in the caption to Figure V.9. The data are taken from Ref 13 (circles), Ref 84 (triangles).

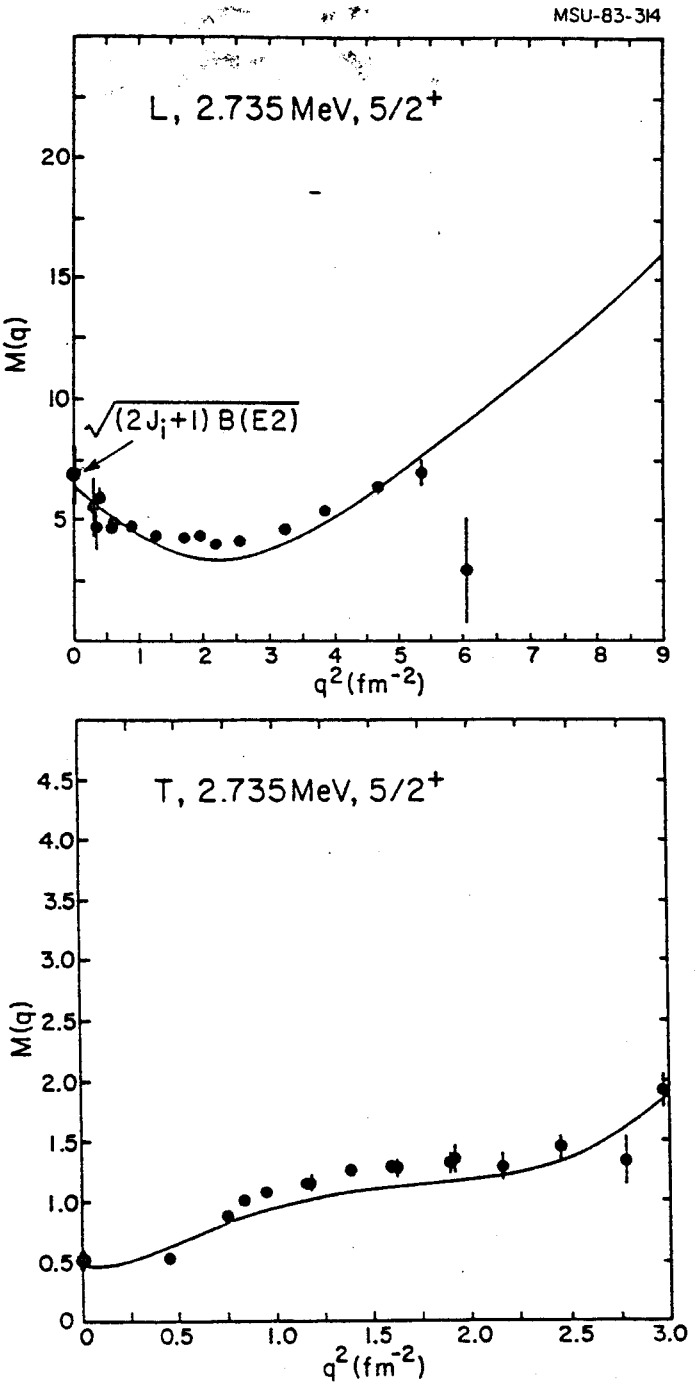

Figure V.13

Figure V.14. Form factors for the (2.98,3.004) MeV, ($3/2_2^+$,$9/2_1^+$) doublet. The convections of the presentation are the same as given in the caption to Figure V.8. The convections for the different multipoles are the same as those in Figure V.10. The data are taken from Ref 13 (circles), Ref 84 (triangles).

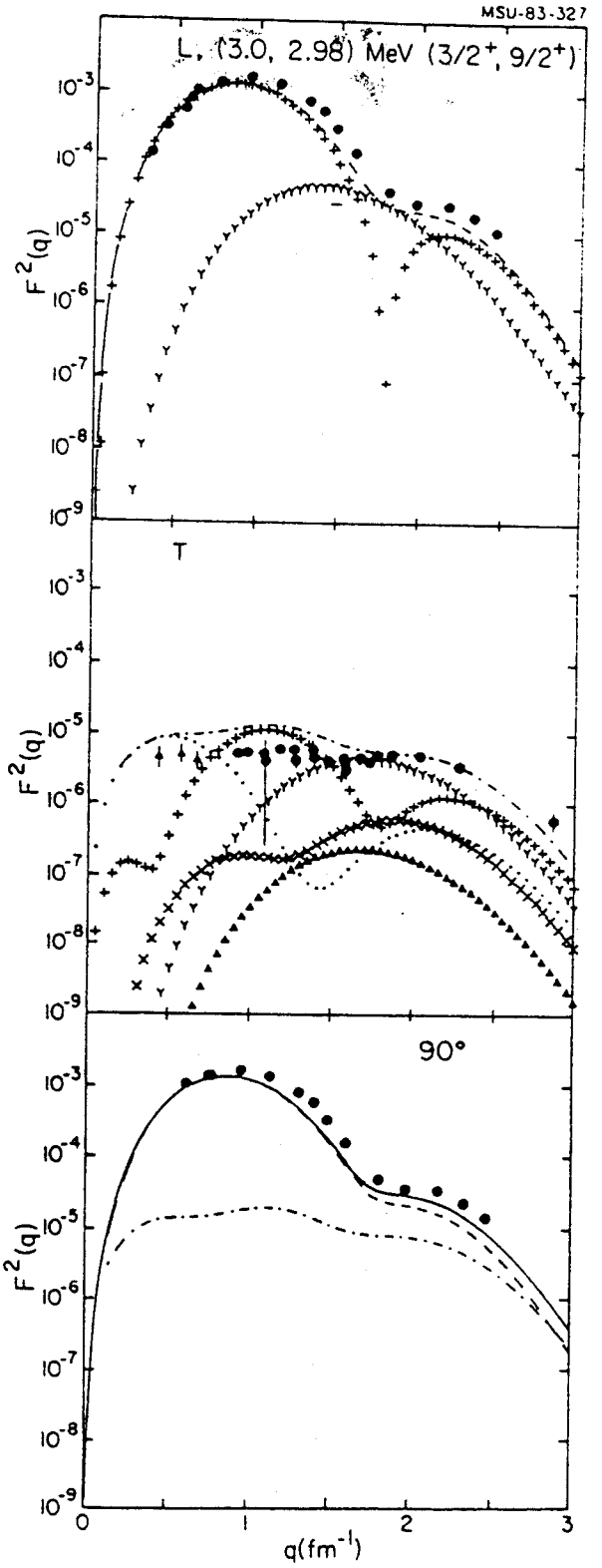

Figure V.14

contribute to the transverse scattering are M1 (dotted line), E2 (plus signs), M3 (cross signs), E4 ("Y" signs) and M5 (triangles). The transverse form factor is dominated by the M1, E2 and E4 multipoles. The shape of the form factor is very well reproduced, but the magnitude is overestimated in the region of $q < 1.5$ fm^{-1} by a factor of 1.5.

The total form factor $F^2(q)$ is shown by the solid line, calculated at $\theta = 90^\circ$. The total form factor is dominated by the longitudinal contribution of the $9/2_1^+$ state.

Reasonable agreement is obtained with the measured B(E2) value of the $9/2_1^+$ state, as shown in Figure V.15 for the longitudinal M(q) plot. The measured B(M1) value of the $3/2_2^+$ state is overestimated, as shown in the transverse M(q) plot.

V.8. The higher-lying states

We present here the shell-model predictions of the form factors for the states above 3.0 MeV which have experimentally known spin and parity assignments. The experimental longitudinal form factors have not been separated from the total form factor measured at 90°. The calculations presented here are for the transverse form factors measured at angles 160° and 180°, and for the total form factors measured at 90°. The decomposition of the different multipoles of the longitudinal scattering are

Figure V.15. Longitudinal and transverse M(q) form factors for the (2.98,3.004) MeV ,($3/2_2^+$,$9/2_1^+$) doublet. The convection of the presentation are the same as given in the caption of Figure V.9. The data are taken from Ref 13 (circles), Ref 84 (triangles).

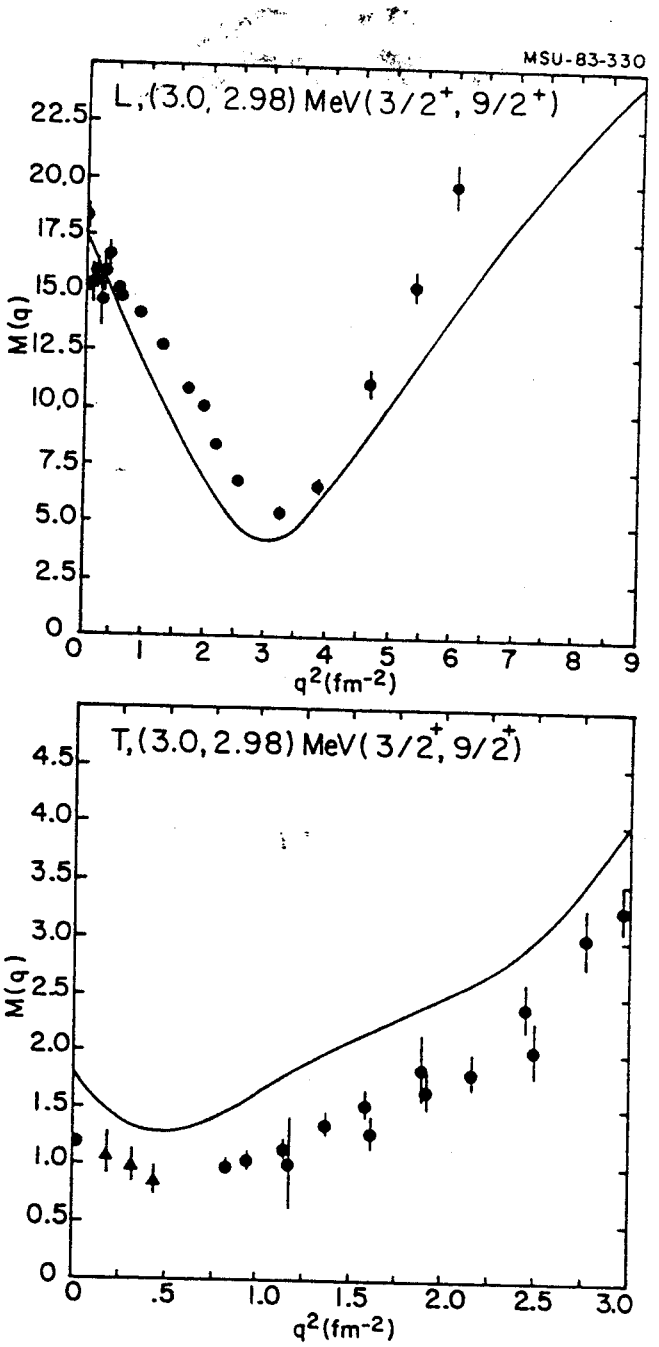

Figure V.15

shown in the total form factor plots.

The form factors for the 3.68 MeV, $1/2_2^+$ state are shown in Figure V.16. The transverse form factor is shown by the dashed-dotted line. It is dominated by the E2 multipole (plus signs), while the M3 multipole (cross signs) has a very small contribution at $q > 2$ fm^{-1}. Good agreement is obtained with the few available data points. The total form factor calculated at $\theta = 90^\circ$ is shown by the solid line. In the the region of $q < 1.5$ fm^{-1}, the scattering is mostly longitudinal (dashed line) and no significant contribution appears from the transverse 1.5 F_T^2 part (dashed-dotted line) at this region of q. In the region of high-q values > 2 fm^{-1}, the scattering is mostly transverse. Reasonable agreement is obtained in shape and magnitude throughout the different momentum transfers regions.

The form factors for the 3.957 MeV, $3/2_3^+$ state are shown in Figure V.17. The transverse form factor is shown by the dashed-dotted line and the different multipoles that contribute to the scattering are M1 (dotted line), E2 (plus signs), M3 (cross signs) and E4 ("Y" signs). The transverse scattering is dominated by the M1 contribution (dotted line). The total form factor calculated at $\theta = 90^\circ$ is shown by the solid line. The scattering is dominated by the transverse 1.5 F_T^2 part (dashed-dotted line) at all q values except in the region of q between 1-2 fm^{-1}, where both longitudinal and transverse parts are important. The

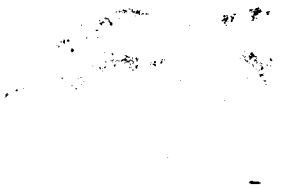

Figure V.16. Form factors for the 3.68 MeV, $1/2_2^+$ state of ^{27}Al. The upper plot represents the transverse form factor (dashed-dotted line). The E2 and M3 multipoles are shown by the plus and cross signs respectively. The lower plot represents the total form factors calculated at $\theta = 90^\circ$ (solid line). The dashed line represents the longitudinal form factor, while the dashed-dotted line represents the transverse form factor including a factor of 1.5. The data are taken from Ref 13.

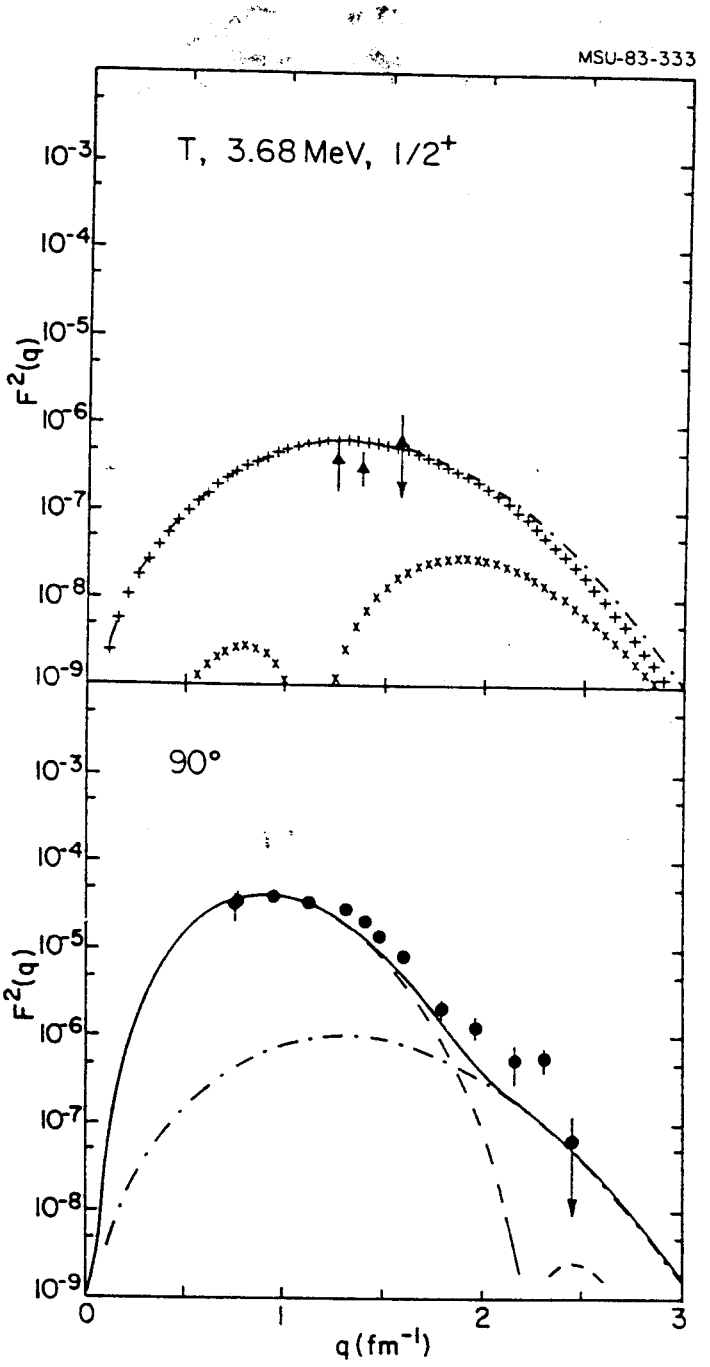
MSU-83-333
T, 3.68 MeV, 1/2+
90°
F2(q)
q(fm-1)
10-3
10-4
10-5
10-6
10-7
10-8
10-9
0
1
2
3

Figure V.16

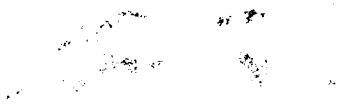

Figure V.17. Form factors for the 3.957 MeV, $3/2_3^+$ state of ^{27}Al. The convections of the presentation are the same as given in the caption to Figure V.16. The decomposition of the multipoles of the transverse form factor are M1 (dotted line), E2 (plus signs), M3 (cross signs), and E4 ("Y" signs). The decomposition of the multipoles of the longitudinal scattering are shown in the total form factor plot as E2 (plus signs) and E4 ("Y" signs).

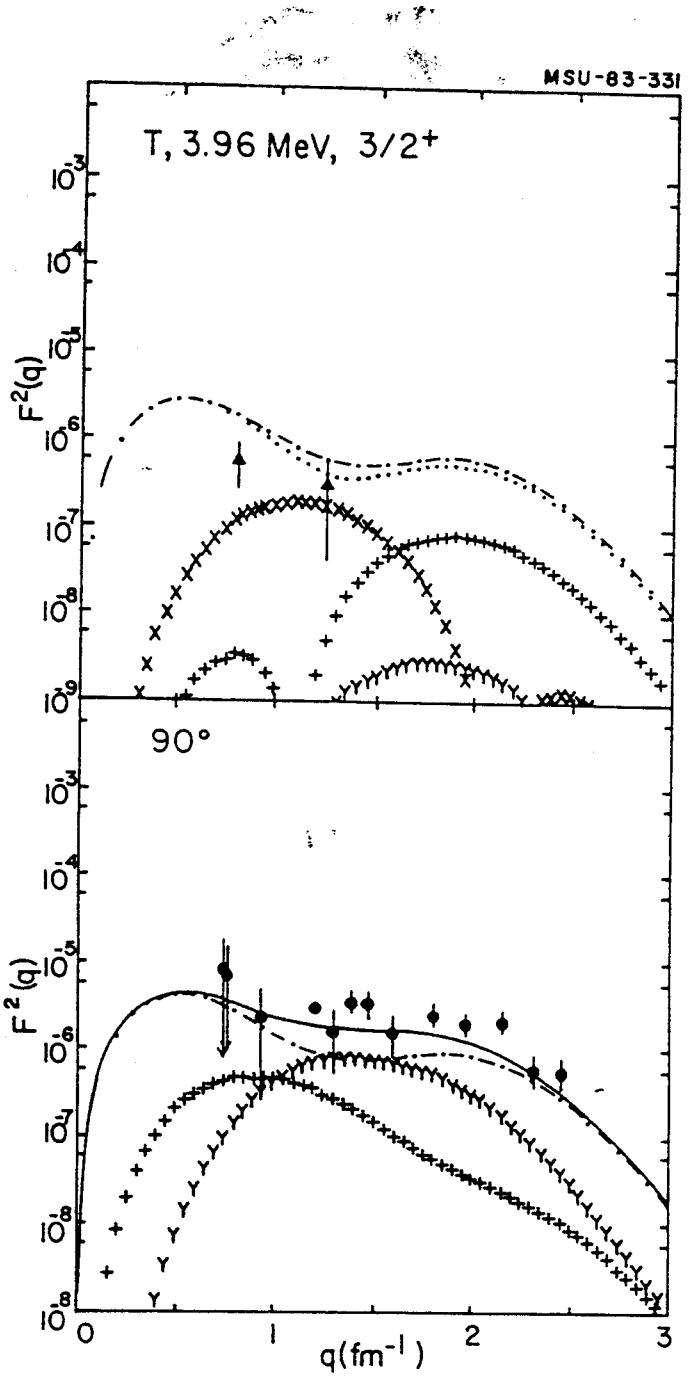

Figure V.17

longitudinal form factor is dominated by the E4 contribution ("Y" signs) in the region of $q > 1$ fm^{-1}, while E2 contribution (plus signs) is more important at $q < 1$ fm^{-1}. An overall agreement is obtained with the experimental data.

In Figure V.18, we show the form factors for the 4.41 MeV, $5/2_3^+$ state. The transverse form factor is shown by the dashed-dotted line and in the region of low-q values the transverse scattering is dominated by the M1 contribution (dotted line). As q increases, E2 (plus signs) and M3 (cross signs) contributions become more important. The contributions from E4 ("Y" signs) and M5 (triangles) multipoles are small and they are important only in the region where E2 and M3 have their second minima. The transverse data are very well reproduced. The total form factor calculated at $\theta = 90^\circ$ is shown by the solid line. In the region of small momentum transfers the scattering is dominated by the transverse part (dashed-dotted line). At $q > 1$ fm^{-1}, the longitudinal part (dashed line) becomes more important up to $q \approx 2.3$ fm^{-1}, where the transverse part becomes again important. The longitudinal form factor contributes to the scattering through the E0 multipole (dotted line), E2 multipole (plus signs) and E4 multipole ("Y" signs). The E4 multipole dominates the longitudinal form factor up to $q \approx 2$ fm^{-1}. In the region of $q > 2$ fm^{-1}, the contributions from E0, E2 and E4 multipoles are all important. The experimental data are very well reproduced

Figure V.18. Form factors for the 4.41 MeV, $5/2_3^+$ state of ^{27}Al. The convections of the presentation are the same as given in the caption to Figure V.16. The decomposition of the multipoles of the transverse form factor are M1 (dotted line), E2 (plusses line), M3 (cross signs), E4 ("Y" signs) and M5 (trianles line). The decomposition of the multipoles of the longitudinal scattering are shown in the total form factor plot as E0 (dotted line), E2 (plus signs) and E4 ("Y" signs).

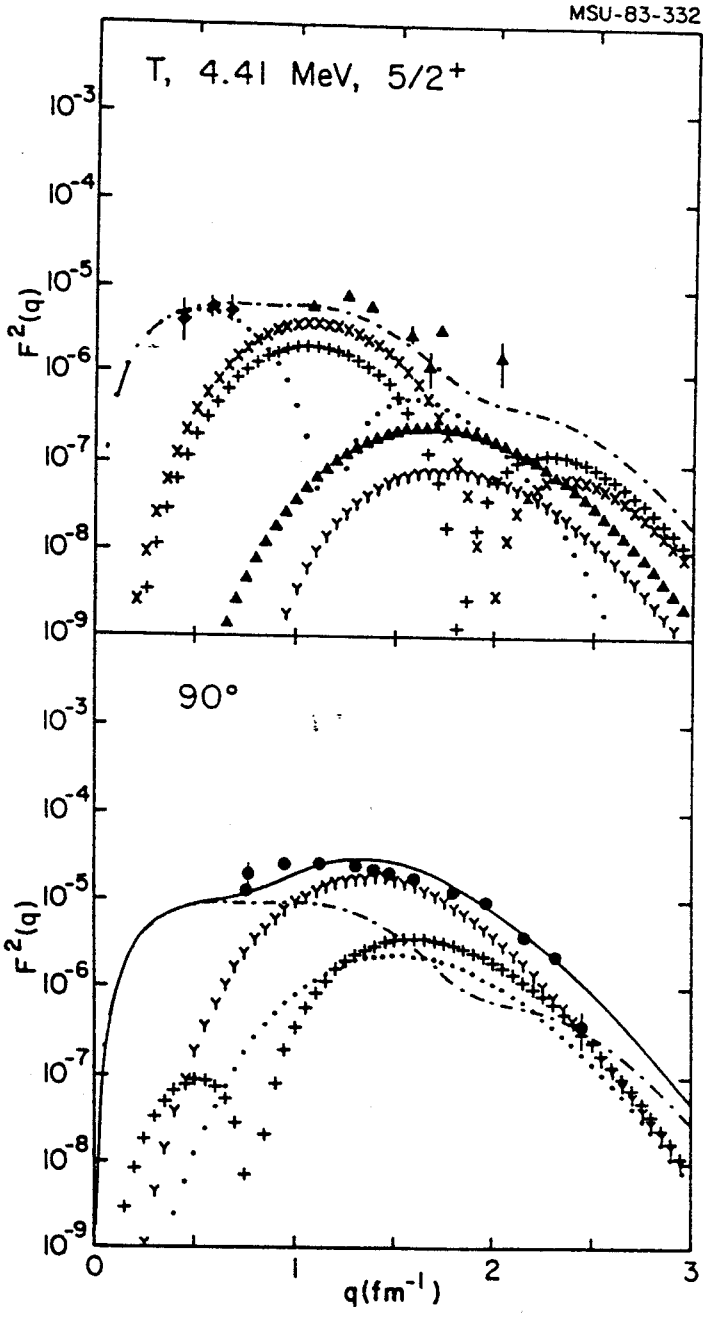

Figure V.18

Figure V.19. Form factors for the 4.51 MeV, $11/2_1^+$ state of ^{27}Al. The convections of the presentation are the same as give in the caption to Figure V.16. The decomposition of the multipoles of the transverse form factor are M3 (cross signs), E4 ("Y" signs) and M5 (trianles). Only E4 multipole contributes to the longitudinal scattering.

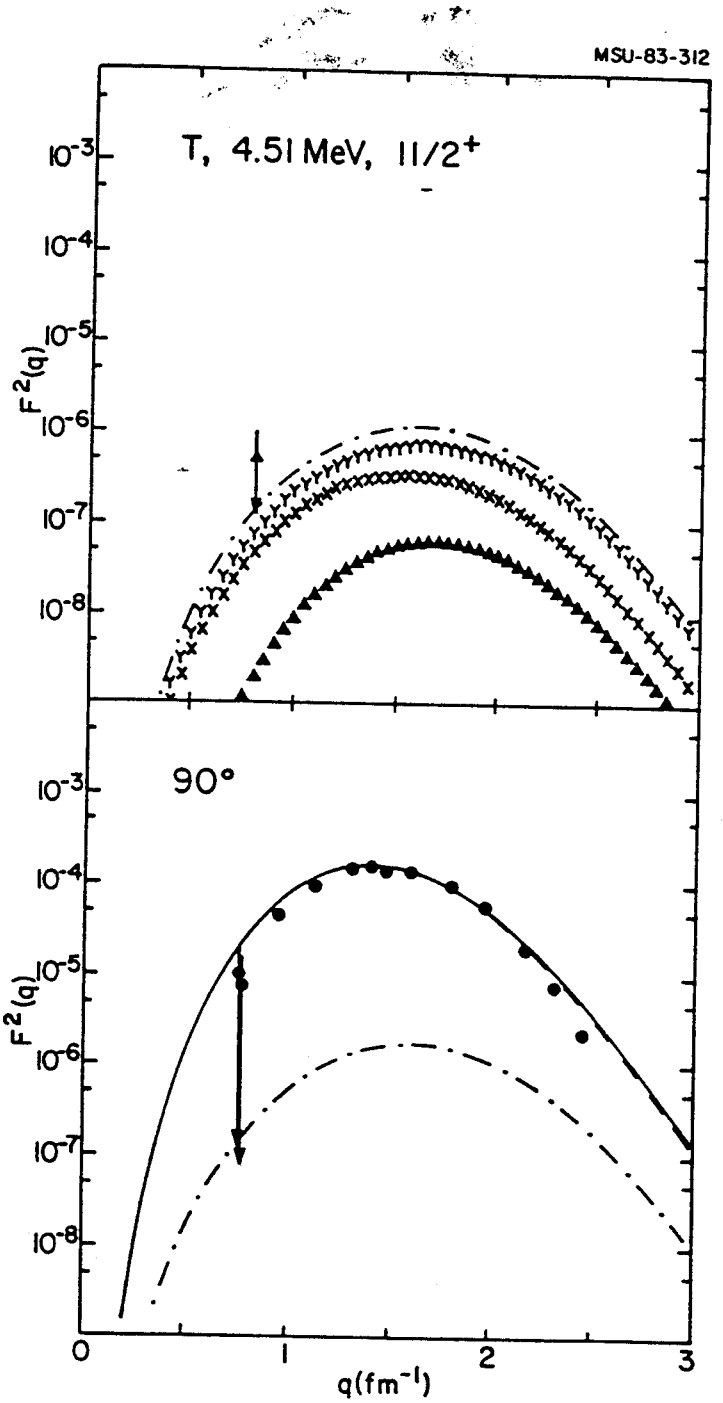

Figure V.19

throughout the different q values.

In Figure V.19, we show the form factors for the 4.51 MeV, $11/2_1^+$ state. The transverse form factor is shown by the dashed-dotted line and it is dominated by the E4 multipole ("Y" signs). The M5 multipole (triangles) makes a negligible contribution. The total form factor calculated at $\theta = 90^\circ$ is shown by the solid line, where the scattering is totally longitudinal (dashed line). Very good agreement is obtained for all q values.

The form factors for the 4.58 MeV, $7/2_2^+$ state are shown in Figure V.20. The transverse form factor is shown by the dashed-dotted line and the different multipoles that contribute to the scattering are M1 (dotted line), E2 (plus signs), M3 (cross signs), E4 ("Y" signs) and M5 (triangles). In the region of $q < 0.5$ fm^{-1}, the M1 multipole dominates the scattering. As q increases the E2 multipole becomes more important up to $q \approx 2$ fm^{-1}. At $q > 2$ fm^{-1}, the transverse scattering is dominated by the E4 multipole. The total form factor calculated at $\theta = 90^\circ$ is shown by the solid line. The scattering is mostly longitudinal (dashed line) and is dominated by the E4 multipole ("Y" signs) in the region of $q > 1$ fm^{-1}. The experimental data are very well reproduced.

V.9. Conclusions

The complete-space shell-model calculations succeed in describing all the positive-parity states of ^{27}Al considered

Figure V.20. Form factors for the 4.58 MeV, $7/2_2^+$ state of ^{27}Al. The convections of the presentation are the same as given in the caption to Figure V.16. The decomposition of the multipoles that contribute to the transverse form factor are M1 (dotted line), E2 (plus signs), M3 (cross signs), E4 ("Y" signs) and M5 (trianles). The decomposition of the multipoles that contribute to the longitudinal scattering are shown in the total form factor plot as E2 (plus signs) and E4 ("Y" signs).

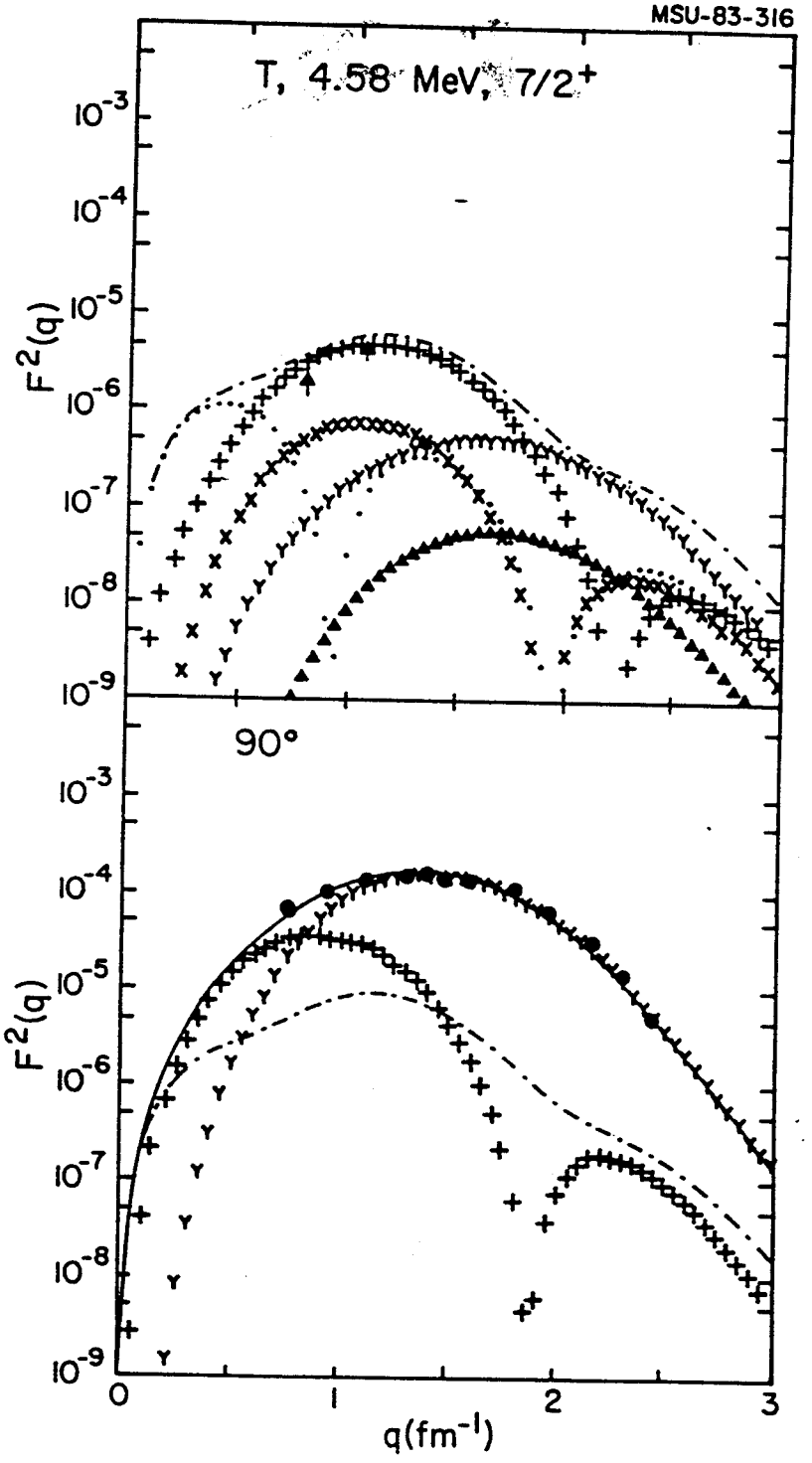
MSU-83-316
T, 4.58 MeV, 7/2+
10^{-3}
10^{-4}
10^{-5}
10^{-6}
10^{-7}
10^{-8}
10^{-9}
$F^2(q)$
90°
10^{-3}
10^{-4}
10^{-5}
10^{-6}
10^{-7}
10^{-8}
10^{-9}
$F^2(q)$
0
1
2
3
$q(fm^{-1})$

Figure V.20

in this study. The longitudinal form factors for the low-lying states of excitation energies below 3.0 MeV are very well described. The B(E2) values are reasonably reproduced with the isoscalar effective charge of 1.7e. The transverse form factors of these states are very well reproduced in shape. However, the magnitudes need to be adjusted for some multipoles to get better explanation of the data for all momentum transfers regions. Quenching the M3 multipole to 60% of the free-nucleon value helps in some cases in describing the low-q values where the M3 multipole is important. The measured B(M1) are not well reproduced for some cases with the free-nucleon g factors of the M1 multipole. This suggests that the M1 multipole needs to be renormalized by using effective g factors. The total form factors of these low-lying states are dominated by the longitudinal scattering.

The higher-lying states, of excitation energies above 3.0 MeV, are also well described. Some of these states are dominated by the longitudinal scattering as in the 4.51 MeV, $11/2_1^+$ and 4.58 MeV, $7/2_2^+$ states. The 3.957 MeV, $3/2_3^+$ state is dominated by the transverse scattering. The other two states are dominated alternatively by the longitudinal and transverse scattering at different q regions.

Table V.1. Calculated one-body transition density matrix elements (OBDM) for [($2J_i$= 5,$2T_i$= 1,N_i= 1) to ($2J_f$,$2T_f$= 1,N_f)] transitions in ^{27}Al for the wave functions of Ref 17

						OBDM(i,f,L,j,j',ΔT)								
			ENERGY			2j-2j'								
$2J_f$	N_f	L	theo.	Exp.	$2\Delta T$	5-5	5-1	5-3	1-5	1-1	1-3	3-5	3-1	3-3
1	1	2	0.912	0.844	0	0.4197	-0.0237	0.3346	0.6674		0.0158	-0.3702	0.0016	0.1503
					2	-0.0584	0.4181	-0.0337	-0.0174		0.0189	-0.0053	-0.0034	0.0217
		3			0	-0.0094	0.3082	0.0238	0.3891			0.0361		-0.0045
					2	0.0481	-0.3610	-0.0540	-0.2760			-0.1165		0.0196
	2	2	3.708	3.680	0	-0.1383	-0.0623	-0.0901	-0.0086		0.0084	0.4426	-0.0358	-0.0875
					2	-0.0364	-0.0572	-0.0362	-0.1937		0.0443	-0.1871	0.0409	0.0072
		3			0	0.1449	-0.1549	0.0250	0.1912			-0.2984		0.0276
					2	-0.0501	0.0483	-0.0124	0.0796			0.0273		0.0112
	3	2	5.607	5.752	0	-0.0297	0.0028	0.0410	-0.0309		-0.0033	-0.0177	-0.0158	-0.0154
					2	-0.0284	0.0427	-0.0241	-0.1360		0.0203	-0.1009	0.0233	0.0096
		3			0	0.0311	-0.0512	-0.0101	0.1348			-0.1326		0.0210
					2	-0.0131	-0.0366	-0.0315	0.0619			-0.0975		0.0168
	4	2	6.786		0	-0.0535	-0.0101	-0.1093	0.1778		0.0192	0.4999	-0.1192	-0.0716
					2	0.0161	-0.0012	-0.0131	0.0661		0.0033	0.0647	0.0011	-0.0060
		3			0	0.0172	-0.0223	0.0247	0.0324			0.0362		-0.0355
					2	-0.0175	0.0029	0.0043	-0.1017			0.2621		-0.0425
	5	2	7.131		0	-0.0328	-0.0689	-0.0321	-0.0823		0.0732	-0.0343	-0.1308	-0.0336
					2	-0.0076	-0.0900	0.0106	-0.0306		0.0842	-0.0543	0.0045	-0.0193
		3			0	0.0375	-0.0126	0.0202	-0.0054			-0.0550		0.0012
					2	-0.0030	0.0627	0.0200	0.0446			-0.0469		0.0002
3	1	1	1.264	1.014	0	0.0488		-0.1136		-0.2019	-0.1228	0.1103	-0.0191	-0.0275
					2	0.0927		0.1243		0.1372	0.0597	-0.1063	0.0684	0.0633
		2			0	-0.3580	-0.4587	-0.1785	-0.9596		0.0128	0.3348	0.0780	-0.1413
					2	-0.0785	-0.0510	-0.1780	0.1572		-0.1675	0.1038	0.0456	-0.0455
		3			0	-0.0979	-0.0239	-0.2365	0.3781			0.1370		0.0201
					2	0.0350	0.0337	0.2181	-0.3911			-0.1176		-0.0526

Table V.1. (cont'd.)

	4			0	-0.0767		0.1701				0.0949			
				2	0.0599		-0.1668				-0.0733			
2	1	2.780	2.981	0	-0.0323		-0.0333		0.2492	-0.0194	0.3772	0.0122	-0.0184	
				2	0.0368		0.0731		-0.2533	-0.0099	-0.2590	-0.1392	-0.0208	
	2			0	0.0295	-0.0320	0.1521	0.1534		0.0124	0.2817	0.0503	0.0345	
				2	-0.0160	0.0871	-0.1869	-0.1051		-0.0063	-0.2575	-0.0446	0.0052	
	3			0	-0.0118	-0.0198	-0.1674	-0.1443			0.3544		-0.0019	
				2	-0.0169	0.0625	0.2039	-0.0133			-0.1135		0.0156	
	4			0	-0.1126		-0.0424				0.5720			
				2	-0.0169		-0.1834				-0.0592			
3	1	4.027	3.957	0	-0.0403		0.0364		0.2009	0.0157	0.1741	0.0007	0.0118	
				2	0.0074		-0.0033		-0.2233	0.0022	-0.1012	-0.0864	-0.0474	
	2			0	-0.0353	0.0687	0.0300	0.0451		0.0219	-0.2112	0.0159	0.0026	
				2	0.0417	0.0114	0.0095	0.1414		0.0457	0.0580	-0.0781	0.0121	
	3			0	0.0325	-0.0392	0.0130	0.1762			-0.4481		0.0117	
				2	0.0525	-0.0383	0.0093	0.0947			0.1469		0.0151	
	4			0	0.1049		-0.0088				-0.0066			
				2	0.0194		-0.0363				0.0241			
4	1	5.765	5.551	0	-0.0149		-0.0038		0.0284	0.0233	-0.0437	0.0068	0.0188	
				2	-0.0179		-0.0082		-0.0364	0.0220	0.0100	0.0168	-0.0161	
	2			0	-0.1020	0.0538	-0.0620	0.0675		0.0560	0.0388	-0.0447	-0.0178	
				2	0.0222	-0.0444	0.0414	0.1595		0.0332	0.1434	-0.0435	-0.0090	
	3			0	0.0284	-0.0504	0.0276	0.2023			-0.1690		-0.0065	
				2	0.0473	-0.0727	-0.0582	0.1198			0.0099		-0.0071	
	4			0	0.1048		0.0058				-0.1142			
				2	0.0199		0.0138				-0.0113			
5	1	6.263		0	0.0640		0.0382		0.0178	0.0106	0.0679	0.0927	-0.1253	
				2	-0.0530		0.0011		0.0263	0.1140	-0.0649	-0.0628	0.0487	
	2			0	0.0997	-0.0104	0.0711	0.0244		-0.0261	-0.0914	0.1037	-0.0126	
				2	-0.0064	0.0270	0.0139	0.0505		-0.0620	0.0031	-0.0336	0.0402	
	3			0	0.0693	-0.0425	-0.0065	0.0564			-0.1062		0.0644	
				2	0.0115	-0.0056	0.0029	0.0759			0.0313		0.0068	
	4			0	-0.0758		-0.0421				0.0469			
				2	0.0266		-0.0173				0.0185			

Table V.1. (cont'd.)

5	1	0	0.000	0.000	0	8.8942			1.7735				
					2	0.6778			0.3134				1.3250
													0.1730
		1			0	0.9419		0.1105		0.0964	0.0084	-0.1105	-0.0084	0.0781
					2	-0.6799		-0.1113		-0.2015	-0.0989	0.1113	0.0989	0.0273
		2			0	-0.6998	-0.4630	-0.4509	-0.4630		0.2096	0.4509	0.2096	-0.1912
					2	0.6068	-0.0796	0.0165	-0.0796		0.0830	-0.0165	-0.0830	0.0080
		3			0	0.6346	-0.1405	0.0358	-0.1405			-0.0358		-0.0112
					2	-0.6095	0.1274	-0.0225	0.1274			0.0225		0.0413
		4			0	-0.5796		-0.0237						
					2	0.5964		-0.0795				0.0237		
												0.0795		
		5			0	0.7276								
					2	-0.7195								
	2	0	2.708	2.735	0	0.1088			-0.3549					
					2	-0.1115			0.3598					0.1178
														-0.1178
		1			0	-0.0200		0.0379		0.2099	-0.1792	0.0920	-0.0676	-0.0280
					2	0.0771		-0.0061		-0.2545	0.1356	-0.0725	0.0672	0.0226
		2			0	-0.0938	-0.2816	-0.2277	-0.4172		0.1076	0.5580	0.2339	-0.1208
					2	-0.1265	-0.0317	-0.0333	-0.1474		-0.1334	-0.2351	-0.1027	0.0234
		3			0	-0.3158	0.0210	-0.0557	-0.4440			0.0909		0.0228
					2	0.2791	0.0150	0.0299	0.3203			-0.0247		-0.0711
		4			0	0.0709		0.1955						
					2	-0.1957		0.0435				-0.4653		
												0.0917		
		5			0	-0.1214								
					2	0.1298								
	3	0	4.139	4.410	0	-0.1985			0.3623					
					2	-0.1036			-0.0177					-0.0130
														0.1394
		1			0	-0.0379		-0.0575		0.0305	0.0645	-0.3701	0.0055	0.0613
					2	0.1316		0.0236		-0.0140	-0.0782	0.2321	0.0424	0.0293
		2			0	0.1233	-0.0555	0.0351	-0.2333		-0.1986	-0.2781	0.0589	0.0027
					2	-0.1755	0.0094	0.0084	0.0175		0.0987	0.2272	-0.0072	0.0427
		3			0	-0.2849	0.1407	-0.0089	-0.5230			0.0147		-0.0103
					2	0.2397	-0.0689	0.0440	0.2677			0.2569		0.0523

Table V.1. (cont'd.)

	4			0	-0.0442		-0.1664				0.4212			
				2	-0.1597		-0.0390				0.0650			
	5			0	-0.1960									
				2	0.1644									
4	0	4.939	4.812	0	-1.0526			1.3616						0.3263
				2	-0.2168			0.3101						0.0463
	1			0	-0.0425		0.0106		0.0472	0.0415	-0.0359	0.0061		0.0646
				2	0.2261		0.0257		-0.1354	-0.0015	-0.0179	-0.0185		
	2			0	-0.0426	-0.0092	-0.0384	-0.0776		-0.1191	0.2889	0.1599		-0.1038
				2	-0.2617	0.0535	-0.0387	-0.1803		0.1131	-0.1453	-0.0423		-0.0198
	3			0	-0.1562	-0.0094	-0.0169	0.0795			-0.0611			-0.0819
				2	0.1538	-0.0300	0.0093	0.1124			-0.0958			0.0214
	4			0	0.3452		0.0946				-0.3042			
				2	-0.2101		0.0299				0.0031			
	5			0	-0.1276									
				2	0.1723									
5	0	5.320		0	-0.0451			0.2654						-0.1325
				2	0.1003			-0.0202						0.1086
	1			0	-0.0105		0.0325		0.0759	-0.0282	0.0500	-0.0207		-0.0044
				2	-0.0510		-0.0742		-0.1754	0.0350	0.0002	-0.0715		0.0082
	2			0	0.0572	0.0709	0.0633	0.0430		0.0472	-0.1703	-0.0256		0.0341
				2	0.0878	-0.0386	0.0033	0.0537		0.0408	0.0764	0.1059		0.0484
	3			0	0.0501	-0.0018	-0.0141	-0.0348			0.0697			-0.0135
				2	-0.0717	-0.0081	-0.0013	-0.0492			0.0184			0.0311
	4			0	-0.0652		-0.0059				0.0270			
				2	0.0869		-0.0021				-0.0207			
	5			0	0.0103									
				2	-0.0622									
7	1	1	2.326 2.211	0	-0.0776		-0.0154		0.0175	-0.1471	-0.1922	-0.0367		0.1396
				2	0.0942		-0.0064		-0.0315	0.1695	0.1470	0.0799		-0.1381
	2			0	0.2908	0.6098	0.4054	1.3689		0.3403	-0.4397	-0.3209		0.2243
				2	-0.1187	-0.0129	0.0182	-0.4292		-0.0567	-0.1417	-0.0338		-0.0359
	3			0	-0.1333	0.0474	0.0029	-0.3473			0.1328			0.0660

Table V.1. (cont'd.)

			2	0.1053	-0.0289	0.0221	0.3722			-0.1650		-0.0271
	4		0	0.0181		-0.1755						
			2	0.0168		0.0114				0.1064		
										0.1469		
	5		0	0.1851								
			2	-0.1725								
2	1	4.665 4.580	0	-0.0038		0.0931		0.0500	0.0240	0.3340	-0.1964	-0.0086
			2	-0.0573		-0.0119		0.0366	-0.0554	-0.1613	0.1347	-0.0240
	2		0	-0.0018	0.0080	-0.0766	-0.1860		-0.0527	0.4077	-0.1206	0.0663
			2	0.0477	-0.0102	-0.0003	0.0131		0.0102	-0.3342	0.0298	-0.0622
	3		0	0.0625	0.0076	0.0032	-0.0627			0.4757		0.0336
			2	-0.0485	0.0520	-0.0238	-0.1912			-0.2747		0.0113
	4		0	-0.1303		-0.2962				0.9294		
			2	-0.0437		-0.0005				-0.1873		
	5		0	-0.1193								
			2	0.0569								
3	1	5.518	0	-0.0236		-0.0034		0.0072	0.0037	-0.0061	-0.0448	0.0419
			2	0.0048		0.0246		0.0906	-0.0339	0.0841	-0.1307	-0.0330
	2		0	0.1041	0.0256	0.1205	0.1894		-0.0813	-0.1748	0.0322	-0.0279
			2	0.0318	-0.0542	-0.0233	-0.0390		0.1006	-0.0413	0.0686	0.0145
	3		0	-0.0814	0.0125	-0.0332	-0.0306			0.0361		-0.1127
			2	-0.0389	0.0139	0.0135	0.0679			0.0399		0.1001
	4		0	0.0201		0.0387				-0.0966		
			2	-0.0220		-0.0073				0.0271		
	5		0	0.0412								
			2	-0.0272								
4	1	5.948	0	-0.0350		0.0723		0.0572	-0.0595	0.2604	-0.2356	0.0474
			2	-0.0282		0.0571		0.1341	0.0015	0.0118	0.1645	-0.0609
	2		0	-0.0426	0.0161	0.0018	-0.0482		-0.0756	0.0240	-0.0560	0.0596
			2	0.0186	-0.0267	0.0079	0.0883		-0.0108	-0.1693	0.1797	-0.0723
	3		0	-0.0569	0.0400	0.0116	0.0819			-0.0891		-0.0188
			2	0.0199	-0.0025	0.0048	0.0241			0.0600		-0.0409
	4		0	0.0440		-0.0398				0.0126		
			2	0.0479		-0.0054				0.0064		
	5		0	0.0241								

Table V.1. (cont'd.)

				2	0.0114								
	5	1	6.187	0	0.0122		-0.0104		-0.0670	0.0696	0.0880	-0.0363	-0.0018
				2	0.0110		-0.0603		-0.1934	0.0300	-0.1819	0.1200	-0.0750
		2		0	-0.0680	0.0501	-0.0837	-0.0868		0.1585	0.1830	-0.1854	0.0474
				2	-0.0061	-0.0116	-0.0116	0.1444		0.0837	0.0463	-0.0854	-0.0055
		3		0	0.0428	-0.0171	0.0198	0.1718			-0.1773		0.0113
				2	0.0733	-0.0754	0.0175	-0.0877			-0.0049		0.0503
		4		0	0.0344		0.0229				0.0211		
				2	0.0365		0.0068				-0.0483		
		5		0	-0.0007								
				2	0.0271								
9	1	2	3.025 3.004	0	0.6853	0.7439	0.5298	0.8187		-0.0042	-0.6710	-0.1582	0.2860
				2	0.0033	-0.0109	-0.0008	0.7215		0.0323	-0.0505	-0.1451	0.0638
		3		0	-0.1593	-0.0401	0.0641	0.3686			-0.3187		-0.0310
				2	0.0175	0.0619	-0.0353	-0.3895			0.1932		0.0568
		4		0	0.1141		-0.1524				0.3662		
				2	-0.0405		0.0006				-0.1234		
		5		0	-0.0816								
				2	0.0670								
	2	2	5.292 4.419	0	-0.0873	0.1483	0.1379	0.2230		0.0113	-0.5120	0.0368	0.1589
				2	-0.0071	-0.0090	-0.0037	-0.1841		0.0189	0.1708	-0.2105	-0.0930
		3		0	0.0353	-0.0626	-0.0005	0.0534			-0.1933		0.0615
				2	0.0379	-0.0133	0.0477	0.0250			0.3068		-0.0171
		4		0	0.0666		-0.1997				0.3295		
				2	-0.0904		0.0163				0.0782		
		5		0	0.0024								
				2	0.0169								
	3	2	5.886	0	0.1787	0.0498	0.2126	-0.3031		-0.0985	-0.8182	-0.0002	0.0152
				2	-0.0826	-0.0019	0.0223	-0.3740		0.0056	-0.3837	0.1747	0.0220
		3		0	0.0278	-0.1045	0.0609	0.4069			0.0307		-0.1021
				2	0.1037	-0.0596	0.0316	-0.0239			0.3859		0.0604
		4		0	-0.1537		-0.0624				0.1617		
				2	-0.0539		0.0137				-0.1370		

Table V.1. (cont'd.)

	5		0	0.0163							
			2	0.0027							
4	2	6.523	0	-0.0310	0.1233	0.0591	-0.0600	0.0571	-0.2959	-0.0864	0.0160
			2	-0.0283	0.0178	0.0138	0.2487	-0.0124	-0.5916	-0.2300	0.0649
	3		0	0.1226	0.0723	0.0128	-0.5504		0.3927		0.1075
			2	0.0625	-0.1091	0.0631	0.1111		0.2577		0.0338
	4		0	-0.0529		0.0630			-0.2028		
			2	-0.0307		-0.0046			0.0009		
	5		0	-0.1019							
			2	0.0294							
5	2	6.718	0	-0.0747	0.0305	-0.0173	-0.0540	-0.0343	-0.0553	0.0651	0.1352
			2	-0.1267	0.0470	-0.0146	-0.0429	0.0169	-0.1182	-0.0176	-0.1137
	3		0	-0.0176	-0.0725	0.0094	0.2628		0.0444		0.0158
			2	0.0718	-0.0260	-0.0232	-0.0931		-0.0327		-0.1288
	4		0	-0.1000		0.0353			-0.0508		
			2	-0.0482		0.0140			-0.0807		
	5		0	0.0429							
			2	0.0431							
11	1	3	4.583 4.510	0	-0.0140	0.1038	0.0656	-0.2718		0.0491	0.1124
				2	-0.0121	0.0095	0.0093	-0.2885		0.6689	-0.0690
	4			0	0.1138		0.3866			-0.9593	
				2	0.0271		0.0073			0.0426	
	5			0	-0.0161						
				2	-0.0460						
2	3	5.400 5.500		0	-0.1074	0.1987	-0.0146	-0.5864		0.4264	-0.0909
				2	-0.1484	0.1584	-0.0716	-0.6085		-0.0280	0.0671
	4			0	0.2068		-0.1710			0.5231	
				2	0.2046		-0.0059			-0.2644	
	5			0	-0.0556						
				2	-0.0553						
3	3	7.503		0	-0.0409	0.1867	-0.0847	-0.4414		-0.5567	0.0413
				2	-0.0504	0.2012	-0.1138	-0.4486		-0.4873	-0.0682

Table V.1. (cont'd.)

	4		0	0.0873		-0.0542		0.2251		
			2	0.0889		-0.0465		0.2792		
	5		0	-0.1179						
			2	-0.0988						
4	3	7.774	0	-0.0398	-0.0841	0.0012	0.1151	0.5099	-0.0717	
			2	0.0725	-0.0422	0.0078	0.0671	0.1128	0.0067	
	4		0	-0.1556		-0.1461		0.5928		
			2	-0.1673		0.0520		-0.3011		
	5		0	-0.0021						
			2	-0.0298						
5	3	8.339	0	-0.0474	0.0094	0.0033	0.0623	-0.0603	-0.0153	
			2	-0.1027	0.0377	0.0158	0.0775	0.0127	-0.0250	
	4		0	0.1416		-0.0054		-0.0238		
			2	0.0683		-0.0107		0.0868		
	5		0	0.0010						
			2	0.0258						
13 1	4	6.745	0	-0.1468		-0.3353		0.8480		
			2	-0.0482		-0.0582		0.8547		
	5		0	0.1426						
			2	0.0396						
2	4	7.317	0	-0.3432		-0.0250		0.2588		
			2	-0.2394		0.0089		0.1789		
	5		0	0.0300						
			2	0.1284						
3	4	9.006	0	-0.1892		0.0547		-0.1417		
			2	-0.1004		0.0109		0.1360		
	5		0	0.0100						
			2	0.0384						
4	4	9.447	0	-0.2634		0.0687		-0.2896		
			2	-0.2090		0.0585		-0.2547		
	5		0	-0.0297						
			2	0.0677						
5	4	9.814	0	-0.0838		-0.0057		0.0266		

Table V.1. (cont'd.)

			2	-0.0749	0.0059	0.0118
	5		0	0.0217		
			2	0.0232		
15	1	5	9.304	0	0.0641	
				2	0.0721	
	2	5	10.339	0	-0.0771	
				2	-0.1151	
	3	5	10.866	0	-0.0249	
				2	-0.0395	
	4	5	11.520	0	0.0224	
				2	0.0151	
	5	5	11.816	0	0.1459	
				2	0.1233	

Table V.2. Calculated occupation numbers for sd-shell orbits in the ground state of ^{27}Al.

p/n	2j= 5	1	3
p	4.108	0.422	0.470
n	4.787	0.602	0.611

APPENDIX

To obtain the one-body density matrix (OBDM) defined in equation (5) in isospin formalism, we can define the operator $\bar{a}$ which is a tensor operator in isospin space,

$$a(t,t_3)= (-1)^{t-t_3}\bar{a}(t,-t_3) \tag{106}$$

then the operator $[a^+(t,t_3) \otimes a(t,t_3)]$ can be written

$$[a^+(t,t_3) \otimes a(t,t_3)]= (-1)^{t-t_3}[a^+(t,t_3) \otimes \bar{a}(t,-t_3)]$$

$$= (-1)^{t-t_3} \sum_{\Delta T \Delta T_z} \langle t\ t_3\ \ t\ -t_3\ |\Delta T\ \Delta T_z\rangle$$

$$[\ a^+ \otimes \bar{a}\ ]^{(\Delta T,\Delta T_z)} \tag{107}$$

where t= 1/2, t_3= 1/2 for proton and -1/2 for neutron, and ΔT_z= 0 and ΔT= 0,1.

$$[a^+(1/2,t_3) \otimes a(1/2,t_3)] = (-1)^{1/2-t_3}\{ \langle 1/2\ t_3\ 1/2\ -t_3 |\ 0\ 0\rangle [a^+ \otimes \bar{a}]^{(\Delta T,0)} + \langle 1/2\ t_3\ 1/2\ -t_3 |\ 1\ 0\rangle [a^+ \otimes \bar{a}]^{(\Delta T,1)}\} \quad (108)$$

$$[a^+(p/n) \otimes a(p/n)] = \sqrt{1/2}\,[a^+ \otimes \bar{a}]^{(\Delta T=0)} +/- \sqrt{1/2}\,[a^+ \otimes \bar{a}]^{(\Delta T=1)} \quad (109)$$

Using Wigner-Eckart theorem, the matrix element of the operator $a^+ \otimes \bar{a}$ is

$$\langle T_f\ T_z |[a^+ \otimes \bar{a}]^{(\Delta T=0)}| T_i\ T_z \rangle = (-1)^{T_f-T_z} \begin{pmatrix} T_f & 0 & T_i \\ -T_z & 0 & T_z \end{pmatrix} \times \langle T_f ||[a^+ \otimes \bar{a}]^{(\Delta T=0)}|| T_i \rangle \quad (110)$$

$$\langle T_f\ T_z |[a^+ \otimes \bar{a}]^{(\Delta T=1)}| T_i\ T_z \rangle = (-1)^{T_f-T_z} \begin{pmatrix} T_f & 1 & T_i \\ -T_z & 0 & T_z \end{pmatrix} \times \langle T_f ||[a^+ \otimes \bar{a}]^{(\Delta T=1)}|| T_i \rangle \quad (111)$$

The OBDM becomes

$$OBDM(p/n)) = \langle f|[a^+(t,t_3) \otimes a(t,t_3)]\,|i\rangle$$

$$= (-1)^{T_f - T_z} \begin{pmatrix} T_f & 0 & T_i \\ -T_z & 0 & T_z \end{pmatrix} \times \sqrt{2} \quad \text{OBDM } (\Delta T=0)/2$$

$$(+/-)\ (-1)^{T_f - T_z} \begin{pmatrix} T_f & 1 & T_i \\ -T_z & 0 & T_z \end{pmatrix} \times \sqrt{6} \quad \text{OBDM } (\Delta T=1)/2 \tag{112}$$

where OBDM(ΔT) is given by

$$\text{OBDM}(i,f,L,\Delta T) = \frac{\langle f||[a^{+}(t) \otimes \bar{a}(t)]^{(\Delta T)}||i\rangle}{\sqrt{(2\Delta T+1)}} \tag{113}$$

Equation (8) follows from reduction in both spin and isospin spaces.

REFERENCES:

1. N. F. Mott, Proc. Roy. Soc. Ser. A, 124, 426 (1929).

2. E. Guth, Anz. Akad. Wiss. Wien Math. Naturw. Kl., 24, 299 (1934).

3. M. E. Rose, Phys. Rev 73, 279 (1948).

4. E. M. Lyman, A. O. Hanson, and M. B. Scott, Phys. Rev 84, 626 (1951).

5. Mamasachlisov, J. Phys., Moscow, 7, 239 (1943).

6. G. B. Collins and B. Waldman, Phys. Rev. 57, 1088 (1940).

7. R. Hofstadter, H. R. Fechter, and J. A. McIntyre Phys. rev.91, 422 (1953).

8. W. C. Barber, Ann. Rev. Nucl. Sci. 12, 1 (1962).

9. T. de Forest and J. D. Walecka, Advan. Phys. 15, 1 (1966).

10. H. Überal, " Electron Scattering from Complex Nuclei", Vols. A and B, Academic Press, New York, (1971).

11. G. A. Peterson, Phys. Lett. 2, 162 (1962).

12. P. M. Endt and C. van der Leun, Nucl. Phys. A310, 1 (1978).

13. P. J. Ryan, R. S. Hicks, A. Hotta, J. Dubach, G. A. Peterson, and D. V. Webb, unpublished.

14. M. G. Mayer and J. H. D. Jensen, "Elementary Theory of Nuclear Shell Structure" (Wiley, New York; 1955).

15. E. C. Halbert, J. B. McGrory, B. H. Wildenthal and S. P. Pandya, "Adv. in Nuclear Physics", edited by M. Baranger and E. Vogt, (Plenum, New York; 1971).

16. J. B. McGrory and B. H. Wildenthal, Ann. Rev. Nucl. Part. Sci. 30: 383 (1980).

17. B. H. Wildenthal, Bull. Am. Phys. Soc. 27, 725 (1982).

18. C. Chitwood and B.H.Wildenthal, unpublished.

19. S. Cohen and D. Kurath, Nucl. Phys. 73, 1 (1965).

20. A. Brown, A. Arima and J. B. McGrory, Nucl. Phys. A277, 77 (1977).

21. P. J. Brussaard and P. W. Glaudemans, " Shell-Model Applications in Nuclear Spectroscopy" (North-Holand, Amstrdam, 1977).

22. B. A. Brown, W. Chung and B. H. Wildenthal, Phys. Rev. 21, 2600 (1980).

23. C. B. Dover and N. Van Giai, Nucl. Phys. A190, 373 (1972).

24. R. D. Woods and D. S. Saxon, Phys. Rev. 95, 577 (1954).

25. B. A. Brown et al., Phys. Rev. C26,

26. R. S. Willey, Nucl. Phys. 40, 529 (1963).

27. K. Arita, Proc. Meeting on Giant Resonances and Related Topics, eds. H. Sagawa et al. (INS, Univ. of Tokyo, 1977) p. 119.

28. H. Sagawa, Phys. Lett. 90b, 21 (1980).

29. A. Bohr and B. R. Mottelson, " Nuclear Structure", Vol. 1 (Benjamin, New York, 1969).

30. B. H. Wildenthal, Proceedings of the Conference on Nuclear Structure and Particle Physics, Oxford, April 6-8, 1981, p.85 (institute of physics).

31. L. J. Tassie, Austr. Jour. Phys. 9,407 (1956).

32. L. J. Tassie and F. C. Barker, Phys. Rev. 111, 940 (1958).

33. B. A. Brown, R. Radhi and B. H. Wildenthal, submitted to Phys. Reports

34. H. Chandra and G. Sauer, Phys. Rev. C13, 245 (1976).

35. J. L. Friar and J. W. Negele "Adv. in Nuclear Physics", edited by M. Baranger and E. Vogt (Plenum, New York, 1975) Vol. 8, p. 219.

36. F. Borkowski, P. Peuser, G. G. Simon, V. H. Walther and R. D. Wendling, Nucl. Phys. A222, 269 (1974).

37. H. Euteneuer, H. Rothhaas, O.Schwentker, J. R. Moreira, C. W. de Jager, L. Lapikas, H. de Vries, J. Flanz, K. Itoh, G. A. Peterson, D. V. Webb, W. C. Barber, and S.

Kowalski, Phys. Rev. C 16, 1703 (1977).

38. S. T. Tuan, L. E. Wright and D. S. Onley, Nucl. Inst. and methods 60, 70 (1968).

39. MIT Bates Laboratory and M.V. Hynes, unpublished.

40. L. Lapikas, A. E. L. Dieperink and G. Box, Nucl. Phys. A 203, 609 (1973).

41. M. W. S. Macauley, R. P. Singhal, R. G. Arthur and E. E. Knight, Kelvin Labroratory, Glasgow, Report (1977).

42. G. C. Li, M. R. Yearian and I. Sick, Phys. Rev. C9, 1861 (1974).

43. A. Arima, Y. Horikawa, H. Hyaunga and T. Suzuki, Phys. Rev. Lett. 40, 1001 (1978).

44. K. Arita, A. Enomoto, S. Oguro, Y. Mizuno, T. Nakazato, S. Ohsawa, T. Terasawa, and Y. Torizuka, Phys. Rev. C 23, 1482 (1981).

45. R. J. McCarthy and J. P. Vary, Phys. Rev. C 25, 73 (1982).

46. T. Suzuki, Phys. Lett. 120B, 27 (1983).

47. C. Williamson, private communication (1983).

48. H. Miessen, (Mainz data) Phd. Thesis, Johannes Gutenberg Univ., prinate communication (1983).

49. H. Miessen, (Bates data) Phd. Thesis, Johannes Gutenberg Univ., private communication(1983).

50. M. V. Hynes, et al., Phys. Rev. Lett. 42,1444 (1979).

51. R. C. York and G. A. Peterson, Phys. Rev. C 19, 574 (1979).

52. Y. Torizuka, Laboratory of Nuclear Science, Tokyo University, Research Report (Private communication), (1977).

53. L. Lapikas, in: Proc. Intern. Conf. on Nuclear Physics with electromagnetic interactions (Mainz, 1979), Lecture Notes in Physics, Vol. 108 (Springer, Berlin, 1979) p.41.

54. C. W. de Jager, Private Communication.

55. B. Desplanques and J. F. Mathiot Nucl. Phys. A358, 381

(1981).

56. B. A. Brown, W. Chung and B. H. Wildenthal, Phys. Rev. Lett 40, 1631 (1978).

57. L. Lapikas, in Proceedings of the Conference on Modern Trends in Elastic Scattering, Amsterdam, (unpublished) and private communication (1978).

58. R. E. Rand, R. Foroch, and M. R. Yearian, Phys. Rev. C 144, 859 (1966).

59. J. C. Bergstrom, S. B. Kowalski and R. Neuhausen, Phys. Rev. C 25 (1982).

60. R. H. Huffman, private communication (1982).

61. G. J. Van Niftrik, L. Lapikas, H. De Vries and G. Box, Nucl. Phys. A174, 173 (1971).

62. J. Lichtenstadt, J. Alster and M. A. Moinester, J. Dubach, R. s. Hicks, G. A. Peterson and S. Kowalski, unpublished.

63. L. Lapikas, G. Box and H. De Vries, Nucl. Phys. A253 324 (1975).

64. G. J. Vanpraet and P. Kossanyi-Demay, Nuovo Cim. 39 388 (1965).

65. R. S. Hicks, J. Dubach, R. A. Lindgren, B. Parker, and G. A. Peterson, Phys. Rev C, 26, 339 (1982).

66. E. B. Dally et al., Phys. Rev. C2,2057 (1970).

67. F. A. Bumiller, F. R. Buskirk, J. N. Dyer and W. A. Manson Phys. Rev. C 5, 391 (1972).

68. C. W. de Jager, H. de Vries, and C. de Vries, At. Data Nucl. Data Tables 14,179 (1974).

69. B. M. Barnett et al., Phys. Lett 97B, 45 (1980).

70. L. S. Cardman et al., Phys. Lett 91B, 203 (1980).

71. G. Fey, H. Frank, W. Schutz, and H. Theissen, talk presented at the Fruhjahrstagung der Deutschen Phys. Geselleschaft, Heidelberg, 1973.

72. M. Miska, B. Norum, M. W. Hynes, W. Bertozzi, S. Kowalski, F. N. Rad,C. P. Sargent, T. Sasanuma, and B. L. Berman, Phys. Lett. 83B, 165 (1979).

73. L. A.Schaller, T. Dubler, K. Kaeser, G. A. Rinker, B.

Robert-Tissot, L. Schellenberg, and H. Schneuwly, Nucl. Phys. 225 (1978).

74. R. Engfer, H. Schneuwly, J. L. Vuilleumier, H. K. Walter, and A. Zehnder, At. Data Nucl. Data Tables 14, 509 (1974).

75. W. J. Briscoe and H. Crannell, in Proceedings of the International Conference on Nuclear Physics with Electromagnetic Interactions, Mainz, 1979 (Springer, Berlin, 1979), p. 2.6.

76. F. Ajzenberg-Selove and T. Lauritsen, Nucl. Phys. A227, 1 (1974).

77. F. ajzenberg-Selove, Nucl. Phys. A248, 1 (1975).

78. F. ajzenberg-Selove, Nucl. Phys. A268, 1 (1976).

79. F. ajzenberg-Selove, Nucl. Phys. A281, 1 (1977).

80. F. ajzenberg-Selove, Nucl. Phys. A300, 1 (1978).

81. P. M. Endt and C. van der Leun, Nucl. Phys. A235 27 (1974).

82. P. M. Endt and C. van der Leun, Nucl. Phys. A214, 1 (1973).

83. R. P. Singhal, A. Johnstone, W. A. Gillespie and E. W. Lees, Nucl. Phys. A279, 29 (2977).

84. B. S. Dolinskii, R. L. Kondratev, N. N. Kostin, V. P. Lisin, V. N. Ponomarev, and A. A. Polonskii, Bull. Acad. Sci. USSR, Phys. Ser. 45, 166 (1981).